


1989

Spectral hole burning studies of Photosystem 1

J. Kevin Gillie
Iowa State University

Follow this and additional works at: <https://lib.dr.iastate.edu/rtd>

 Part of the [Biophysics Commons](#), and the [Physical Chemistry Commons](#)

Recommended Citation

Gillie, J. Kevin, "Spectral hole burning studies of Photosystem 1" (1989). *Retrospective Theses and Dissertations*. 8935.
<https://lib.dr.iastate.edu/rtd/8935>

This Dissertation is brought to you for free and open access by the Iowa State University Capstones, Theses and Dissertations at Iowa State University Digital Repository. It has been accepted for inclusion in Retrospective Theses and Dissertations by an authorized administrator of Iowa State University Digital Repository. For more information, please contact digirep@iastate.edu.

INFORMATION TO USERS

The most advanced technology has been used to photograph and reproduce this manuscript from the microfilm master. UMI films the text directly from the original or copy submitted. Thus, some thesis and dissertation copies are in typewriter face, while others may be from any type of computer printer.

The quality of this reproduction is dependent upon the quality of the copy submitted. Broken or indistinct print, colored or poor quality illustrations and photographs, print bleedthrough, substandard margins, and improper alignment can adversely affect reproduction.

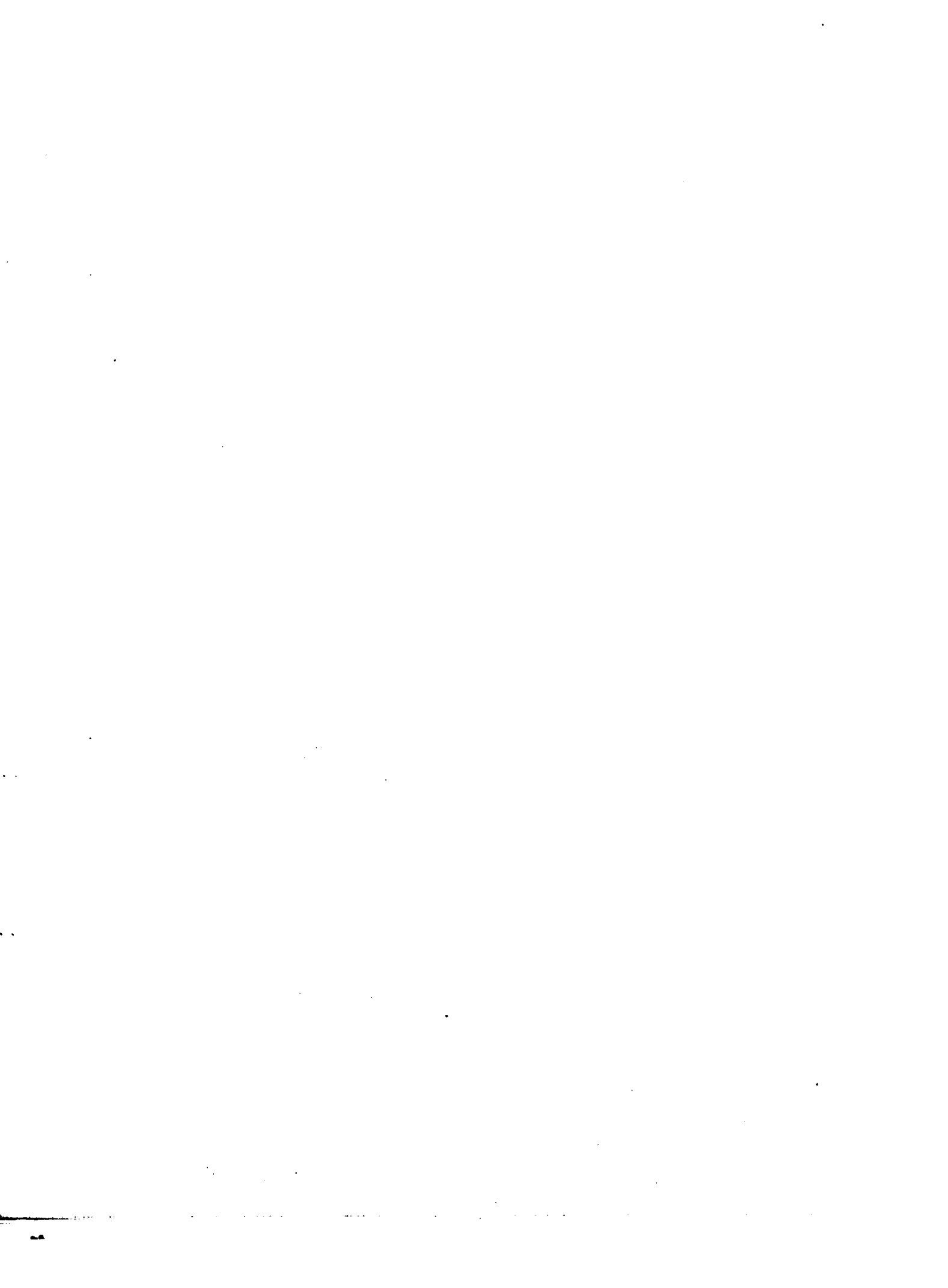
In the unlikely event that the author did not send UMI a complete manuscript and there are missing pages, these will be noted. Also, if unauthorized copyright material had to be removed, a note will indicate the deletion.

Oversize materials (e.g., maps, drawings, charts) are reproduced by sectioning the original, beginning at the upper left-hand corner and continuing from left to right in equal sections with small overlaps. Each original is also photographed in one exposure and is included in reduced form at the back of the book. These are also available as one exposure on a standard 35mm slide or as a 17" x 23" black and white photographic print for an additional charge.

Photographs included in the original manuscript have been reproduced xerographically in this copy. Higher quality 6" x 9" black and white photographic prints are available for any photographs or illustrations appearing in this copy for an additional charge. Contact UMI directly to order.

U·M·I

University Microfilms International
A Bell & Howell Information Company
300 North Zeeb Road, Ann Arbor, MI 48106-1346 USA
313/761-4700 800/521-0600



Order Number 8920132

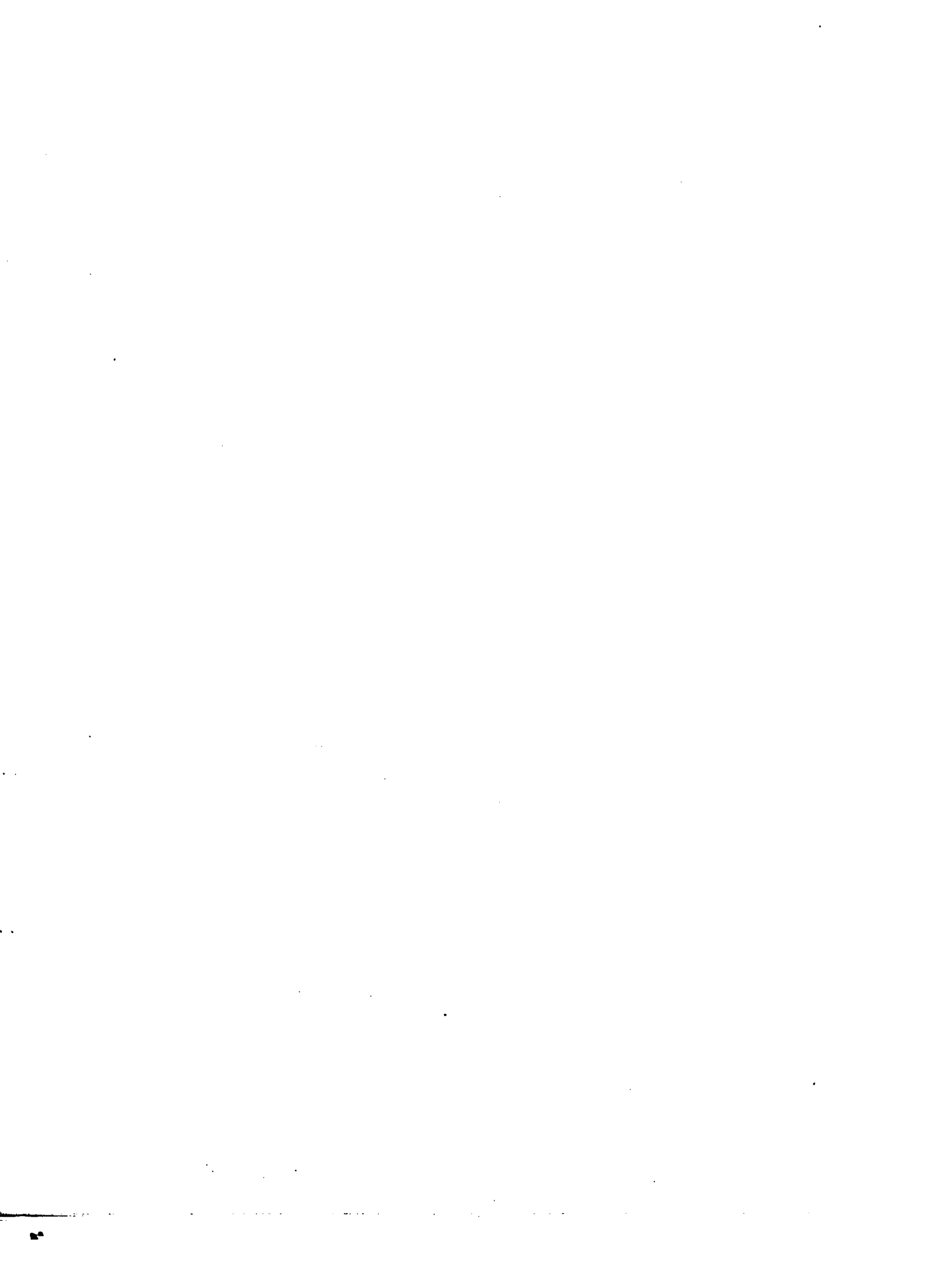
Spectral hole burning studies of Photosystem I

Gillie, J. Kevin, Ph.D.

Iowa State University, 1989

U·M·I

**300 N. Zeeb Rd.
Ann Arbor, MI 48106**



Spectral hole burning studies of Photosystem 1

by

J. Kevin Gillie

**A Dissertation Submitted to the
Graduate Faculty in Partial Fulfillment of the
Requirements for the Degree of
DOCTOR OF PHILOSOPHY**

**Department: Chemistry
Major: Physical Chemistry**

Approved:

Signature was redacted for privacy.

~~In Charge of Major Work~~

Signature was redacted for privacy.

~~For the Major Department~~

Signature was redacted for privacy.

~~For the Graduate College~~

**Iowa State University
Ames, Iowa**

1989

TABLE OF CONTENTS

	page
EXPLANATION OF DISSERTATION FORMAT	iv
GENERAL INTRODUCTION	1
EXPERIMENTAL METHODS	15
REFERENCES	20
SECTION I. PHOTOCHEMICAL HOLE BURNING OF P700	24
INTRODUCTION	25
PAPER I. PERSISTENT HOLE BURNING OF THE PRIMARY DONOR STATE OF PHOTOSYSTEM I: STRONG LINEAR ELECTRON-PHONON COUPLING	32
INTRODUCTION	34
RESULTS AND DISCUSSION	36
CONCLUSIONS	46
REFERENCES	47
PAPER II. THEORY FOR SPECTRAL HOLE BURNING OF THE PRIMARY DONOR STATE OF PHOTOSYNTHETIC REACTION CENTERS	50
INTRODUCTION	52
THEORY	55
CALCULATIONS	65
RESULTS	67
DISCUSSION	90
CONCLUSIONS	99
REFERENCES	102
ADDITIONAL RESULTS	106
CONCLUSIONS	120
REFERENCES	121

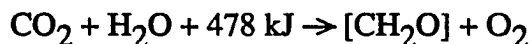
	page
SECTION II. NONPHOTOCHEMICAL HOLE BURNING OF THE ANTENNA COMPLEX OF PHOTOSYSTEM I	127
INTRODUCTION	128
PAPER I. HOLE BURNING SPECTROSCOPY OF A CORE ANTENNA COMPLEX	146
INTRODUCTION	148
EXPERIMENTAL	151
RESULTS AND DISCUSSION	152
REFERENCES	159
PAPER II. NONPHOTOCHEMICAL HOLE BURNING OF THE NATIVE ANTENNA COMPLEX OF PHOTOSYSTEM I (PSI-200)	162
INTRODUCTION	164
EXPERIMENTAL	166
RESULTS	168
DISCUSSION	184
CONCLUSION	200
REFERENCES	201
ADDITIONAL RESULTS	206
REFERENCES	215
ACKNOWLEDGMENTS	223

EXPLANATION OF DISSERTATION FORMAT

This dissertation contains the candidate's original work on spectral hole burning of Photosystem I. Section I contains two published papers which describe a linear electron-phonon coupling theory that was developed to model the spectral properties of the primary electron donor states of photosynthetic systems and application of the theory to P700 of Photosystem I. Section II contains two published papers which report hole burning experiments performed on the light harvesting chlorophyll complex of Photosystem I and application of multiphonon excitation energy transport theory to these results. Each section contains an introduction, two papers, and additional results. The references for the introduction and additional results of each section are located at the end of that section. The references for each paper are found at the end of that paper.

GENERAL INTRODUCTION

Photosynthesis is one of the many fascinating biophysical energy conversion processes that occur in nature. It is unique, however, since the energy source for the basic photosynthetic equation



is sunlight. That is, photosynthesis utilizes solar energy to reduce carbon dioxide to carbohydrates. One einstein (one mole of photons) at 680 nm contains only ~ 175 kJ. It is recognized then, that nature had to construct sophisticated systems to collect and convert solar energy. The first evidence for such systems was provided by Emerson and Arnold [1] when they demonstrated that large numbers of chlorophylls (Chl) cooperated to produce oxygen via photosynthesis. Although the basic photosynthesis equation is simple, the processes occurring in the thylakoid membranes are complicated. The primary events of light harvesting and charge separation are the concern of this work.

The thylakoid membrane of green plant chloroplast contains hundreds of protein bound pigments arranged into two functional groups: i) the reaction centers and ii) the light harvesting complexes. The physical organization of the thylakoid membranes has been extensively reviewed [2 and refs. therein] and is shown in Fig. 1. The thylakoid membrane consist of two photosynthetic units (PSU), Photosystem I (PSI) and Photosystem II (PSII), which function cooperatively in photosynthesis. The reaction centers (RC) are labeled P700 (for PSI) and P680 (for PSII) to indicate the position, 700 nm and 680 nm, of the maximum of the light induced absorption decrease.

The light harvesting chlorophyll protein complexes (LHCI and LHCII) contain

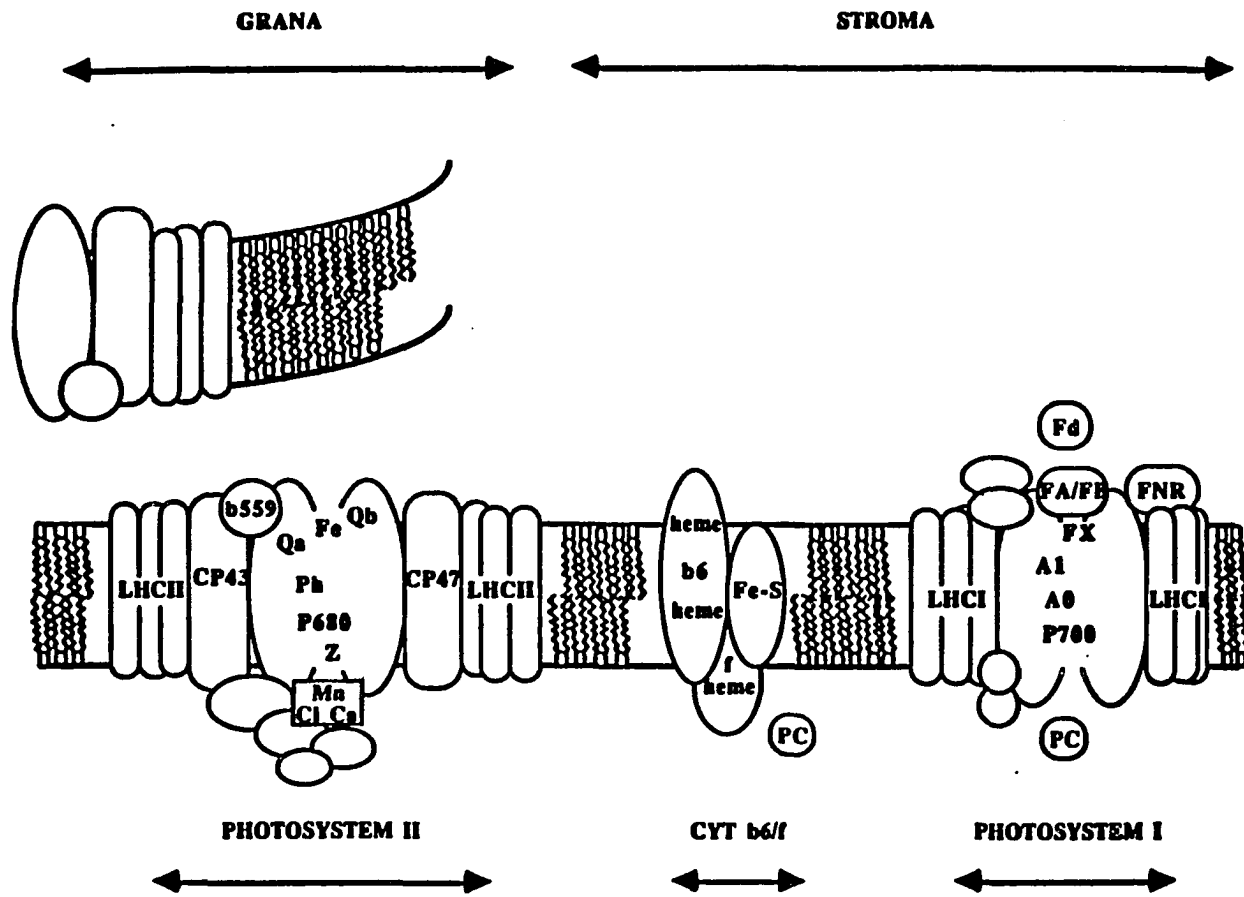


Figure 1. The physical organization of the Photosystem I, cytochrome *b6/f*, and Photosystem II protein complexes within the thylakoid membrane. The cytochrome *b6/f* complex transfers an e^- from PSII to PSI via plastocyanine (PC) (reprinted from ref. 3).

protein bound chlorophyll a (Chl a) and chlorophyll b (Chl b). These protein complexes and the core Chl a protein complexes serve the RCs as antenna complexes to collect and transfer solar energy to the RC. For PSI, there are about 200 Chls per reaction center. The antenna complexes serve to increase the amount of the solar spectrum that is employed by broadening the photosystem's absorption (different spectral forms of Chls) [4-7] and by increasing the absorptivity (additive in number of molecules) over the isolated RC absorption profile.

Since the quantum yield for photosynthesis is ~ 1 [8], it is interesting to consider how energy can be transferred over large spatial distances in the antenna in a manner that competes successfully with other radiative and non-radiative decay channels. The orientation of the proteins with respect to the RC, the organization of the Chls within the proteins, the dynamical role of the proteins and the electronic states of the Chls are important components of any answer to this question.

The energy delivered by the antenna complex is photoconverted at the RC to a stabilized charge separation. In PSII, excitation of the primary electron donor (PED), P680, leads to electron transfer to a pheophytin (Pheo) acceptor [9-11] and subsequent transfer to a quinone where the charge is stabilized [12]. The P680 \rightarrow Pheo e^- transfer occurs in ~ 3 psec [13,14]. The charge separation in PSI occurs within ~ 3 psec [15] at room temperature with production of the charge separated state $P700^+A_0^-$ (A_0 is the primary acceptor) within ~ 14 psec [16]. Overall, the RCs produce an energy change of 1.22V.

The e^- necessary for reducing $P680^+$ is provided by splitting H_2O . Eight photons are required to produce one molecule of oxygen. The e^- produced in charge stabilized P680 reaction center is passed into the cytochrome b₆/f (cyt b₆/f) complex where it is ultimately used to reduced $P700^+$. This process translocates a proton

across the membrane thereby producing a pH and electric field gradient which is used for generating ATP. The electron available from P700 excitation is passed to the ferredoxin (Fd) and reduces NADP^+ to NADPH. It is NADPH and ATP which the dark reactions (Calvin cycle) use to reduce CO_2 to carbohydrates. As in the antenna complex, acceptor orientation, protein dynamics, and electronic states play important roles in efficient charge separation and stabilization.

The PSI protein complex is shown schematically in Fig. 2 [see refs. 3,17-20 for reviews]. The structure has not yet been determined by X-ray crystallography so this represents a proposal based on a large volume of biochemical evidence [3,17]. CP1, the P700 chlorophyll a-protein, contains the core antenna complex, active P700 and A_0 , and A_1 . It is a subset of the core protein which includes, along with CP1, the e^- acceptors A_1 and F_x and the high molecular weight (82 and 83 kDa) polypeptides. The enriched PSI core complex is the smallest fully functional RC particle. It contains P700, the e^- acceptors A_0 , A_1 , F_x , F_a/F_b and ~7 polypeptides including the core antenna complex. The identity of the acceptors is given in Table I. The PSI core complex is enriched to ~30 Chl a per reaction center. The "native" PSI particle contains, in addition to the core complex, LHCI and is the most physiologically intact particle. The LHCI complex contains ~170 Chl with a Chl a /Chl b ratio of ~6 [21,22]. The overall Chl a/Chl b ratio in PSI-200 is ~3.5 [21,23,24].

A proposed structure for P700 is shown in Fig. 3. It is based on biochemical evidence and reflects the structure determined for the purple photosynthetic bacteria Rhodospseudomonas viridis (Rps. viridis) [25-28] and Rhodobacter sphaeroides (Rb. sphaeroides) [29,30]. It maintains the pseudo-symmetry (C_2) found in the purple bacteria and suggested for PSII. The precise structural arrangement awaits X-ray

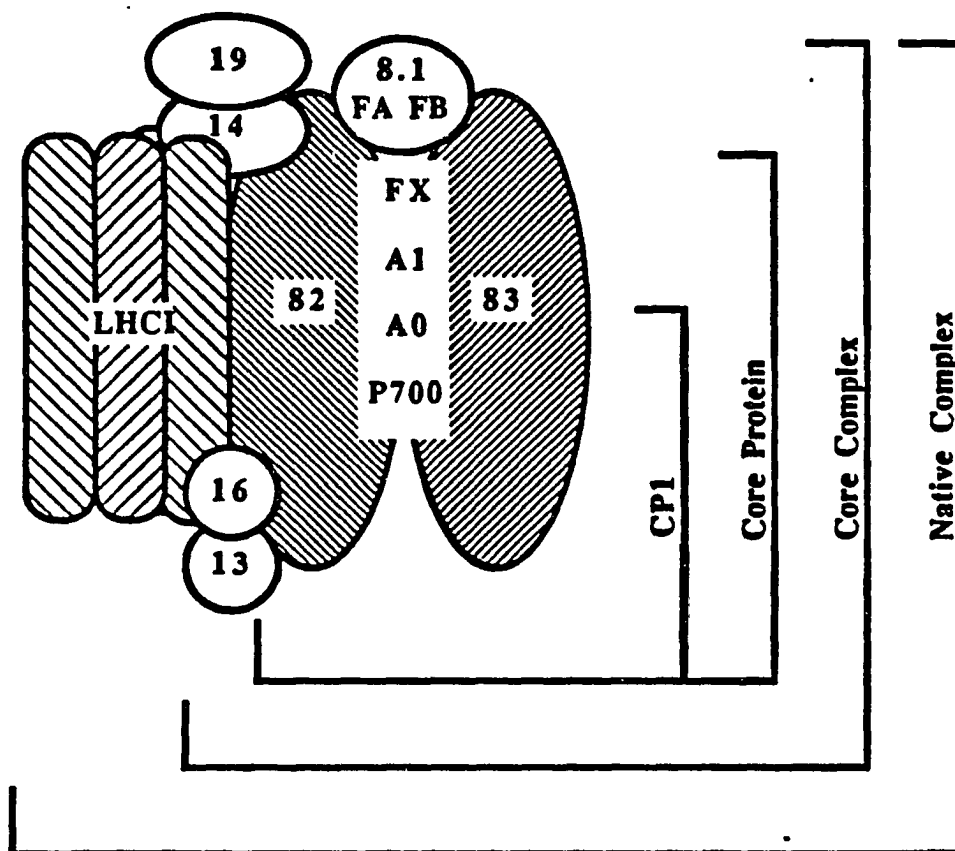


Figure 2. A schematic of the Photosystem I protein complex indicating the polypeptide composition of the isolatable particles. The shaded polypeptides represented chlorophyll-bearing proteins (reprinted from ref. 3).

Table I. Donor/acceptor identity of the Photosystem I polypeptides

Donor/Acceptor	Identity
P700	Chlorophyll dimer
A _O	Chlorophyll monomer
A ₁	Vitamin K ₁
F _X	[XFe - XS]Cluster (X=2,4)
F _B	[4Fe - 4S]Cluster
F _A	[4Fe - 4S]Cluster
F _D	Ferredoxin
FNR	Ferredoxin:NADP ⁺ oxidoreductase

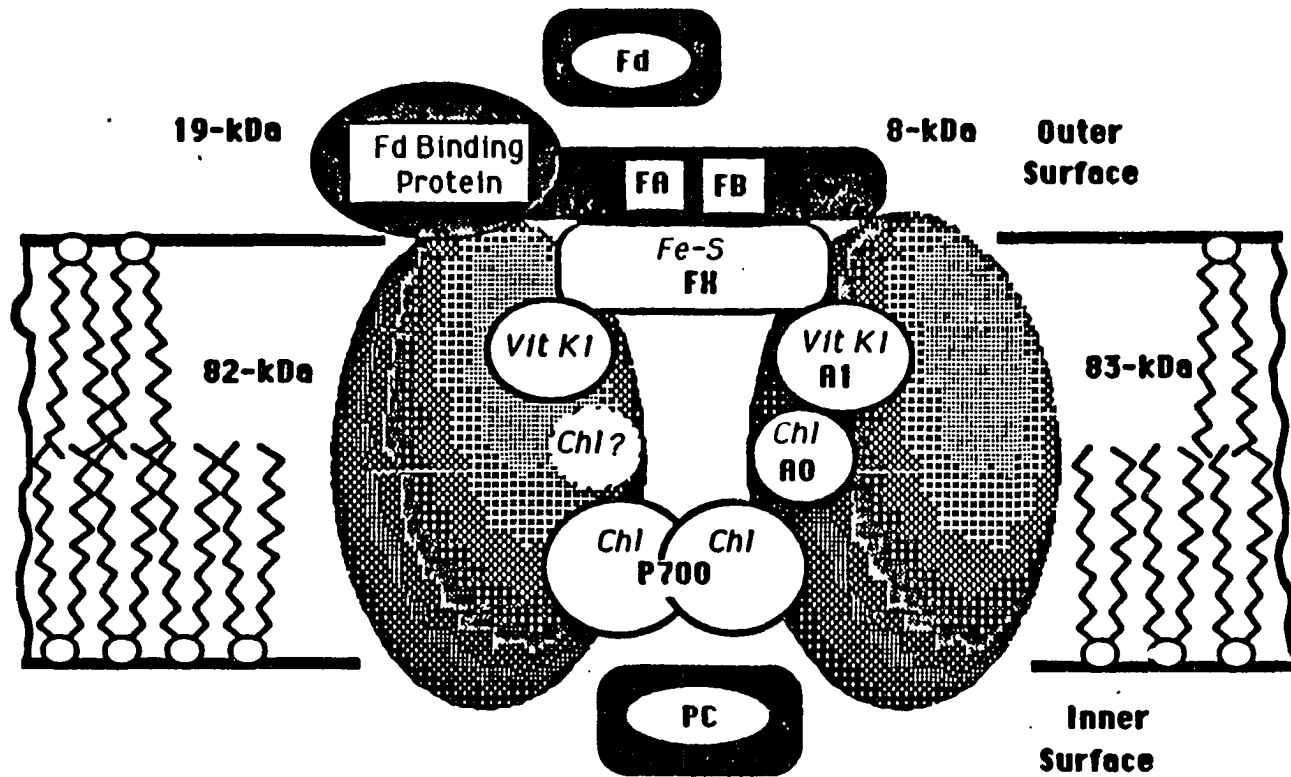


Figure 3. A proposed structure for the Photosystem I reaction center. It reflects biochemical evidence and the structure determined for the reaction center of purple photosynthetic bacteria (reprinted from ref. 3).

structure analysis of the recently crystallized PSI complex from cyanobacteria [31,32].

The absorption spectrum of PSI at room temperature is shown in Fig. 4. The dominant absorption feature is the lowest excited singlet state ($S_1 \leftarrow S_0$) transition, the Q_y transition, of the protein bound Chl a antenna complex at 670 nm. The Q_y transition for Chl b is at 650 nm. The $S_2 \leftarrow S_0$ or Q_x transition lies at about 575 nm for Chl a. The primary electron donor state, P700, has its maximum absorption at ~700 nm, a shift of ~750 cm^{-1} from monomer Chl a. To a first approximation, the shift is a result of excitonic interactions between pigment pairs. The carotenoids associated with PSI absorb in the 450-500 nm range and the Chl $S_3 \leftarrow S_0$ and higher transitions, the Soret transitions, lie at <450 nm.

The absorption spectrum sharpens only slightly in cooling the sample to 4.2 K, and it is still dominated by the broad (350 cm^{-1} width) profile of the Chl a Q_y transition. At this temperature it is possible to distinguish the Chl b absorption at 650 nm and the P700 absorption (in enriched particles). The broad profile hides important information - homogeneous linewidths, intramolecular vibrational frequencies, and low energy lattice vibration (phonon) frequencies - about the excited state of the system. The broad low temperature absorption character is similar to that observed for molecules doped into amorphous (glassy) materials. In this case, site selective spectroscopies, spectral hole burning and fluorescence line narrowing, are employed to "trick" the system into mimicking a perfect crystal.

Molecules doped into amorphous materials, e.g., ionic dyes in organic glasses, exhibit a broad absorption spectrum (typically several hundred cm^{-1}) even after cooling to near 0 K. In contrast, molecules doped into perfect crystals exhibit sharp absorption lines (typically <1 cm^{-1}) which correspond to the various electronic

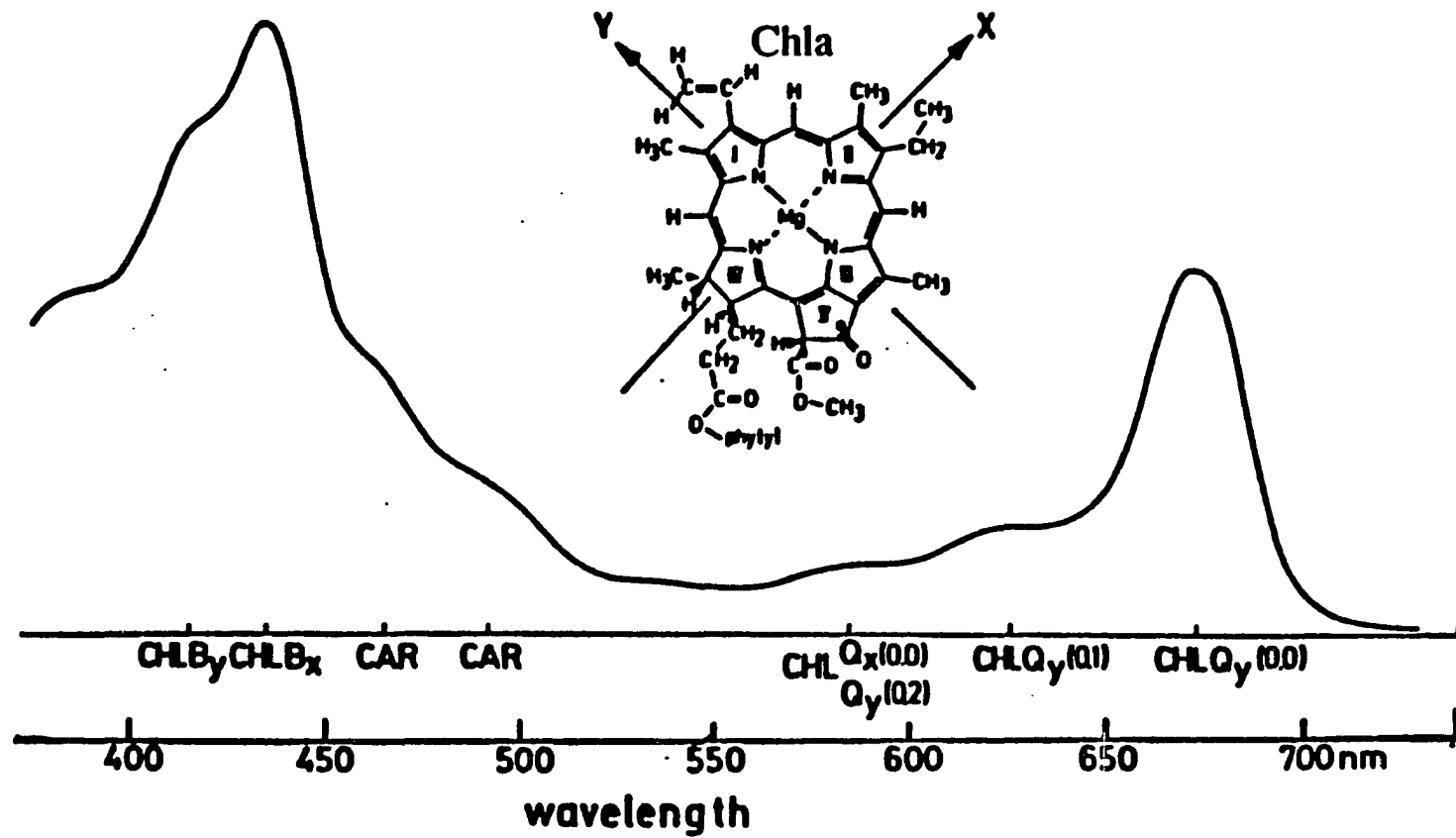


Figure 4. The room temperature absorption spectrum of PSI. The inset shows the conventional axis assignment for Chl a.

(vibronic) transitions of the molecule. The different behaviors are a result of the impurity's microenvironment. For a perfect crystal each impurity molecule has the same environmental interactions and hence the electronic transitions overlap producing the observed homogeneously broadened lines. One important characteristic of amorphous materials is the variation in microscopic site-impurity interactions. Each impurity molecule experiences slightly different environmental interactions which cause the electronic transitions to be distributed around a center frequency. The resulting spectrum is said to be inhomogeneously broadened and consist of the convolution of the homogeneously broadened absorption profile of the individual impurity molecule. This is illustrated in Fig. 5a.

Site selection spectroscopies utilize narrow band (preferably less than the homogeneous linewidth) light sources such as lasers to select a narrow energy window (isochromat) for excitation. The number of molecules excited represents just a small fraction of the total number of molecules in the system and the resulting spectral features are narrow mimicking that of a perfect crystal. The inhomogeneity has been circumvented.

An impurity molecule in a glass can undergo two types of transformations, one photochemical the other photophysical, while in its excited state. In either case, the dopant loses memory of its initial state which results in a depletion of the number of absorbers coincident with the the excitation frequency. This is manifested by a dip or "hole" in the impurity's absorption spectrum, hence the term spectral hole burning. As long as the sample is kept cold (near 0 K), the spectral holes are persistent (transient hole burning via a population bottleneck is also possible). There are two processes that result in spectral holes. Photochemical hole burning, as the name implies, occurs in systems that undergo photochemistry, e.g., proton

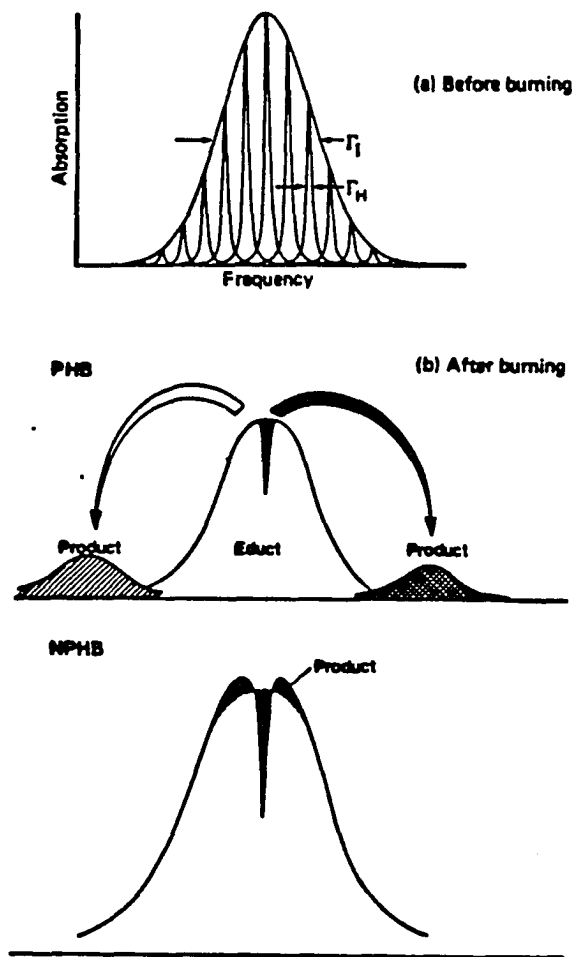


Figure 5. The inhomogeneously broadened absorption spectrum (a) of an impurity in a glass- Γ_h (homogeneous line width) $< 1 \text{ cm}^{-1}$; Γ_{inh} (inhomogeneous line width) \sim a few hundred cm^{-1} for organic molecules in glasses. The absorption profile after (b) photochemical hole burning and (c) nonphotochemical hole burning.

tautomerization of H₂-phthalocyanine during irradiation with a laser [33]. As shown in Fig. 5b the products from photochemical hole burning (PHB) typically absorb several hundred cm⁻¹ away from the spectral hole. Nonphotochemical hole burning is a result of host configuration changes that occur while the impurity is in its excited state. The host-impurity interaction changes are small so typically the anti-hole (product absorption) is displaced <100 cm⁻¹ from the spectral hole, Fig. 5c. Hayes and Small [34,35] proposed that the mechanism for nonphotochemical hole production is phonon assisted tunneling between the glassy states two level systems. Two level systems had already been proposed to explain other glassy state anomalous behavior [36,37].

The spectral linewidth of the hole is related to the time domain by the equation $T_2 = (\pi \Delta\nu_h)^{-1}$ where T_2 , the total dephasing time, is given by $1/T_2 = 1/2T_1 + 1/T_2^*$. T_1 processes are those that lead to depopulation of initially prepared excited states and include fluorescence, intersystem crossing, and internal conversion. When a system of molecules is irradiated with a coherent source, they begin to oscillate in phase with themselves and with the radiation field. When the coherent source is removed, the molecules, through their interactions with low energy lattice phonons, begin to lose phase coherence. This process is termed pure dephasing and has a characteristic lifetime T_2^* . T_1 processes occur even at 0 K whereas pure dephasing processes should cease at 0 K. Because of the frequency-time domain relation interesting glassy state properties, e.g. spectral diffusion and dephasing, can be probed with spectral hole burning. A large number of different impurities and host matrices have been shown to produce spectral holes. The science and application of hole burning has been extensively discussed [35,38-40]. Of particular interest here is spectral hole burning of biological pigments hosted in their natural proteins.

Phonons resulting from the displacement of the excited nuclear coordinates of the impurity, relative to its ground state, induce low energy lattice distortions. The strength of the coupling of the excited state potential to the lattice is measured by the Huang-Rhys factor defined as

$$S = \frac{1}{2} \Delta^2$$

where Δ is the displacement of the normal coordinates. The phonon transitions build on the "pure" zero-phonon transition and are reflected in the absorption profile as broad bands at higher energy, relative to the zero-phonon transition, by a mean phonon frequency (typically $10\text{-}50\text{ cm}^{-1}$). The relative intensities of the r-phonon process is given by the Poisson distribution $e^{-S} S^r / r!$ [41 and refs. therein] with S defined as above. For large electron-phonon coupling strengths, the phonon absorption will dominate the spectrum.

The absorption cross-section of the impurity at any particular frequency consist of the overlap of zero-phonon transitions, phonon transitions and vibronic transitions. Spectral hole burning can occur through any of these features. For example, if one chooses a burn frequency on the low energy side of the absorption profile it is possible to produce a zero-phonon hole coincident with the laser. At higher energies in the absorption profile, there is significant overlap of zero-phonon and phonon transitions. A zero-phonon hole coincident with the burn frequency and a pseudo-phonon sideband hole (pseudo-PSBH) to lower energy are produced by irradiation. The pseudo-PSBH is the convolution of zero-phonon transitions that have absorbed radiation through their phonon wings. The mean phonon frequency can be measured from the displacement of the pseudo-PSBH from the zero-phonon

hole. If the sample is irradiated in the congested vibronic regions, vibronic satellite hole structure can be burned into the origin bands. That is, excitation occurs through vibronic transitions and results in the depletion of the number of zero-phonon absorbers in the origin band. The displacement of the satellite holes from the burn frequency gives the excited state vibrational frequencies. By tuning the burn frequency, it is possible to determine all the Franck-Condon active modes.

A number of phenomena affect hole burning. Spectral diffusion and dephasing processes alter the zero-phonon linewidth. The extent to which these processes alter the observed linewidths is much debated [38,39,42-45]. It is an important limitation to the calculation of T_1 lifetimes. Spontaneous hole filling (SPHF) and laser induced hole filling (LIHF) also affect the hole burning. The mechanisms for these phenomena have been investigated for ionic dyes doped in organic glasses [46,47]. Spontaneous hole filling defines the time frame of the hole burning experiment, i.e., one would want to probe the hole before significant hole filling occurs. SPHF has not been observed in the pigment-protein complexes of PSI at 1.6 K.

Application of spectral hole burning to pigment-protein systems is a recent and exciting development. The only requirement is that the pigments absorb in a region accessible to lasers. Probing the primary events of photosynthesis, reaction center and antenna dynamics, with spectral hole burning is the subject of this dissertation.

EXPERIMENTAL METHODS

Samples

The Photosystem I particles with various P700 enrichment levels (actually, antenna chlorophyll depleted) are generously supplied to us by John Golbeck. The particles are prepared following the procedure of Mullet and coworkers [48] and Golbeck [49]. Fragmented thylakoid membranes of spinach chloroplast are obtained by homogenizing leaf spinach with a high speed blender in a buffered (pH 7.8) solution. The freed chloroplast are osmotically shocked, suspended in EDTA to remove loosely bound proteins, and sonicated to produce the fragmented thylakoid membranes. The thylakoid membranes are washed with a non-ionic detergent (Triton X-100) in a buffered solution to produce the "native" PSI-200 particle. Subsequent washing with Triton X-100 results in depletion of the Chl antenna proteins. The Chl to P700 ratio is assayed by photo-oxidizing P700. The extinction coefficient for P700 is $\epsilon_{700\text{nm}} = 64 \text{ mM}^{-1} \text{ cm}^{-1}$.

The particles, suspended in a buffered glycerol/water mixture (pH 8.0) containing 0.1% Triton X-100, are stored at 77 K until needed. The optical density of the samples was adjusted by dilution to the appropriate value with a buffered (pH 8.3) glycerol/water (70:30) solution containing 100 mM Tris [tris(hydroxymethyl) aminomethane] and 0.1% triton X-100. 1 mM ascorbic acid is added to pre-reduce P700.

The samples were held in the dark for a few minutes before being quickly cooled (< 10 minutes) to 4.2 K. This procedure is required to aid pre-reduction of P700. Subsequent exposure to light is held to a minimum.

Cryogenic Equipment

All liquid samples were placed in a 1 cm diameter polystyrene tube chosen because it minimized sample cracking at low temperatures. The sample tube is held in a brass container of local design which allowed for optical access of the sample. The samples were cooled to 4.2 K in a Janis Model 8-DT Super Vari-Temp liquid Helium cryostat. By pumping with an auxiliary vacuum pump it is possible to take helium past its lambda point (2.25 K) and achieve a temperature of 1.6 K. The sample temperature was monitored using a silicon diode thermometer (Lake Shore Cryogenic model DT-500K) calibrated over the range from 1.4 K to 300 K.

Experimental Apparatus

Figure 6 shows the configuration of the apparatus used for hole burning and subsequent reading. The laser system consist of a 5W argon ion laser (Coherent Innova 90-5) which was used to pump a single frequency passively stabilized ring dye laser (Coherent 699-21). A three plate birefringent filter provides wavelength selection. Narrow laser linewidths (0.002 cm^{-1}) are accomplished with two low finesse intra-cavity etalons having free spectral ranges of 10 GHz and 100 GHz which combined with the birefringent filter ($\sim 380 \text{ MHz}$) forces single longitudinal mode operation. The laser dyes used were DCM and LD688 (Exciton).

The output of the ring laser was monitored for single frequency operation by directing, by means of a beamsplitter, a portion of the laser beam to a confocal spectrum analyzer (Spectra-Physics model 470-40, FSR= 8 GHz). The output of the spectrum analyzer was displayed on an oscilloscope. The laser wavelength was determined by sending a portion of the beam to a 1/3 meter monochromator (McPherson model 218). Laser powers were set using a variable attenuator

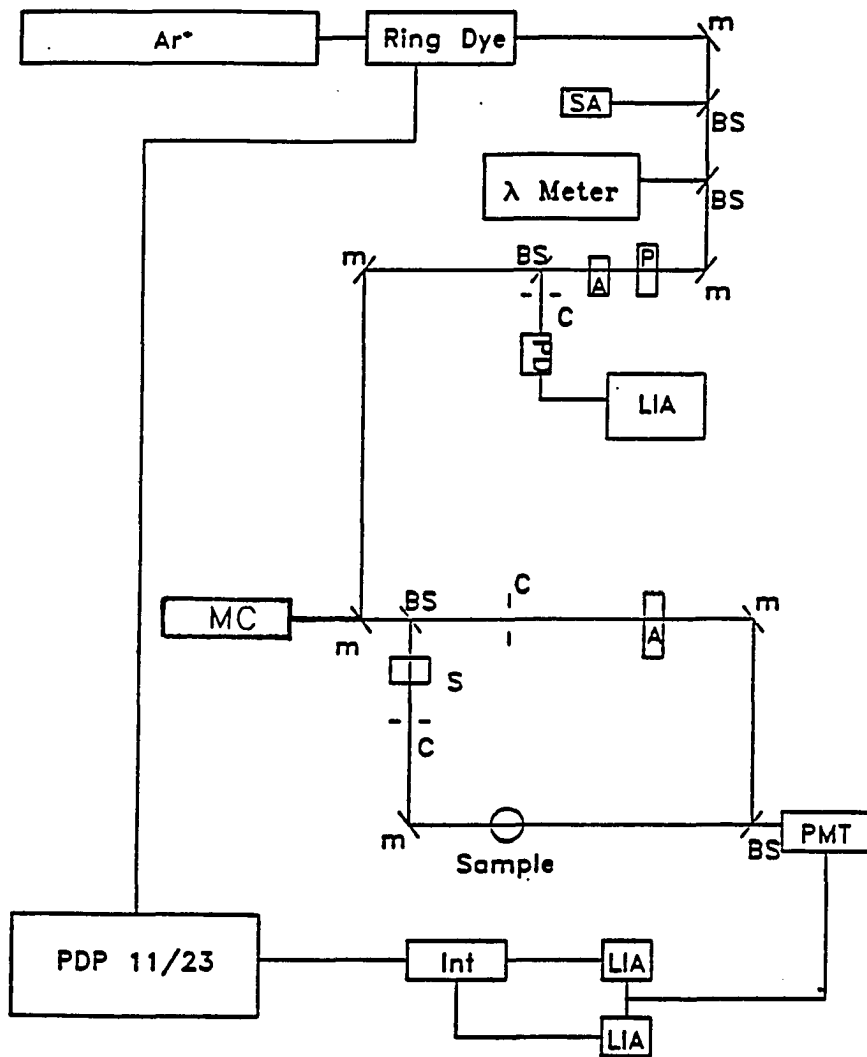


Figure 6. Experimental absorption/hole burning apparatus. Ar^+ -argon ion laser; M -mirror; BS -beamsplitter; SA -spectrum analyzer; λ meter wavemeter; P -polarizer; A -attenuator; C -chopper; PD -photodiode; LIA -lock-in amplifier; S -shutter; PMT -photomultiplier tube; INT integrator; MC - monochromator.

(Newport Corporation model 935-3) and neutral density filters. Part of the attenuated beam was extracted, modulated with a mechanical chopper (PAR model 125), and monitored for intensity with a photodiode detector (Molelectron 4P-141) and lock-in amplifier (PAR model 124 with a model 118 preamplifier). The laser beam was then directed by mirrors to a home built double beam spectrometer [50,51]. There are two sources available for scanning the holes. The ring dye laser can be scanned through 30 GHz (1 cm^{-1}) by an intra-cavity angle tuned brewster plate. Resolution is 0.002 cm^{-1} . Low resolution ($\sim 0.2 \text{ cm}^{-1}$) spectra were taken using light from a 500 W short-arc Xenon lamp (Canrad-Hanovia model 959C1980) dispersed by a 1.5 M monochromator (Jobin-Yvon HR1500). The monochromator has a linear dispersion of 0.19 nm/mm (2400 groves/mm grating). Either source could be utilized for hole scanning by retraction of a mirror. In either case, the ring dye laser is employed for burning.

The light incoming onto the double apparatus is split into a reference leg and a sample leg by a beamsplitter. Each leg contains identical optics. The reference leg intensity can be attenuated (Newport Corporation model 925B) to match optical losses on the sample leg caused by scattering from the cryostat and sample. Each leg is modulated at different frequencies with mechanical choppers (Laser Precision CTX-534). The beams are recombined and sent to a cooled photomultiplier tube (RCA C31034 in a PFR PR-1400-RF thermoelectrically cooled housing). The signal is then detected by two lock-in amplifiers (Ithaco model 97EO) referenced to the mechanical choppers. The output from the lock-in amplifiers is integrated (at multiples of 1/60 second) and digitized with an integrator/coupler (Ithaco model 385EO-2) and sent to a microcomputer (Digital Equipment Corporation Micro PDP-11/23+ with RT11 operating system) where it is converted into absorbance and

stored. The computer also drives the scanning of the monochromator and ring dye laser.

Stark Apparatus

The Stark cell was built from polystyrene. A round polystyrene tube was cut to provide a center section about 3 mm thick with parallel sides. Thin polystyrene sheets (0.0015 inches) onto which gold had been vapor deposited were attached to the parallel sides of the tube section with model cement (Testor). Electrical connection is made by means of small screws. The Stark cell is placed in a teflon holder with optical and electrical access and provides electrical insulation. The holder is attached to a sample rod and lowered into the cryostat. DC voltage is supplied by a high voltage supply (Sorenson 1030-20) and measured using a high voltage probe (Fluke 80F-15).

REFERENCES

1. Emerson, R.; Arnold, W. *J. Gen. Physiol.* 1932, 15, 391; *J. Gen Physiol.* 1932, 16, 191.
2. Staehelin, L. A. In Photosynthesis III: Photosynthetic Membranes and Light Harvesting Systems; Staehelin, L. A., Arntzen, C. J., Eds.; Springer-Verlag: Berlin, 19, p 1.
3. Golbeck, J. H. *Biochim. Biophys. Acta* 1987, 895, 167.
4. Seely, G. R. *J. Theor. Biology* 1973, 40, 173.
5. Glazer, A. N. *Annu. Rev. Biochem.* 1983, 52, 125.
6. Davis, R. C.; Ditson, S. L.; Fentiman, A. F.; Pearlstein, R. M. *J. Amer. Chem. Soc.* 1981, 103, 6823.
7. Maggoria, L. L.; Maggoria, G. M. *Photochem. Photobiol.* 1984, 39, 847.
8. Lien, S.; San Pietro, A. In An Inquiry into Biophotolysis of Water to Produce Hydrogen; a report sponsored by NSF under RANN Grant G140253, 1976.
9. Nuijjs, A. M.; van Gorkom, H. J.; Plijter, J. J.; Duysens, L. N. M. *Biochim. Biophys. Acta* 1986, 848, 167.
10. van Gorkom, H. J.; Nuijjs, A. M. In Primary Processes in Photobiology; Kobayashi, T., Ed.; Springer-Verlag: Berlin, 1987, p 61.
11. Klimov, V. V.; Klevanik, A. V.; Shuvalov, V. A.; Krasnovsky, A. *FEBS. Lett.* 1977, 82, 183.
12. van Gorkom, H. J. *Photosyn. Res.* 1985, 6, 97.
13. Wasielewski, M. R.; Johnson, D. G.; Seibert, M.; Govindjee *Proc. Natl. Acad. Sci. USA*, 1989, 86, 524.

14. Jankowiak, R. J.; Tang, D.; Small, G. J.; Seibert, M. J. *Phys. Chem.*, 1989, 93, 1649.
15. Owens, T. G.; Webb, S. P.; Mets, L.; Alberte, R. S.; Fleming, G. R. *Proc. Natl. Acad. Sci. USA* 1987, 84, 1532.
16. Wasielewski, M. R.; Fenton, J. M.; Govindjee *Photosyn. Res.* 1987, 17, 181.
17. Golbeck, J. H. *J. Membrane Sci.* 1987, 33, 151.
18. Rutherford, A. W.; Heathcote, P. *Photosyn. Res.* 1985, 6, 295.
19. Mathis, R.; Rutherford, A. W. In Photosynthesis; Ames, J., Ed.; Elsevier: Amsterdam, 1987, p 63.
20. Malkin, R. In The Light Reactions; Barber, J., Ed.; Elsevier: Amsterdam, 1987, p 495.
21. Malkin, R.; Ortiz, W.; Lam, E.; Bonnerjea, J. *Physiol. Veg.* 1985, 23, 619.
22. Ortiz, W.; Lam, E.; Ghiradi, M.; Malkin, R. *Biochim. Biophys. Acta* 1984, 766, 505.
23. Lam, E.; Ortiz, W.; Mayfield, S.; Malkin, R. *Plant Physiol.* 1984, 74, 650.
24. Haworth, P.; Watson, J. L.; Arntzen, C. J. *Biochim. Biophys. Acta* 1983, 724, 151.
25. Deisenhofer, J.; Epp, O.; Miki, K.; Huber, R.; Michel, H. *J. Mol. Biol.* 1984, 180, 385.
26. Deisenhofer, J.; Epp, O.; Miki, K.; Huber, R.; Michel, H. *Nature* 1985, 318, 618.
27. Michel, H.; Epp, O.; Deisenhofer, J. *EMBO J.* 1986, 5, 2445.
28. Michel, H.; Deisenhofer, J. *Chemica Scripta* 1987, 27B, 173.

29. Chang, C. -H.; Tiede, D.; Tang, J.; Smith, U.; Norris, J.; Schiffer, M. FEBS Lett. 1986, 205, 82.
30. Allen, J. P.; Feher, G.; Yeates, T. O.; Rees, D. C.; Deisenhofer, J.; Michel, H.; Huber, R. Proc. Natl. Acad. USA 1986, 83, 8589.
31. Ford, R. C.; Picot, D.; Garavito, P. M. EMBO J. 1987, 6, 1581.
32. Witt, I.; Witt, H. T.; Gerken, S.; Saenger, W.; Dekker, J. P.; Roegner, M. FEBS Lett. 1987, 221, 260.
33. Gorokhovski, A. A.; Kaarli, R. K.; Rebane, L. A. JETP Lett. 1974, 20, 216.
34. Hayes, J. M.; Small, G. J. Chem. Phys. 1978, 27, 151.
35. Small, G. J. In Spectroscopy and Excitation Dynamics of Condensed Molecular Systems; Agranovich, V. M., Hochstrasser, R. M., Eds.; North-Holland: Amsterdam, 1983, p 515.
36. Anderson, P. W.; Halperin, B. I.; Varma, C. M. Phil. Mag. 1972, 25, 1.
37. Phillips, W. A. J. Low Temp. Phys. 1972, 7, 351.
38. Jankowiak, R.; Small, G. J. Science 1987, 237, 618.
39. Persistent Spectral Hole Burning: Science and Application; Moerner, W. E., Ed.; Springer-Verlag: West Berlin, 1988.
40. Freidrich, J.; Haarer, D. Angew. Chem., Int. Ed. Engl. 1984, 23, 113.
41. Hayes, J. M.; Gillie, J. K.; Tang, D.; Small, G. J. Biochim. Biophys. Acta 1988, 932, 287.
42. Freidrich, J.; Haarer, D. In Optical Spectroscopy of Glasses; Zschokke, I., Ed.; Reidel: Dordrecht, Netherlands, 1986, p 149.
43. Optical Linewidths in Glasses, J. Lumin. 1987, 4&5, 1987.

44. van den Berg, R.; Visser, A.; Völker, S. *Chem. Phys. Lett.* 1988, 144, 105.
45. Berg, M.; Walsh, C. A.; Narasimhan, L. R.; Littau, K. A.; Fayer, M. D. *Chem. Phys. Lett.* 1987, 139, 66.
46. Fearey, B. L.; Carter, T. P.; Small, G. J. *Chem. Phys.* 1986, 101, 279.
47. Fearey, B. L.; Small, G. J. *Chem. Phys.* 1986, 101, 269.
48. Mullet, J. E.; Burke, J. J.; Arntzen, C. J. *Plant Physiol.* 1980, 65, 814.
49. Golbeck, J. H. *Methods in Enzymol.* 1980, 69, 129.
50. Carter, T. P. Ph. D. Dissertation, Iowa State University, 1986.
51. Fearey, B. L.; Carter, T. P.; Small, G. J. *J. Phys. Chem.* 1983, 87, 3590.

SECTION I.

PHOTOCHEMICAL HOLE BURNING OF P700

SECTION I. PHOTOCHEMICAL HOLE BURNING OF P700

INTRODUCTION

The determination of the structure of the reaction center (RC) of Rhodospseudomonas viridis [1-4] and subsequently Rhodobacter sphaeroides [5,6] has given new impetus to the debate concerning the description of the excited electronic states of the RC pigment complex. That is, the debate has turned from a discussion of which pigments comprise the RC and their arrangement to how the pigments interact to efficiently stabilize the electron in the charge transfer process [7-10].

The structure of the RC is shown in Fig. 1. It is comprised of a special pair bacteriochlorophyll dimer [P], two accessory bacteriochlorophylls [B], two bacteriopheophytins [H], a quinone, and a nonheme iron. The RC complex possesses an approximate C_2 symmetry with the two arms labeled L and M for light weight and medium weight protein structures. The center to center distances between pigments are given in Å. Upon excitation of the special pair (the primary electron donor [PED]), an electron is transported down the the L branch and is stabilized at the quinone [7-9]. This is the source of the transmembrane charge separation that drives photosynthesis.

Several remarkable photophysical features present themselves. The first important feature is that the absorption band of the PED is displaced to the red $\sim 2200 \text{ cm}^{-1}$ for Rps. viridis from the monomer absorption in solution [10]. A similar shift is observed for Rb. sphaeroides [7]. The cause of the shift is best associated with excitonic interactions and this led to the hypothesis of the special

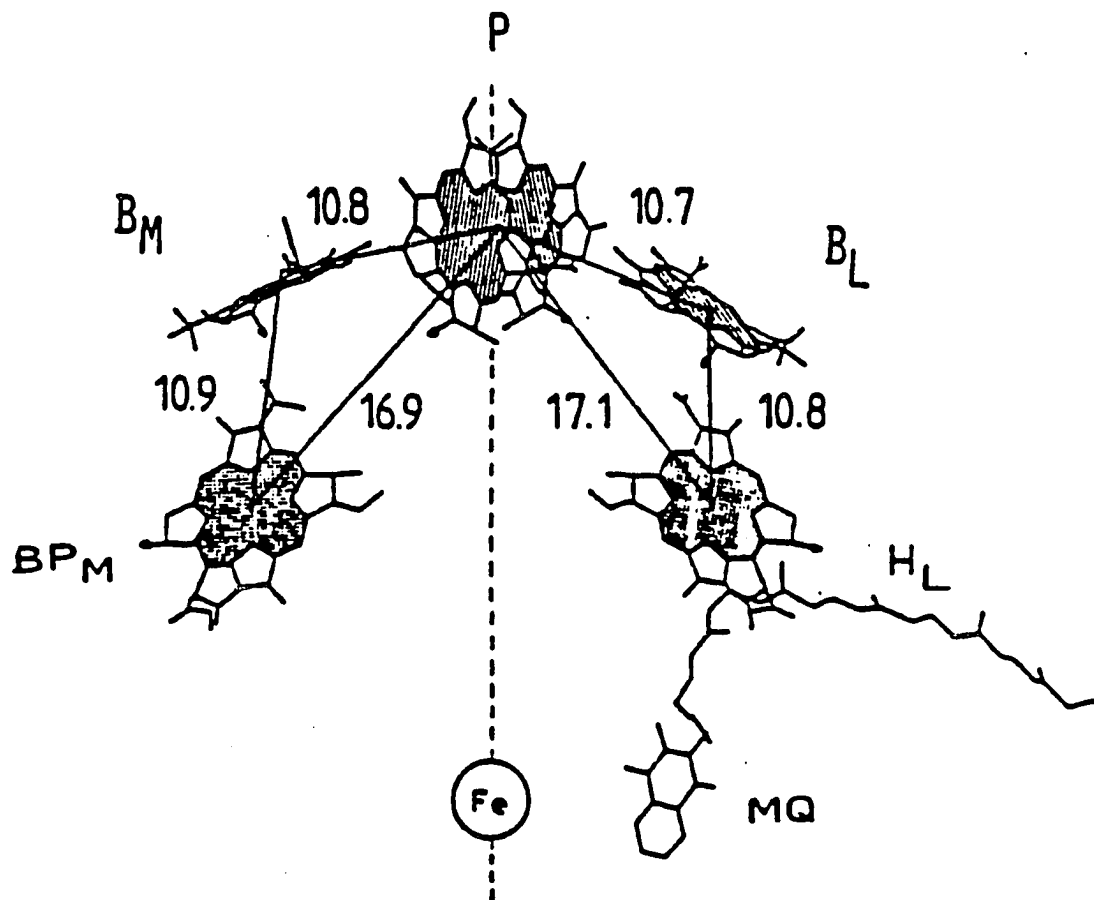


Figure 1. An overview of the structure of the reaction center of *Rhodospseudomonas viridis*. The center-to-center distances are given in Å. P - special bacteriochlorophyll dimer; B - accessory bacteriochlorophyll; H - bacteriopheophytin; MQ - menaquinone; Fe non-heme iron.

pair [11,12]. The pigment interactions are now believed to be more complicated and current models generally mix charge transfer characteristics into the exciton manifold [13] or extend the dipole interaction to include all the RC pigments [14-16].

A second interesting feature is the observation that the e^- transfer occurs only along the L branch of the RC [7-9]. Currently, research here is focused on the role of the RC proteins. Fortuitous placement of point charges from amino residues of the surrounding protein complex can alter the relative energetic positions of electronic states [4,8,17-19]. Protein vibrations may also be important in the events leading to stabilized charge separation [20-23].

A third feature is that the transfer of the e^- from the special pair to the BPh occurs in about 3 psec [24] at room temperature apparently without the involvement of the accessory BChl molecule [7,8]. By 1986, experiments monitoring the BChl and BPh absorption with a few psec resolution had confirmed, at least on this time scale, no involvement of the accessory BChl in the e^- transport process [26, 27 and refs. therein]. It is interesting from a dynamical viewpoint how an e^- could transfer over 17Å at such rates (the rate is generally thought to depend on $\exp(-2\alpha R)$ with $\alpha \sim 0.7 \text{ \AA}^{-1}$ and R the intermolecular distance [8,28]) without accessory BChl involvement.

Several proposals have been forwarded to address the role of the accessory BChl. The most straightforward proposal is that the time scale of the special pair \rightarrow BChl electron transfer is faster than the time resolution of the picosecond absorption experiments. In this case the charge separated state involving the BChl monomer is a real intermediate state in the e^- transfer. Recent experiments with 100 femtosecond time resolution did not find evidence for direct BChl participation in e^-

transfer [7,8,24,25]. A second proposal is that the e^- reaction occurs via a superexchange mechanism. In this case the state involving the BChl monomer is considered a virtual state and is not observed because it lies at an energy higher than P^* [9,29-33]. The description of the states (charge transfer character, excitonic character) and their relative energetic ordering is much debated [31,32].

Spectral hole burning is a frequency domain technique and as such circumvents the time domain problems of producing ultrafast light pulses (in the required wavelength range) and detecting ultrafast absorption changes. Using transient spectral hole burning, Boxer et al. [34,35] and Meech et al. [36,37] recorded the hole burned spectrum of the PED for Rb. sphaeroides and Rps. viridis. The holes produced were $\sim 400 \text{ cm}^{-1}$ broad which gives, if the hole is homogeneously broadened, an excitation depopulation lifetime of the initial excited state of ~ 25 fsec. There are, however, two important observations. The first is that the hole maximum is not necessarily coincident with the burn frequency, and secondly the hole position remains invariant (or slightly varying) to changes in the burn wavelength. Boxer et al. [34,35] suggested that the hole may be dominated by phonon bands that result from very large displacement of the PED excited state potential surface thereby suppressing a narrow zero-phonon line. One possible mechanism for the large displacement would be direct excitation of a charge transfer state with significant charge transfer character [35,37].

Hayes and coworkers [38,39] explored the effect a highly displaced excited state would have on the observed absorption and hole profile of the PED. The spectra were modeled in terms of an arbitrarily strong electron-phonon coupling. This approach is consistent with the displacement of the excited state in a charge transfer complex. The theory is fully developed in Paper II of this section. The

absorption and hole profiles are calculated using the electron-phonon coupling strength S , the phonon frequency and phonon linewidth, the homogeneous linewidth of the zero-phonon transition, and the inhomogeneous linewidth of the profile. The zero-phonon hole (ZPH) width corresponds to the e^- transfer rate for the special pair \rightarrow BPh process [40,41]. The temperature dependence of the absorption and fluorescence, and the Stokes shift (between absorption and fluorescence maximum) are used to verify the values of the parameters used to fit the profiles. It is found that the magnitude of the electron-phonon coupling combined with the inhomogeneous broadening causes the broad holes and apparent lack of sharp zero-phonon holes. That is, for large S , multiphonon transitions dominate the spectrum. The holewidths are not a manifestation of an ultrafast charge separation process. The theory presents a unified description of the absorption profile, the hole profile, and the wavelength behavior of the holes for the PED for Rps. viridis, Rb. sphaeroides, Photosystem I, and Photosystem II.

An alternate proposal to model the spectral features is suggested by Won and Friesner [42-44]. The WF theory includes a set of low frequency inter- and intramolecular vibrational modes strongly coupled into the excitonic manifold. Lattice phonons and inhomogeneous broadening are treated phenomenologically. The crucial theoretical conjecture is the resonant coupling of a charge transfer state to the vibrationally coupled excitonic state. Once the exchange coupling strength (J in WF's notation) is "turned on" the broad absorption and hole profile results from chaotic spreading of oscillator strength caused by a breakdown of the Born-Oppenheimer approximation. Coupling to the CT state suppresses the zero-phonon line. In this picture the PED profiles are homogeneously broadened. By setting the energy gap between the special pair excited state and the CT state to $\Delta=2000 \text{ cm}^{-1}$

(the internal CT state of the special pair is higher in energy than the excited state) and the coupling strength to $J=240\text{ cm}^{-1}$, WF successfully models the hole burning data of Boxer and coworkers [34,35] and Meech and coworkers [36,37].

Both theories (Hayes and coworkers and WF) share certain features, e.g., inhomogeneous broadening and linear-electron vibration coupling. However, weak electron-mode coupling (i.e., $S < 1$) is assumed in the WF model for all modes (low frequency monomer intramolecular and phonons). The ultra-fast chaotic electronic decay due to strong coupling with some type of close lying charge-transfer is eliminates sharp features in the hole spectra for the WF model. The ZPHs include the one coincident with ω_B and the vibronic satellite holes [45]. Based on the recently obtained data for the antenna Chl a and Chl b of PSI [46,47], however, one would not expect to observe sharp vibronic satellite holes of any significant intensity since the intramolecular vibronic Franck-Condon factors are very small (≤ 0.04) and no excited state vibrations with a frequency less than 260 cm^{-1} are active. The Franck-Condon factors for the low frequency intramolecular vibronic modes ($\leq 200\text{ cm}^{-1}$) of BChl a in a glass at 5 K are estimated at ≤ 0.02 based on fluorescence excitation spectra [48].

A critical test of the linear electron-phonon coupling theory is the observation of a narrow zero-phonon hole coincident with the laser frequency. Both models for calculating the hole profiles for PEDs allow for such an observation. However, the conditions for this observation ($J=0$ and/or $\Delta > 2000\text{ cm}^{-1}$) in the WF model causes the absorption profile to become highly structured, contrary to observation. Maslov et al. [49] had reported a sharp hole (no broad hole) coincident with the laser frequency in the PED absorption profile of the PSI reaction center from the bacteria Chlamydomonas reinhardtii. If this is taken as evidence to support the linear

electron-phonon coupling model, it suggests that the excited state is radically different for green photosynthetic systems. The dynamics of charge separation and stabilization would be different for green and purple photosynthetic systems.

Paper I of this section reports spectral hole burning studies of the PSI reaction center complex P700 obtained from spinach chloroplasts. A persistent hole burned spectrum is reported that is comprised of both a broad (350 cm^{-1}) hole and a narrow zero-phonon hole. The hole shapes are modeled using the linear electron-phonon coupling theory. Paper II outlines the linear electron-phonon theory which is shown to model the absorption profiles, hole profiles, and the temperature dependent line broadening data for the PED of purple photosynthetic bacteria and the hole profiles of PHB and NPHB experiments performed on the antenna and P700 complex of PSI. Chemical bleaching and white light bleaching of P700 followed by laser irradiation of the PED produced only narrow hole coincident with the laser frequency. Thus, the possibility exists that the narrow hole is not associated with P700 that is photoactive at liquid helium temperatures. Finally, new results of spectral hole burning on P700 are presented which show production of only a broad hole. The theory of Hayes and coworkers is used to fit the profiles.

**PAPER I. PERSISTENT HOLE BURNING OF THE PRIMARY DONOR STATE
OF PHOTOSYSTEM I: STRONG LINEAR ELECTRON-PHONON COUPLING**

**Persistent Hole Burning of the Primary Donor State
of Photosystem I: Strong Linear Electron-Phonon
Coupling**

**J. K. Gillie, B. L. Fearey, J. M. Hayes, G. J. Small
and J. H. Golbeck**

Chemical Physics Letters 1987, 134, 316.

INTRODUCTION

An adequate understanding of photochemical events in photosynthetic reaction centers (RC) requires, in part, knowledge of the RC structure and an accurate description for the electronically excited states of the RC pigment system. With the recent determination of the structures for Rps. viridis [1] and Rh. sphaeroides [2], theoretical calculations of their excited state structure have reached a more sophisticated level [3,4]. The calculations of Parson et al. [4] indicate that the primary donor state, P960, associated with the special bacteriochlorophyll bpair (BC_p) of Rps. viridis has significant charge-transfer (CT) character, arising from mixing of the lowest neutral excitonic state of BC_p with intra-dimer CT states. However, the effect of electron-phonon coupling on the familiar excitonic coupling models has not been explored.

Recently [5] we have suggested that the electron-phonon (lattice) coupling associated with P960 and P870 of Rb. sphaeroides is very strong, rivaling that observed for 100% CT states of π -molecular donor-acceptor complexes [6]. The line of reasoning used is based on a theory for photochemical hole burning (PHB) valid for arbitrarily strong linear electron-phonon coupling [5]. This coupling defines the extent to which the lattice surrounding the BC_p and the dimer itself change their equilibrium configuration upon excitation of the primary donor state. Using the analysis of T-dependent absorption and fluorescence data given by Scherer et al. [7] as a guide, the theory was used to account for the PHB results of Boxer et al. [8,9] on P870 and P960 and of Meech et al. [10] on P870 [5]. Time domain studies had previously shown that electron transfer from the special pair to a bacteriopheophytin occurs in about 2 and 5 psec for Rb. sphaeroides and Rps.

viridis, respectively, at cryogenic temperatures [11,12]. These decays correspond to homogeneous line broadenings of 2.5 and 1 cm^{-1} . By contrast, the PHB experiments yielded holewidths at $T \sim 1.5$ K equal to $\sim 400 \text{ cm}^{-1}$, a significant fraction of the absorption linewidths for P870 and P960. That is, no sharp zero-phonon holes are observed and thus, the question of whether or not the holewidths represent homogeneous broadening became important. Meech et al. [10] interpreted the holewidth of P870 in terms of an ultrafast (25 fsec) dynamical charge separation process within the special pair following preparation (excitation) of the neutral pair excitonic state. This charge separation precedes electron transfer from BC_p to the bacteriopheophytin. This interpretation was also considered by Boxer et al. [8,9], in addition to an inhomogeneous broadening mechanism based on strong electron-phonon coupling. The theoretical calculations of ref. [5] establish that the latter interpretation is entirely plausible. For P870, the Huang-Rhys factor (S) determined is ~ 8 and the average frequency for the Franck-Condon active phonons is $\sim 30 \text{ cm}^{-1}$. Availability of more accurate absorption and fluorescence thermal broadening data for P870 and theoretical refinements may lead to modest changes in these numbers.

Equally intriguing are the earlier PHB results of Maslov et al. [13] on P700 of intact cells of a mutant strain of Chlamydomonas reinhardtii. By contrast, only a sharp zero-phonon hole (full width $\sim 1.2 \text{ cm}^{-1}$, uncorrected for monochromator resolution) coincident with the laser burn wavelength, λ_B , was observed at $T = 4.2$ K. An obvious question is whether the apparent very different PHB behavior for the primary donor state P700 means that its electronic structure is markedly different from those of P870 and P960. Such might be expected if, for example, P700 is a monomer rather than a dimer, a point of continuing controversy [14].

RESULTS AND DISCUSSION

These questions and others are addressed here where we report some of our results from PHB experiments on P700 of enriched (~35:1; Chl a:P700) Photosystem I particles from spinach chloroplast. The particles were isolated following the procedure of Golbeck [15] and dissolved in a glycerol:water solvent (glass forming). The hole burning apparatus has been described previously [16]. Briefly, a computer-controlled double beam spectrophotometer operating with a resolution of 0.20 cm^{-1} was used for hole reading. An excimer-pumped dye laser with a linewidth of 0.04 cm^{-1} was used for hole burning. Burn intensities ranging between 1.0 and $100 \mu\text{W}/\text{cm}^2$ were employed.

The absorption spectrum of the Photosystem I particles is shown in Fig. 1 for the samples used to obtain the PHB spectrum of Fig. 3. In Fig. 1, P700 appears as a low E shoulder riding on the Chl a absorption centered at 675 nm. Thus far, persistent sharp zero-phonon holes for λ_{B} ranging from 700 to 720 nm have been observed. Initially, we were puzzled by the fact that the saturated (maximum) hole depths represented only a 3-5% OD change depending on λ_{B} . The mechanism which leads to stable or persistent holes is irreversible charge separation between P700 and the terminal electron acceptors $F_{\text{a}}/F_{\text{B}}$ which occurs at helium temperature [17]. However, this process is known to lead to about 70% of P700 being photobleached [18]. Thus if only zero-phonon PHB occurs, one would expect a comparable OD change for the hole. The OD changes observed by Maslov et al. [13] for Ch. reinhardtii appear to be comparable to ours. Resolution of the above puzzle emerges from extended read scans. Fig. 2 shows one such scan following a burn at $\lambda_{\text{B}}=710.8 \text{ nm}$. The shallow zero-phonon hole in the lower trace is indicated

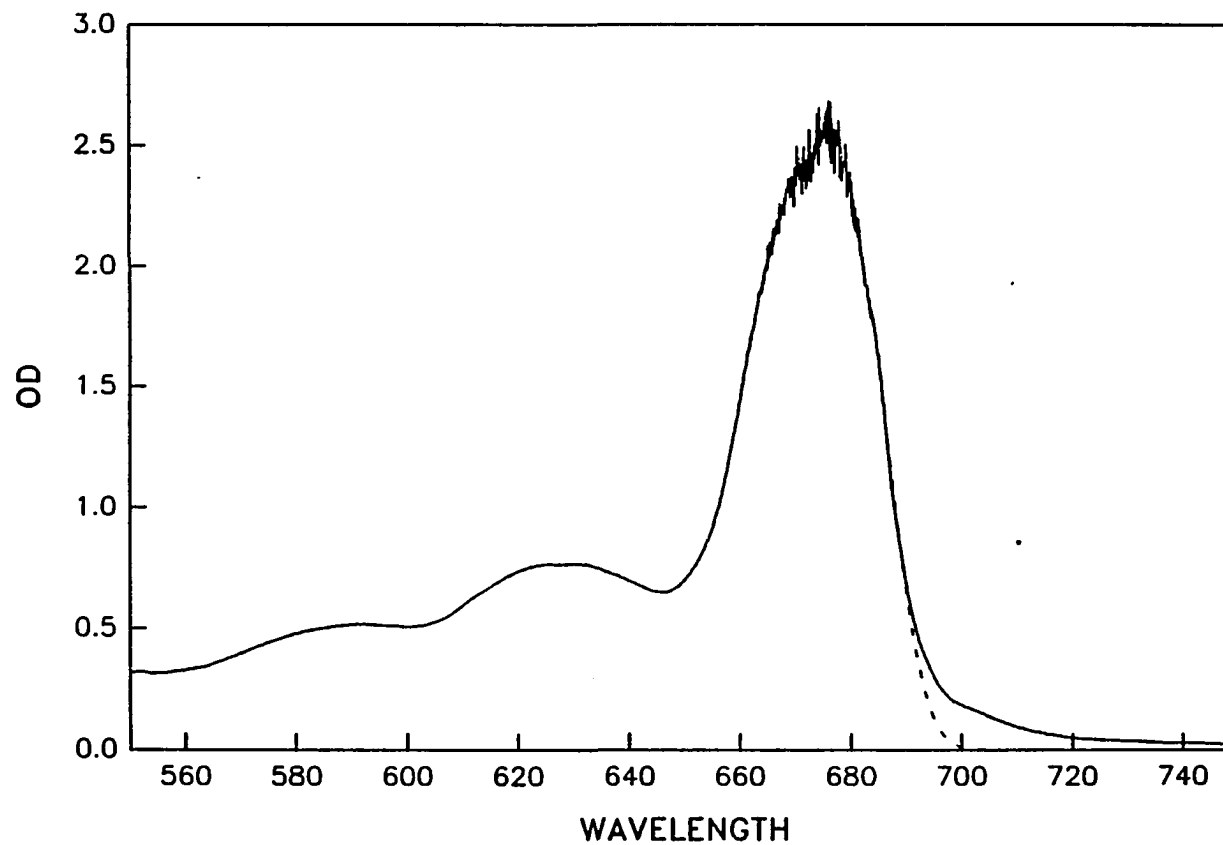


Figure 1. Absorption spectrum of enriched Photosystem I particles in a glycerol/water glass at 1.6 K. The dashed line is a calculation of the extent of overlap of the absorption peaked at 675 nm with the P700 absorption based on a Gaussian fit to the low energy side of the 675 nm band.

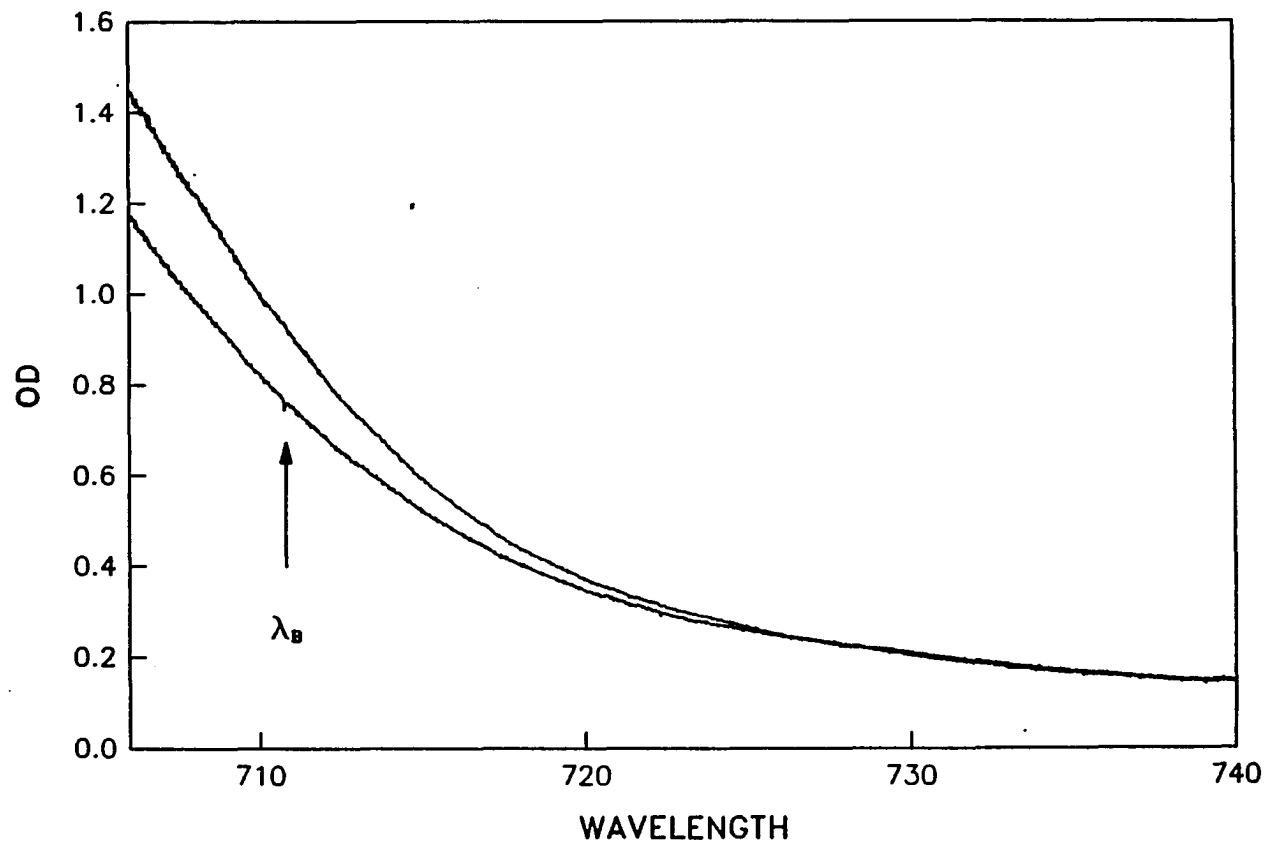


Figure 2. A portion of the absorption spectra of enriched Photosystem I particles before (top) and after (bottom) laser excitation at 710.8 nm. The holes were burnt for 30 min with $\sim 100 \mu\text{W}/\text{cm}^2$ at 1.6 K.

by the λ_B arrow. The upper trace is the absorption prior to the burn. Fig. 2 suggests that hole-burned spectrum consists of a sharp hole superimposed on a very broad hole and, consequently, that the P700 hole spectrum may indeed bear a close relationship to those of P870 and P960 (a broad hole for Ch. reinhardii was not reported by Maslov et al. [13]). We now pursue this line of thought further. Fig. 3 presents a ΔOD spectrum that is unique in the annals of hole burning. It results from a burn at $\lambda_b=700.0$ nm. (The inset spectrum will be addressed later.) The zero-phonon hole (indicated by the λ_B arrow) is just discernible and was positively identified by slower, less extended scans. Notice that it is superimposed on a broad hole possessing a width of ~ 300 cm^{-1} . The absorption increase at 688 nm is due, in part at least, to electrochromic shifts of surrounding chlorophylls resulting from charge separation [18,19].

We now give a brief account of our theory and apply it to Fig. 3. A detailed account is forthcoming [20]. For the development of a theory of PHB valid for arbitrarily strong linear electron-phonon coupling it is first necessary to derive the single site absorption profile. Our approach is based on a time correlation function method [21] and employs the Condon approximation. Defining ν as the single site zero-phonon transition frequency and ω_m as the maximum frequency of the one-phonon absorption profile (relative to ν), the single site absorption profile takes the form

$$L(\lambda) = e^{-S} I_0(\lambda - \nu) + \sum_{r=1}^{\infty} \frac{S^r e^{-S}}{r!} I_r(\lambda - \nu - r\omega_m) \quad (1)$$

in the $T \rightarrow 0$ K limit of interest here. The values of $r=0,1,2,\dots$ correspond to zero-, one-, etc., phonon transitions and S is the Huang-Rhys factor. To a reasonable

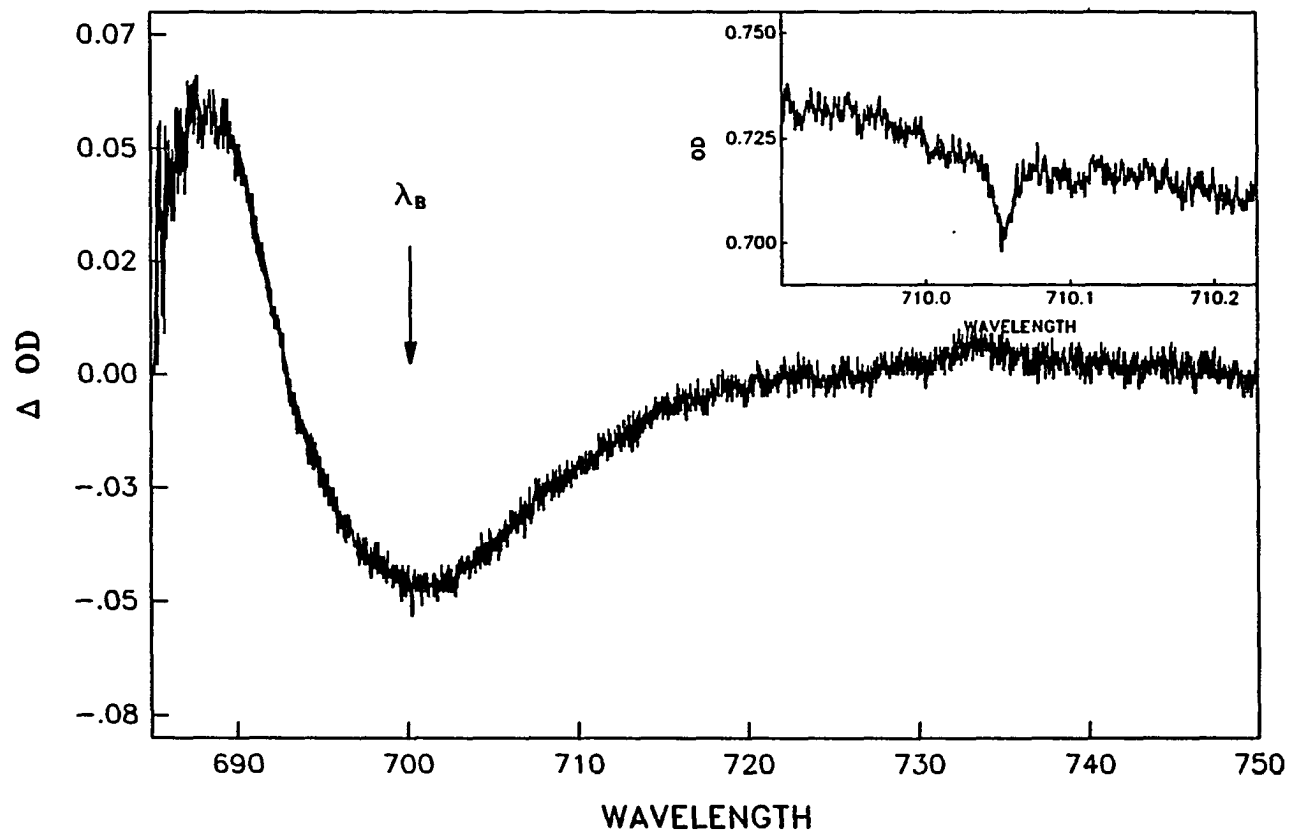


Figure 3. Difference absorption spectrum of enriched Photosystem I particles before and after laser excitation at 700.1 nm. Excitation was for 10 min with $100 \mu\text{W}/\text{cm}^2$. The inset shows a high resolution scan about the excitation wavelength for a sample burnt for 10 minutes at 710.06 nm with $1.0 \mu\text{W}/\text{cm}^2$. For both spectra the sample was 1.6 K.

accuracy, $2S\omega_m$ is the familiar Stokes shift. The r -phonon profile is the result of convolving the one-phonon profile r times with itself. If the one-phonon profile is taken to be a Gaussian or Lorentzian with width Γ , the r -phonon profile has a width of $r^{1/2}\Gamma$ or $r\Gamma$, respectively, and is centered at $r\omega_m$. In order to present an expression for the hole profile in a closed and physically transparent form, we will utilize Lorentzians for I_r ($r \geq 1$) with a width given by $r^{1/2}\Gamma$. The important features of our calculations will not be affected by utilization of more realistic lineshapes, e.g. asymmetric Gaussians. For the zero-phonon line (ZPL), I_0 can be a Lorentzian with a linewidth γ . We note that Eqn. 1 is valid for coupling to either a "sea" of delocalized phonons or a single pseudolocalized phonon.

The approach taken to derive the hole lineshape function with Eqn. 1 is, with suitable modification for strong electron-phonon coupling, that of Friedrich et al. [22]. We present only the result in the short burn time limit [22] for which our data are applicable:

$$\begin{aligned}
A_0(\Lambda) - A_r(\Lambda) = & \sum_{r,r'=0}^{\infty} \frac{S^r e^{-S}}{r!} \frac{S^{r'} e^{-S}}{r'!} \\
& \times \left(\frac{\Gamma_{inh} + \Gamma_r}{(\Lambda - \nu_m - r\omega_m)^2 + [(\Gamma_{inh} + \Gamma_r)/2]^2} \frac{\Gamma_r + \Gamma_{r'}}{[\Lambda - \omega_B + \omega_m(r'-r)]^2 + [(\Gamma_r + \Gamma_{r'})/2]^2} \right. \\
& + \frac{\Gamma_{inh} + \Gamma_{r'}}{(\omega_B - \nu_m - r'\omega_m)^2 + [(\Gamma_{inh} + \Gamma_{r'})/2]^2} \frac{\Gamma_r + \Gamma_{r'}}{[\Lambda - \omega_B + \omega_m(r'-r)]^2 + [(\Gamma_r + \Gamma_{r'})/2]^2} \\
& \left. + \frac{\Gamma_{inh} + \Gamma_{r'}}{(\omega_B - \nu_m - r'\omega_m)^2 + [(\Gamma_{inh} + \Gamma_{r'})/2]^2} \frac{\Gamma_{inh} + \Gamma_r}{(\Lambda - \nu_m - r\omega_m)^2 + [(\Gamma_{inh} + \Gamma_r)/2]^2} \right), \quad (2)
\end{aligned}$$

the desired result. We have defined $\Gamma_r \equiv \gamma$, for $r=0$. For $r \geq 1$, $\Gamma_r \equiv r^{1/2}\Gamma$. The width Γ_{inh} is that of the site excitation energy distribution function (SDF) determined by disorder. The SDF has a maximum at the frequency ν_m . The terms A_0 and A_t represent the absorption spectrum prior to and after the burn, respectively.

Considering the complexity of the problem, Eqn. 2 is gratifyingly simple as well as physically transparent [5].

The value of S for P700 can be obtained directly from our PHB spectra since e^S is the ratio of the areas for the zero-phonon hole and the broad hole [20]. From a high resolution scan of the zero-phonon hole and after correcting the high energy side of the broad hole for distortion due to the increase in absorption at 688 nm, we obtain $S \sim 7$. From Eqn. 1, the weighting factor for the r -phonon process is $P_r = e^{-S} S^r / r!$. With $S \sim 7$, it is clear that the zero-phonon transition is highly Franck-Condon forbidden. In fitting Eqn. 2 to the main spectrum of Fig. 3, values of $\gamma = 0.06 \text{ cm}^{-1}$ (vide infra) and $\Gamma_{inh} = 300 \text{ cm}^{-1}$ were used. The latter is judged to be a physically reasonable value based on our fit to the 675 nm absorption band using a convolution of several Gaussians with widths of $\sim 300 \text{ cm}^{-1}$. Chlorophyll monomer is a significant contributor to the 675 nm band. In addition, a value of 300 cm^{-1} is consistent with low T spectra of the Q_y transition of chlorophylls in glasses. With S , γ , and Γ_{inh} fixed, only ω_m and the width of the one-phonon absorption profile, Γ , remain to be specified. They were varied and acceptable fits to Fig. 3 could only be obtained for low values of ω_m . The calculated hole spectrum of Fig. 4 was obtained for $\omega_m = 30 \text{ cm}^{-1}$ and $\Gamma = 30 \text{ cm}^{-1}$. The latter is reasonable based on one-phonon sidebands in fluorescence line narrowed spectra of many impurity/glass systems. The ω_m value corresponds to excited state phonon modes. If it is assumed that it is the same for the ground state, the Stokes shift ($\sim 2S\omega_m$) is 420 cm^{-1} . Unfortunately

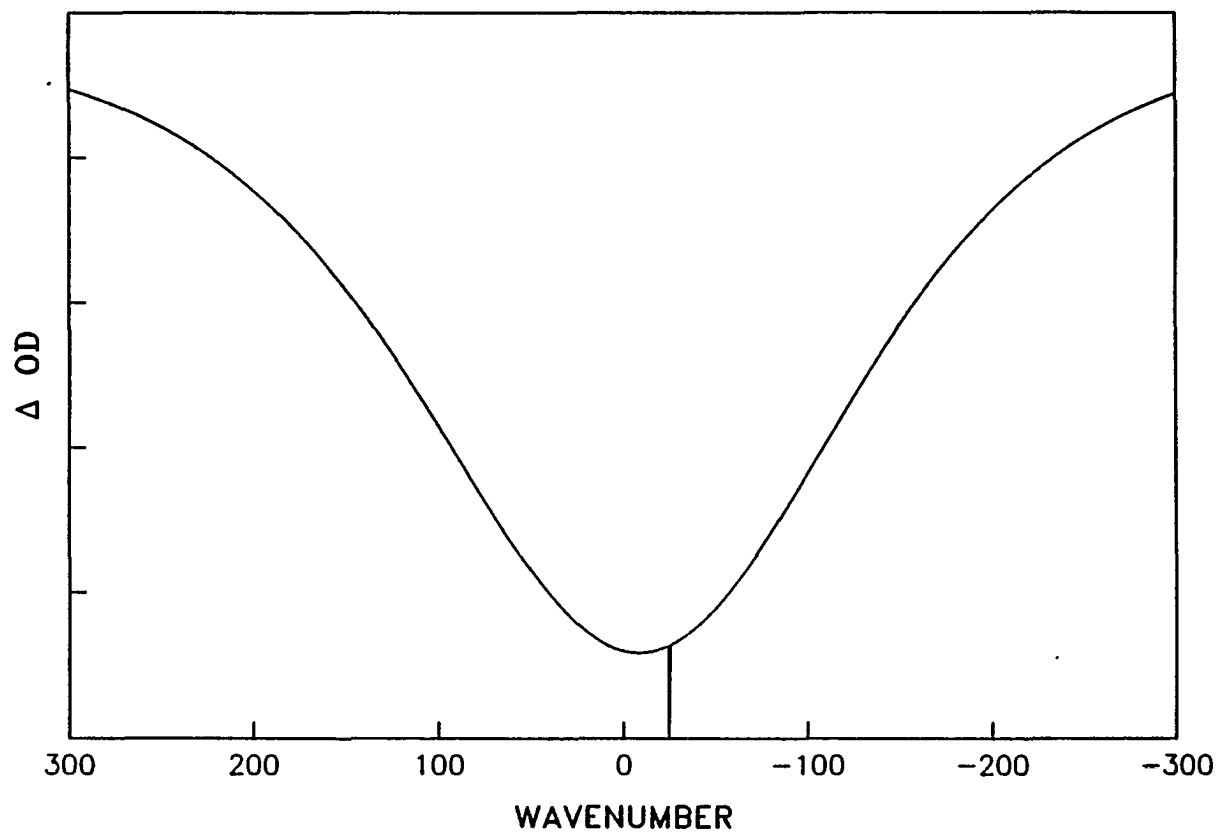


Figure 4. Computed hole spectra for $S = 7$, $\omega_m = 30.$, $\gamma = 0.06$, $\Gamma = 30.$, and $\Gamma_{inh} = 300$. The hole burnt at $\omega_B = 25 \text{ cm}^{-1}$ relative to the peak of the site distribution function at 0. The peak of the inhomogeneous absorption band was found to be $+175 \text{ cm}^{-1}$ from the peak of the SDF.

a reliable experimental value is not available. For P870 and P960 of Rb. sphaeroides and Rps. viridis, the Stokes shift is $\sim 500 \text{ cm}^{-1}$ [5].

The calculation, Fig. 4, succeeds not only in reproducing the shape of the PHB spectrum but also in accounting for the displacement between λ_B and the maximum of the broad hole which varies as λ_B is tuned. Indeed, from the data of Fig. 2, $\lambda_B \sim 700 \text{ nm}$ was chosen as the wavelength at which the hole maximum- λ_B displacement would be close to zero. The accuracy of this choice is verified in Fig. 3. The calculated broad hole maximum for Fig. 2 is close to that shown in Fig. 2 (it could not be measured due to the high OD of the sample used for Fig. 2). Our calculations show [23] that ω_m and Γ cannot be varied too much from the above values. It is possible that ω_m could approach $\sim 40 \text{ cm}^{-1}$. Values much higher than this do not provide a good fit to Fig. 3. Furthermore, our calculations do not exclude the possibility that higher frequency modes ($\sim 120 \text{ cm}^{-1}$ due, for example, to out-of-plane intramolecular deformation of Chl a) are not active provided their $S \lesssim 1$. The key point is that the hole burned spectrum (and low T absorption spectrum) is dominated by low frequency "phonons" characterized by strong coupling.

We note that if the lifetimes of P870 and P960 were as long as 90 psec (for P700 and corresponding to $\gamma=0.06 \text{ cm}^{-1}$), zero-phonon holes would be observable for $S \sim 8$ and $\omega_m \sim 30 \text{ cm}^{-1}$. That is, the absence of zero-phonon holes for P870 and P960 may be due more to lifetime shortening (zero-phonon hole broadening) than slight differences in linear electron-phonon coupling strength relative to P700. Thus, we conclude that P700, P870, P960 are all characterized by the very strong coupling expected only from a state with significant CT character. As we can conceive of no mechanism by which a Chl monomer can support such character, we

suggest that P700 must be a dimer. Indeed, Chl monomers are known to exhibit weak electron-phonon coupling [24-27].

Referring to Fig. 3, the inset spectrum shows the narrowest P700 zero-phonon hole profile measured at 1.6 K for λ_B in a region where Chl a monomer is negligible. The burn intensity used was $\sim 1.2 \mu\text{W}/\text{cm}^2$. Increasing the burn intensity by a factor of approximately ten did not broaden the hole. The holewidth is 0.29 cm^{-1} which, when corrected for the monochromator resolution, yields a value of $\sim 0.12 \text{ cm}^{-1}$. Within experimental uncertainty ($\pm 0.02 \text{ cm}^{-1}$), the value obtained for a burn temperature of 3.2 K is the same. Thus, it appears that pure dephasing and spectral diffusion (both T-dependent processes [28]) do not contribute significantly to the holewidth at 1.6 K. Since the homogeneous holewidth is twice the homogeneous linewidth [22], we calculate a T_1 lifetime for P700 of ~ 90 psec at 1.6 K. This is a factor of about three [29-31] and six [32] times longer than those determined by picosecond studies at room temperature. A lengthening by 2-3 with reduction in temperature is observed for P870 and P960 [11,12]. It should be noted that significant thermal broadening of the P700 holes occurs for $T_B \gtrsim 5$ K.

CONCLUSIONS

In summary, the present results for P700 and those for P870 [5] and P960 [20] establish that these primary donor states share common features. Their very large Huang-Rhys factors are consistent with the findings of Parson et al. [4]. That is, significant CT character leads to a large permanent excited state dipole moment which, in turn, gives rise to strong linear electron-phonon coupling [6]. A dimer structure for P700 is indicated. In terms of the low T absorption spectrum of a single primary donor site, the values of the Huang-Rhys factor obtained mean that a long phonon progression with $\omega_m \sim 30 \text{ cm}^{-1}$ must build on a highly Franck-Condon forbidden zero-phonon origin transition. A number of questions emerge from our findings that the electron-phonon coupling is very strong and that the primary donor state is subject to significant inhomogeneous line broadening. The former is comparable to the special pair exciton resonance interaction of several hundred cm^{-1} [3] and, thus, its neglect [3,4] in the calculation of excitonic structure may not be justified [33]. Site inhomogeneous line broadenings of $300\text{-}400 \text{ cm}^{-1}$ suggest that the two monomers within a given pair may be energetically inequivalent by a comparable amount. How would this inequivalence together with the electron-phonon coupling and proposed CT character of the primary donor state affect the familiar excitonic coupling schemes? And finally what, if any, role do the phonons associated with the strong electron-phonon coupling have in energy transfer from the antenna system to the primary donor state or electron transfer from the donor state to the primary acceptor?

REFERENCES

1. Deisenhofer, J.; Epp, O.; Miki, K.; Huber, R.; Michel, H. *Nature* 1985, 318, 618.
2. Chang, C. H.; Schiffer, M.; Tiede, D. M.; Smith, U.; Norris, J. *J. Mol. Biol.* 1985, 186, 201.
3. Zinth, W.; Knapp, E. W.; Fischer, S. F.; Kaiser, W.; Deisenhofer, J.; Michel, H. *Chem. Phys. Lett.* 1985, 119, 1.
4. Parson, W. W.; Scherz, A.; Warshel, A. In Antennas and Reaction Centers of Photosynthetic Bacteria; Michel-Beyerle, M. E., Ed.; Springer-Verlag: Berlin, 1985, p 122.
5. Hayes, J. M.; Small, G. J. *J. Phys. Chem.* 1986, 90, 4928.
6. Haarer, D.; Philpott, M. R. In Spectroscopy and Excitation Dynamics of Condensed Molecular Systems; Agranovich, V. M., Hochstrasser, R. M., Eds.; North-Holland: Amsterdam, 1983, p 27.
7. Scherer, P. O. J.; Fischer, S. F.; Hörber, J. K. H.; Michel-Beyerle, M. E. In Antennas and Reaction Centers of Photosynthetic Bacteria; Michel-Beyerle, M. E., Ed.; Springer-Verlag: Berlin, 1985, p 122.
8. Boxer, S. G.; Lockhart, D. J.; Middendorf, T. R. *Chem. Phys. Lett.* 1986, 123, 476.
9. Boxer, S. G.; Middendorf, T. R.; Lockhart, D. J. *FEBS Lett.* 1985, 200, 287.
10. Meech, S. R.; Hoff, A. J.; Wiersma, D. A. *Chem. Phys. Lett.* 1985, 121, 287.
11. Parson, W. W.; Woodbury, N. W. T.; Becker, M.; Kirmaier, C.; Holten, D. In Antennas and Reaction Centers of Photosynthetic Bacteria; Michel-Beyerle, M. E., Ed.; Springer-Verlag: Berlin, 1985, p 278.

12. Holten, D.; Windsor, M.W.; Parson, W. W.; Thorber, J. P. *Biochim. Biophys. Acta* 1978, 501, 112.
13. Maslov, V. G.; Chunaev, A. S.; Tugarinov, V. V. *Mol. Biol.* 1981, 15, 788.
14. Rutherford, A. W.; Heathcote, P. *Photosynth. Res.* 1985, 6, 295, and references therein.
15. Golbeck, J. H. In Methods in Enzymology; San Pietro, A., Ed.; Academic: New York, 1980, Vol. 69, p 129.
16. Fearey, B. L.; Carter, T. P.; Small, G. J. *J. Phys. Chem.* 1983, 87, 3590.
17. Bearden, A. J.; Malkin, R. *Biochim. Biophys. Acta* 1972, 283, 456.
18. Sétif, P.; Mathis, P.; Vänngård, T. *Biochim. Biophys. Acta* 1984, 767, 404.
19. Schaffernicht, H.; Junge, W. *Photochem. Photobiol.* 1981, 34, 223.
20. Hayes, J. M.; Gillie, J. K.; Tang, D.; Small, G. J. *Biochim. Biophys. Acta* 1988, 932, 287.
21. Pryce, H. M. L. In Phonons in Perfect Lattices with Point Defects; Stevenson, R. W. H. Ed.; Oliver and Boyd: London, 1965, p 403.
22. Friedrich, J.; Swalen, J. D.; Haarer, D. *J. Chem. Phys.* 1980, 73, 705.
23. Hayes, J. M.; Gillie, J. K.; Tang, D.; Small, G. J. *Biochim. Biophys. Acta* 1988, 932, 287.
24. Völker, S.; Mcfarlane, R. M.; van der Waals, J. H. *Chem. Phys. Lett.* 1978, 53, 8.
25. Avarmaa, R.; Muring, K.; Suisalu, A. *Chem. Phys. Lett.* 1981, 7, 88.
26. Rebane, K. K.; Avarmaa, R. A. *Chem. Phys.* 1982, 68, 191.
27. Carter, T. P.; Small, G. J. *Chem. Phys. Lett.* 1985, 120, 178.

28. Hayes, J. M.; Jankowiak, R.; Small, G. J. In Persistent Spectral Hole Burning: Science and Application; Moerner, W. E., Ed.; Springer-Verlag: West Berlin, 1988, p 153.
29. Shuvalov, V. A.; Klevanik, A. V.; Kryulov A. V.; Ke, B. FEBS Lett. 1979, 107, 313.
30. Shuvalov, V. A.; Ke, B.; Dolan, E. FEBS Lett. 1979, 100, 5.
31. Shuvalov, V. A.; Nuijjs, A. M.; van Gorkum, H. J.; Smit, H. W. J.; Duysens, L. N. M. Biochim. Biophys. Acta 1986, 850, 319.
32. Wasielewski, M. R.; Fenton, J.; Govindjee Photosynth. Res. 1987, 12, 181.
33. Small, G. J. In Excited States; Lim, E. C., Ed.; Academic: New York, 1982, and references therein.

**PAPER II. THEORY FOR SPECTRAL HOLE BURNING OF THE PRIMARY
DONOR STATE OF PHOTOSYNTHETIC REACTION CENTERS**

**Theory for Spectral Hole Burning of the Primary
Donor State of Photosynthetic Reaction Centers**

J. K. Gillie, J. M. Hayes, D. Tang, G. J. Small

Biochimica et Biophysica Acta 1988, 932, 287

INTRODUCTION

In attempts to understand electronic excitation transport and electron transfer in photosynthetic units a variety of spectroscopic techniques have been utilized. Most recently, frequency domain spectral hole burning [1-7], which complements ultra-fast time-domain techniques, has been applied to the primary electron donor state of photosystem I [8,9] and the bacterial systems Rhodobactersphaeroides [10,11] and Rhodospseudomonas viridis [12,13]. In addition, hole burning has been reported for the core antenna complex (C670) of PSI [14]. Irrespective of whether the hole-burning mechanism is photochemical [5] (as is the case for the primary electron donor state) or nonphotochemical [4,7] (as is the case for the core antenna complex C670 of Photosystem I [14]), the data relate to several important questions. Included are the intramolecular vibronic activity in the pigment absorption, pigment site inhomogeneity within the protein complex, electronic excitation transport and electron transfer dynamics and the electron-phonon coupling. By phonon is meant low-frequency ($\leq 100 \text{ cm}^{-1}$, or $\leq 3 \cdot 10^{12} \text{ Hz}$) modes of the pigment-protein complex.

The role of the electron-phonon coupling in nonadiabatic electronic excitation transport from the antenna to the primary electron donor state of the reaction center and electron transfer within the reaction center poses an interesting question. From the point of view of dynamics, one is asking about the function of the protein beyond that of a glue which defines the relative orientations of the photosynthetic pigments. Phonons (approx. 100 cm^{-1}) have recently been implicated as the key modes for nuclear tunneling associated with the quinone reduction and its subsequent charge recombination in the reaction center of Rb.sphaeroides [15,16]. Hole-burning studies on C670 and the primary electron donor state P700 of PSI

have led to the conclusion that low-frequency (approx. 30 cm^{-1}) phonons are the primary acceptor modes for nonadiabatic electronic excitation transport from the antenna to P700 [14]. At the same time, theoretical analysis of the hole-burning data for P700 [14] and P870 [17] showed that these primary electron donor states are characterized by strong electron-phonon coupling. The nature of these phonons remains an open question.

The primary purpose of this paper is to present a unified picture for the linear electron-phonon coupling associated with the primary electron donor states P700, P870, P960 of PSI, *Rb. sphaeroides* and *Rps. viridis*. To this end, the details of the theory for hole burning in the presence of arbitrarily strong linear electron-phonon coupling are presented along with refined calculations of the hole spectra for the above three states. A brief discussion of the theory has been given in ref. 17 where it was applied to the data of Boxer and coworkers [10] on P870. Exceedingly broad holes (approx. 400 cm^{-1}) were observed at 1.5 K for several burn frequencies ω_B located within the P870 absorption profile. The maximum of the hole did not generally coincide with ω_B and its position was invariant to variations in ω_B . Furthermore, the holewidth was observed to increase with increasing ω_B . Time domain studies had earlier shown that electron transfer from the special pair (P870) to the bacteriopheophytin of the reaction center takes place in about 2 psec at cryogenic temperatures [16]. The width of a zero-phonon hole corresponding to this transfer time is approx. 2.5 cm^{-1} . Thus, the absence of a sharp hole for P870 was particularly interesting [10]. The hole-burning properties of P870 were shown to be consistent with (i) strong linear electron-phonon coupling defined by a Huang-Rhys factor $S \sim 8$ and a mean phonon frequency $\omega_m \sim 30 \text{ cm}^{-1}$ and (ii) a site inhomogeneous absorption linewidth contribution of $\Gamma_{inh} \sim 400 \text{ cm}^{-1}$ [17]. The S

and ω_m values were chosen to be consistent with the analysis by Scherer et al. [18] of absorption and fluorescence thermal broadening and Stokes shift (approx. $2S\omega_m$) data for P960. The thermal broadening data were a compilation of results from several different laboratories. Data are presented here that are far more precise and used to refine the hole-burning calculations for P870.

These thermal broadening data together with the same for P960 are also used to conclude that Γ_{inh} for P870 is approx. 200 cm^{-1} greater than for P960. As a result, the hole-burning characteristics for P960 [12] can be understood with one and the same model which accounts for the data for P870. The key difference between the data is that the broad hole maximum frequency for P960 is insensitive to variations in ω_B [12].

Gillie et al. [9] have shown that the hole profiles for P700 of enriched PSI particles from spinach consist of a very weak but sharp zero-phonon hole (coincident with ω_B) superimposed on an intense but broad hole whose width is comparable to those observed for P870 and P960. Maslov et al. [8] had earlier observed the sharp feature for P700 of intact cells of a mutant strain of Chlamydomonas reinhardtii. The data of ref. 9 were also shown to be consistent with strong linear electron-phonon coupling plus significant site inhomogeneous line broadening. Refined calculations for P700 presented here are discussed in terms of those for P870 and P960.

THEORY

The Single-site Absorption Profile

For the case of arbitrarily strong electron-phonon coupling it is convenient to determine the Fourier transform of the absorption lineshape function $G(\Lambda)$ [19]:

$$g(t) = \int d\Lambda G(\Lambda) e^{i\Lambda t} \quad (1)$$

where

$$G(\Lambda) = \langle \sum_n | \langle f n' | \mathbf{d} | n \rangle |^2 \delta(\Lambda - (E_{f,n'} - E_{o,n})/\hbar) \rangle_T \quad (2)$$

and $\langle \rangle_T$ denotes a thermal average over initial phonon levels n of the ground state. The subscripts f and n' denote the excited electronic state and its phonon levels, respectively and \mathbf{d} is the electric dipole moment operator. In the adiabatic approximation the transition dipole takes the form

$$\langle f n' | \mathbf{d} | n \rangle = M_0 \prod_{\alpha} \langle n'_{\alpha} | n_{\alpha} \rangle + \sum_{\alpha} m_{\alpha} \langle n'_{\alpha} | \mathbf{q}_{\alpha} | n_{\alpha} \rangle \prod_{\beta \neq \alpha} \langle n'_{\beta} | n_{\beta} \rangle \quad (3)$$

where the first and second terms represent the Condon and phononic contributions, respectively. The phonon coordinates \mathbf{q}_{α} are those of the ground state and the m_{α} are the induced electronic transition dipoles. The phonons are comprised of all intermolecular modes and provide a density of states, $\rho(\omega)$. We consider the case where the phonons are sufficiently delocalized so that for each and every \mathbf{q}_{α} its displacement, a_{α} , in the excited electronic state is of the order $N^{-1/2}$, where N is the number of molecular entities comprising the system. We discuss at the end the case

where a pseudolocalized [20] phonon exist and undergoes a large displacement. The displacement a_α is defined by expressing the excited-state potential as

$$E_f(\mathbf{q}) = E_f(0) + \sum_{\alpha} A_{\alpha} q_{\alpha} + 1/2 \sum_{\alpha, \beta} B_{\alpha\beta} q_{\alpha} q_{\beta} \quad (4)$$

in the harmonic approximation. The second term represents the linear electron-phonon coupling. For our application the phonon normal coordinate rotation can be ignored, i.e., $B_{\alpha\beta} = \omega'_{\alpha}{}^2 \delta_{\alpha\beta}$ and, further, we take $\omega'_{\alpha} = \omega_{\alpha}$ (ground state frequency). Equation 4 can be rewritten as

$$E_f(\mathbf{Q}) = E_f(0') + 1/2 \sum_{\alpha} \omega_{\alpha}^2 Q_{\alpha}^2 \quad (5)$$

where the $Q_{\alpha} = q_{\alpha} + a_{\alpha}$ are the excited-state phonon coordinates and $a_{\alpha} = A_{\alpha} / \omega_{\alpha}^2$. The term

$$E_f(0') - E_f(0) = 1/2 \sum_{\alpha} (a_{\alpha} \omega_{\alpha})^2 \quad (6)$$

represents the difference between the vertical and adiabatic absorption transition frequencies. And so for $\omega_{\alpha} = \omega'_{\alpha}$ the Stokes shift at T=0 K (energy difference between the intensity maxima in absorption and fluorescence) is

$$\text{Stokes shift}(T=0 \text{ K}) = \sum_{\alpha} (a_{\alpha} \omega_{\alpha})^2 \quad (7)$$

We consider this shift for finite temperatures later.

For the case of delocalized phonons and $|\underline{m}_{\alpha}| \sim N^{-1/2} |\underline{M}_0|$ the right hand side of Eqn. 3 is readily evaluated perturbatively. The procedure involves using the

ground-state phonon wavefunctions as a zero-order basis set with the perturbation $\sum_{\alpha} A_{\alpha} Q_{\alpha}$ to determine the excited-state phonon wavefunctions. We will, however, consider here only the Condon contributions, since our application is to a strongly allowed electronic transition, i.e., $|\mu_{\alpha}| \ll N^{-1/2} |M_0|$. It follows that

$$g(t) = e^{i\nu t} \prod_{\alpha} \{ [1 - 1/2 (\gamma_{\alpha}^{1/2} a_{\alpha})^2] [(2\langle n_{\alpha} \rangle_T + 1)(1 - \cos \omega_{\alpha} t) - i \sin \omega_{\alpha} t] \} \quad (8)$$

to order N^{-1} , where ν is the zero-phonon transition frequency, $\gamma_{\alpha} = \omega_{\alpha} \hbar$ and $\langle n_{\alpha} \rangle_T$ is the phonon thermal occupation number equal to $[\exp(\hbar \omega_{\alpha} / kT)]^{-1}$. The product \prod_{α} term can be expressed as

$$1 - \frac{1}{2} \sum_{\alpha} (\gamma_{\alpha}^{1/2} a_{\alpha})^2 \left\{ \left(\coth \frac{\hbar \omega_{\alpha}}{2kT} \right) (1 - \cos \omega_{\alpha} t) - i \sin \omega_{\alpha} t \right\}$$

and the sum replaced by

$$\sum_{\alpha} \rightarrow \hbar^{-1} \int_0^{\omega_M} d\omega \omega a_{\omega}^2 \rho(\omega)$$

where $\rho(\omega)$ is the phonon density of states and ω_M the maximum fundamental phonon frequency. Defining

$$A(\omega) = 1/2 \omega a_{\omega}^2 \rho(\omega) \quad (9)$$

it follows that

$$g(t) = e^{i\nu t} e^{-S(1-\xi(t))} \quad (10)$$

Here S is the Huang-Rhys factor,

$$S = \sum_{\alpha} (\langle n_{\alpha} \rangle_T + 1/2) (\gamma_{\alpha}^{1/2} a_{\alpha})^2 = \int d\omega A(\omega) \coth \frac{\hbar\omega}{2kT} \quad (11)$$

and

$$\xi(t) = S^{-1} \int d\omega \left[\cos \omega t \coth \frac{\hbar\omega}{2kT} + i \sin \omega t \right] A(\omega) \quad (12)$$

Eqn. 10 is exact to order N^{-1} . Now

$$G(\Lambda) = \frac{1}{2\pi} \int dt g(t) e^{-i\Lambda t} \quad (13)$$

which with Eqn. 10 becomes

$$G(\Lambda) = e^{-S} \sum_{r=0}^{\infty} \frac{S^r}{r!} B_r(\Lambda) \quad (14)$$

with

$$B_r(\Lambda) = \frac{1}{2\pi} \int dt e^{i(v-\Lambda)t} (\xi(t))^r. \quad (15)$$

The r values 0,1,2, correspond to zero-, one-, two-, etc. phonon transitions in which no single phonon undergoes a quantum number change greater than 1. Thus, $B_r(\Lambda)$ is the line shape function for the r -phonon ($|n' - n| = r$) process and is normalized to unity as written. From Eqn. 15 the zero-phonon line is a delta-function centered at v as expected because no allowance for dephasing has yet been made. It is also apparent that the r -phonon lineshape is the result of convolving $B_1(\Lambda)$ r -times with itself, *vide infra*. With Eqns. 12 and 15 it follows that

$$B_1(\Lambda) = S^{-1} \int d\omega A(\omega) \left(\frac{\delta(\nu - \Lambda + \omega)}{1 - e^{-\hbar\omega/kT}} + \frac{\delta(\nu - \Lambda - \omega)}{e^{\hbar\omega/kT} - 1} \right) \quad (16)$$

where the first and second terms correspond to one-phonon creation and annihilation, respectively. Equation 16 serves to underscore the fact that $B_r(\Lambda)$ takes due account of all phonon transitions for which $|\sum_{\alpha} (n'_{\alpha} - n_{\alpha})| = r$ subject to the aforementioned constraint. Because $B_r(\Lambda)$ is normalized to unity the weighting factor for the r -phonon process is

$$P_r = e^{-S} \frac{S^r}{r!}. \quad (17)$$

From Eqn. 16 it is evident that the function A determines, aside from the thermal factors, the shape of the one-phonon spectrum. In the $\lim_{T \rightarrow 0}$ only the first term survives and $A(\lambda - \nu)$ is completely determining. This function is difficult to calculate, cf. Eqn. 9, and so we turn to experiment as a guide. Fluorescence-line-narrowed spectra of impurities in organic glasses and polymers exhibiting weak electron-phonon coupling ($S < 1$) often exhibit a one-phonon line shape which can be approximated by a Gaussian at low T [21]. It is the low T limit we now focus our attention on and we consider two possibilities: either A is a Gaussian or A is a Lorentzian. Considering the latter with a FWHM = Γ and peaked at ω_m and noting that

$$\lim_{T \rightarrow 0} \left[\int d\omega \xi(t) \right]^r = e^{-r\Gamma t/2} e^{ir\omega_m t} \quad (18)$$

it follows that

$$\begin{aligned}
B_r(\Lambda, T=0) &= \pi^{-1} \operatorname{Re} \int_0^{\infty} dt e^{i(v-\Lambda+r\omega_m+ir\Gamma/2)t} \\
&= \frac{r\Gamma/2\pi}{(\Lambda-v-r\omega_m)^2 + (r\Gamma/2)^2}
\end{aligned} \tag{19}$$

Thus, with one-phonon spectrum centered at $v+\omega_m$ and possessing a width Γ , the r -phonon spectrum is centered at $v+r\omega_m$ with a width of $r\Gamma$. Utilization of a Lorentzian for A likely overestimates the dependence of the linewidth on r relative to a Gaussian, which, for coupling to delocalized phonons, may be a more realistic shape. It is readily shown that for a Gaussian the linewidth of the r -phonon spectrum is $r^{1/2}\Gamma$.

In the following subsection we utilize the $T=0$ K limit of $g(\Lambda)$ (Eqn. 14) to develop the shape of the hole-burned spectrum. The formalism admits any shape for $A(v-\Lambda)$ but in order to obtain an expression for the hole profile which is simple and physically transparent we will utilize the following single site absorption profile

$$L(\Lambda-v) = e^{-S} l_0(\Lambda-v) + \sum_{r=1}^{\infty} \frac{S^r e^{-S}}{r!} l_r(\Lambda-v-r\omega_m). \tag{20}$$

Here, l_r is given by Eqn. 19 but for model calculations the width $r\Gamma$ is replaced by $r^{1/2}\Gamma$ so that the second term in Eqn. 20 is a reasonable approximation to a sum of Gaussians, especially for large S -- the case of interest. The zero-phonon line shape is taken as homogeneously broadened with the FWHM of l_0 equal to γ .

Finally, we consider the case where a pseudo-localized or resonant phonon mode [20] associated with the impurity dominates the phonon spectrum and is characterized by strong coupling ($S>1$). It is well known [22] that the $T=0$ K

absorption spectrum also has the functional form of Eqn. 20 although the linewidths for the r -phonon transitions ($r \geq 1$) are determined by resonant relaxation of the r -phonon level into the continuum of delocalized phonons [20] as well as the dispersion in the pseudolocalized phonon frequency due to site inhomogeneity. Thus, our expression for the hole profile can also be utilized for pseudolocalized phonons.

The Hole Profile

With suitable modifications mandated by strong electron-phonon, our approach follows that of Friedrich and Haarer [5]. We define $N_0(\nu-\nu_m)/N$ as the probability of finding a site with a zero-phonon transition frequency equal to ν . For amorphous solids or protein environments a Gaussian distribution is usually used but, for reasons already mentioned, we employ a Lorentzian:

$$\frac{N_0(\nu-\nu_m)}{N} = \frac{\Gamma_{inh}/2\pi}{(\nu-\nu_m)^2 + (\Gamma_{inh}/2)^2} \quad (21)$$

for the pre-burn distribution. Given the approximate form of $L(\Lambda-\nu)$ (Eqn. 20), utilization of a Lorentzian should introduce little additional error for strong coupling. Let the absorption cross-section, laser intensity and photochemical quantum yield equal σ , I and ϕ , respectively. Then following a burn for time τ [5]

$$N_\tau(\nu-\nu_m) = N_0(\nu-\nu_m) e^{-\sigma I \phi \tau L(\omega_B - \nu)} \quad (22)$$

where ω_B is the laser burn frequency and $L(\omega_B - \nu)$ is given by Eqn. 20. To obtain the absorption spectrum, A_τ , following the burn we must convolve Eqn. 22 with $L(\Lambda - \nu)$ and integrate over ν . Thus,

$$A_\tau(\Lambda) = \sum_{r=0}^{\infty} \frac{S^r e^{-S}}{r!} \int d\nu N_0(\nu - \nu_m) e^{-\sigma I \phi \tau L(\omega_B - \nu)} l_r(\Lambda - \nu - r\omega_m). \quad (23)$$

For simplicity we employ the short-burn-time limit where the exponential can be expanded as $1 - \sigma I \phi \tau L(\omega_B - \nu)$. This approximation need not be made, although the resulting expressions are very cumbersome if it is not. The hole spectrum in the short-burn-time limit is simply

$$A_0(\lambda) - A_\tau(\lambda) = \sigma I \pi \tau \sum_{r,r'=0}^{\infty} \frac{e^{-S} S^r}{r!} \frac{e^{-S} S^{r'}}{r'!} \int d\nu \times N_0(\nu - \nu_m) l_r(\lambda - \nu - r\omega_m) l_{r'}(\omega_B - \nu - r'\omega_m) \quad (24)$$

Because we are interested in holes whose widths are comparable to Γ_{inh} we cannot assume, as in ref. 5 that $N_0(\nu - \nu_m)$ is constant in Eqn. 24. The convolution of the three Lorentzians can be performed using the method of residues but the procedure is tedious. A far more facile approach is to express each of the Lorentzians as the Fourier transform of the appropriate exponential time decay. Performing the frequency integration ($d\phi$) first yields $2\pi\delta(t+t'+t'')$. Taking due account of the possible time orderings in the time integration immediately yields

$$\begin{aligned}
A_o(\Lambda) - A_r(\Lambda) = & \frac{\sigma\phi\tau}{3(2\pi)^2} \sum_{r,r'=0}^{\infty} \frac{S^r e^{-S}}{r!} \frac{S^{r'} e^{-S}}{r'!} \\
& \times \left(\frac{\Gamma_{inh} + \Gamma_r}{(\Lambda - v_m - r\omega_m)^2 + [(\Gamma_{inh} + \Gamma_r)/2]^2} \frac{\Gamma_r + \Gamma_{r'}}{[\Lambda - \omega_B + \omega_m(r'-r)]^2 + [(\Gamma_r + \Gamma_{r'})/2]^2} \right. \\
& + \frac{\Gamma_{inh} + \Gamma_{r'}}{(\omega_B - v_m - r'\omega_m)^2 + [(\Gamma_{inh} + \Gamma_{r'})/2]^2} \frac{\Gamma_r + \Gamma_{r'}}{[\Lambda - \omega_B + \omega_m(r'-r)]^2 + [(\Gamma_r + \Gamma_{r'})/2]^2} \\
& \left. + \frac{\Gamma_{inh} + \Gamma_{r'}}{(\omega_B - v_m - r'\omega_m)^2 + [(\Gamma_{inh} + \Gamma_{r'})/2]^2} \frac{\Gamma_{inh} + \Gamma_r}{(\Lambda - v_m - r\omega_m)^2 + [(\Gamma_{inh} + \Gamma_r)/2]^2} \right) \quad (25)
\end{aligned}$$

the desired result. For compactness, we have defined $\Gamma_r = \gamma$ for $r=0$ and $=r^{1/2}\Gamma$ for $r \geq 1$, where γ is the damping constant for the zero-phonon transition. Considering the complexity of the problem, Eqn. 25 is simple as well as physically transparent. For example, consider strong coupling where $S > 1$ and phonon processes with large r the most probable, r_{max} . Consider next the burn frequency ω_B located in the high-energy tail of the absorption profile where transitions with $r' > r_{max}$ are predominantly excited. From the first factor of the second term of Eqn. 25 we have $\omega_B = v_m + r'\omega_m$ which when inserted into the second factor of the same term yields the resonance $\Lambda - v_m - r\omega_m$. The factor $S^r e^{-S}/r!$ favors $r \sim r_{max} < r'$, so that the hole maximum may well be red shifted relative to ω_B . The other two terms indicate a red shift as well. In the same way one can argue that for ω_B in the low-energy tail the hole may be blue shifted relative to ω_B . The extents of these shifts and the

value of $\omega_{\mathbf{B}}$ for which the hole is coincident are determined by the interplay between S , Γ_{inh} , and Γ .

CALCULATIONS

In order to simulate spectra Fortran computer programs for calculating the single site absorption (Eqn. 20), the inhomogeneously broadened absorption (the convolution of Eqn. 20 with the site distribution function (Eqn. 21)) and the hole spectrum (Eqn. 25) were written. Input data required for the programs were the one-phonon absorption width, Γ , the one-phonon displacement frequency, ω_m , the excited state lifetime, γ^{-1} , the inhomogeneous width, Γ_{inh} , and the Huang-Rhys factor, S . The effects of varying each of these parameters will be discussed in the following section.

In addition to these parameters the frequency interval at which the spectra were calculated could be specified. The step size selected is similar to the spectroscopic resolution in experimental spectra, although it is not exactly analogous. If the step size is small compared to the narrowest spectral feature, then the spectra will be undistorted. However, if the step size is comparable to or greater than the width of the spectral features then distortions will occur. In particular, if the step size and starting positions are such that calculations are carried out half a step size away from a sharp maximum, then the maximum will be diminished relative to the same results obtained with the calculated points shifted half a step so that the value at the maximum is calculated. Although it would be preferable to perform the calculations with a small step size to avoid these distortions, the time required to perform a computation can become quite large. However, the hole spectra were all calculated so that a value was calculated at the peak of the sharp features. The effect of this is more easily seen in the noise-free calculations than they would be in actual experimental data.

One final point to be made about the calculations is how the infinite sums (or double sums) over multi-phonon processes were handled. In general these sums were performed for $r=0$ to $r=20$. The accuracy of truncating at this point is dependent upon the value for S . For $S=4$, this truncation resulted in neglecting $2 \cdot 10^{-7}\%$ of the intensity at each point. For $S=8$, 0.009% of the intensity was neglected.

The calculations were performed on a Digital Equipment Corporation VAX-11/780.

RESULTS

Computed Profiles

Ultimately the aim of the computer simulations is to compare the computed spectra with experimental spectra and thereby obtain reasonable estimates for parameters such as the Huang-Rhys factor, S , the mean phonon frequency to which the transition is coupled, ω_m , and the inhomogeneous broadening, Γ_{inh} . It is instructive, however, to consider first the various spectral shapes themselves, apart from any experimental data to appreciate the effect of the various parameters on the spectral profile.

Single site absorption profile

The single site absorption spectrum or profile is not experimentally measurable. Its computed shape, however, does allow the effects of variations in S , Γ , ω_m , and γ to be assessed without the complications introduced by the site inhomogeneous distribution. Fig. 1 illustrates for fixed Γ , ω_m , and γ , the variation in the single site absorption shape as S is consecutively doubled from 0.5 to 8. Since the area under each of the bands is equal, as the bands broaden with increasing S the peak intensities decrease by two orders of magnitude. Hence the spectra have been normalized to unity at the frequency of the most strongly absorbing point of the spectrum. In the absence of this normalization it would not be possible to present the five shapes on the same coordinate system. For ease of inspection the spectra for $S > 0.5$ have been shifted in steps of 150 cm^{-1} relative to the $S=0.5$ spectrum.

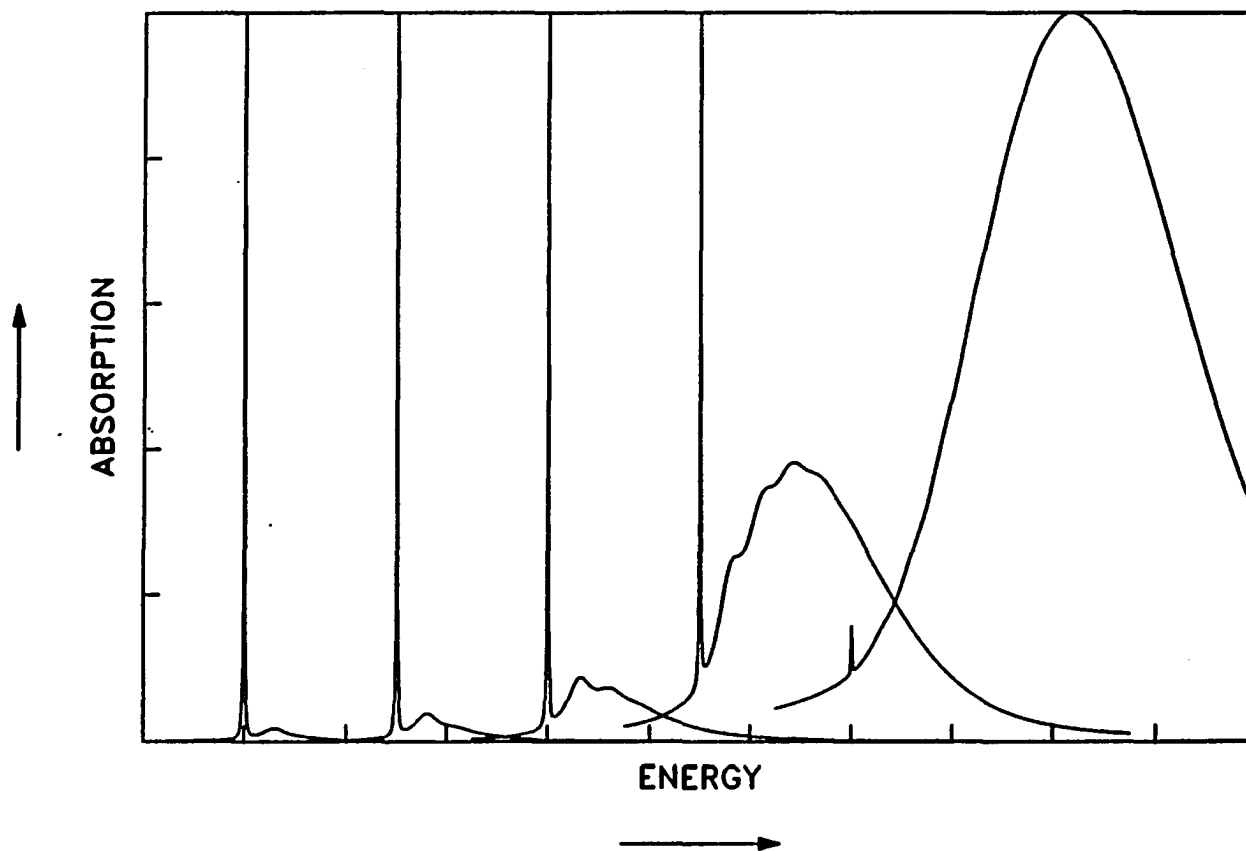


Figure 1. Single site absorption profiles calculated according to Eqn. 20 with $\Gamma = \omega_m = 30$ and $\gamma = 1$. From left to right the values of S are 0.5, 1., 2., 4., 8. For ease of inspection the $S = 1-8$ spectra are artificially shifted in steps of 150 cm^{-1} relative to the $S = 0.5$ spectrum.

From Eqn. 20, it can be seen that the intensity of the zero-phonon contribution to the line shape is e^{-S} . Thus in Fig. 1, the zero-phonon lines are 60.0, 36.8, 13.5, 1.83, and 0.039% of the total intensity for $S=0.5, 1.0, 2.0, 4.0,$ and $8.0,$ respectively. Note also, that the peak of the phonon absorption increases with increasing S and is maximum at approx. $S\omega_m$. The width of the phonon wing of the single-site absorption also increases significantly as S increases and is also dependent upon Γ , the one-phonon absorption width.

Convolution with Γ_{inh} - the inhomogeneous absorption profile

To obtain the inhomogeneously broadened absorption spectrum involves the convolution of Eqn. 20 with the site distribution function, Eqn. 21. The resulting absorption shape is

$$A_o(\Lambda) = \sum_{r=0}^{\infty} \frac{e^{-S} S^r}{r!} l_{r,inh}(\Lambda - \nu - r\omega_m) \quad (26)$$

where $l_{r,inh}$ is a Lorentzian with a peak at $\nu + r\omega_m$ and a width equal to $\Gamma_r + \Gamma_{inh}$, where as before $\Gamma_r = \gamma$ for $r=0$ and $\Gamma_r = r^{1/2}\Gamma$ for $r > 0$. Since every term of the sum has a width greater than Γ_{inh} , there will no features sharper than Γ_{inh} . In general, the profile will be structureless unless ω_m is comparable to or greater than Γ_{inh} . In that case, peaks or shoulders with a separation of ω_m will be discernible, although if the phonon absorption widths are large, these features may again be obscured

The calculated absorption bands are asymmetric, tailing more slowly on the high-energy side. A measure of the degree of asymmetry is the comparison of the full width at half maximum intensity with twice the width measured from the peak frequency to the half maximum intensity point on the low-energy side of the band.

Widths measured in that latter manner are as much as 15% narrower than the full widths. The absorption width, Γ_{abs} , is given approximately by

$$\Gamma_{\text{abs}} = \Gamma_{\text{inh}} + S\omega_{\text{m}} \quad (27)$$

Deviations from this relation increase as S increasing.

The peak of the absorption can deviate considerably from the peak of the site distribution function. The displacement is approximately $S\omega_{\text{m}}$. This shift can be understood from the single site absorption profiles. The maximum Franck-Condon factor occurs for $S=r$, corresponding to an r -phonon process shifted from the zero-phonon frequency by $r\omega_{\text{m}}$. Thus the frequency at which there is a maximum number of absorbers, i.e., the maximum of the site distribution function, ν_{m} , will produce an absorption maximum similarly shifted. As will be seen, hole burning results can lead to a determination of ω_{m} . In conjunction with the inhomogeneous absorption spectrum, this allows determination of $S\omega_{\text{m}}$.

The computed inhomogeneous absorption profiles are used to check that the parameters used for the hole burning simulations produced absorption shapes with asymmetries, widths and peak wavelength consistent with the experimental absorption shapes.

The hole spectrum

The hole spectrum in the short burn time limit is given by Eqn. 25. Figs. 2 and 3 illustrate holes calculated according to this equation with the same parameters as used for Fig. 1, viz., $\omega_{\text{m}}=30$, $\Gamma=30$, $\gamma=1.0$. and $S=0.5, 1.0, 2.0, 4.0, 8.0$. The additional parameters needed for evaluation of Eqn. 25 are the burn frequency, ω_{B} ,

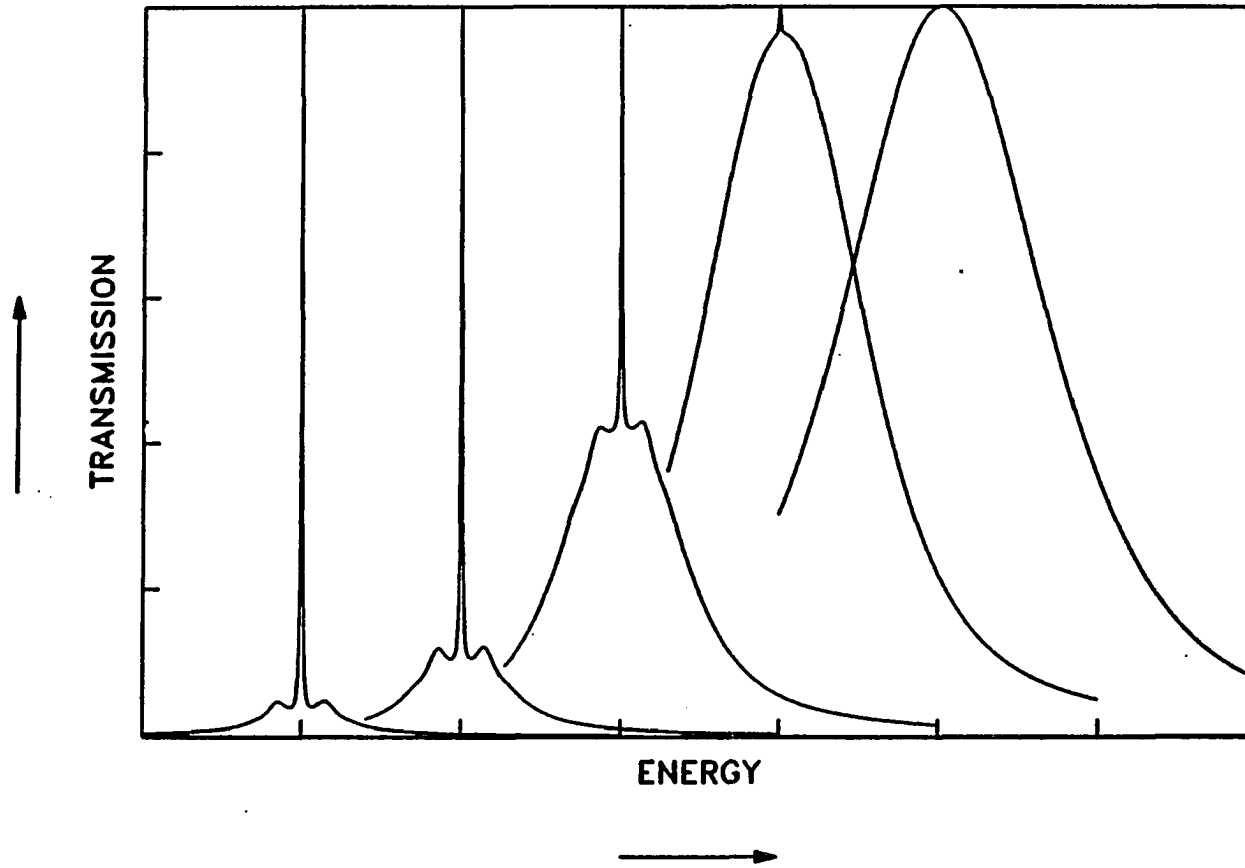


Figure 2. Hole profiles calculated according to Eqn. 25 with $\Gamma = \omega_m = 30$, $\gamma = 1$, $\Gamma_{inh} = 300$, and $\omega_B = 0$. From left to right the values of S are 0.5, 1., 2., 4., 8. The hole profiles are artificially displaced from each other for ease of inspection, see text.

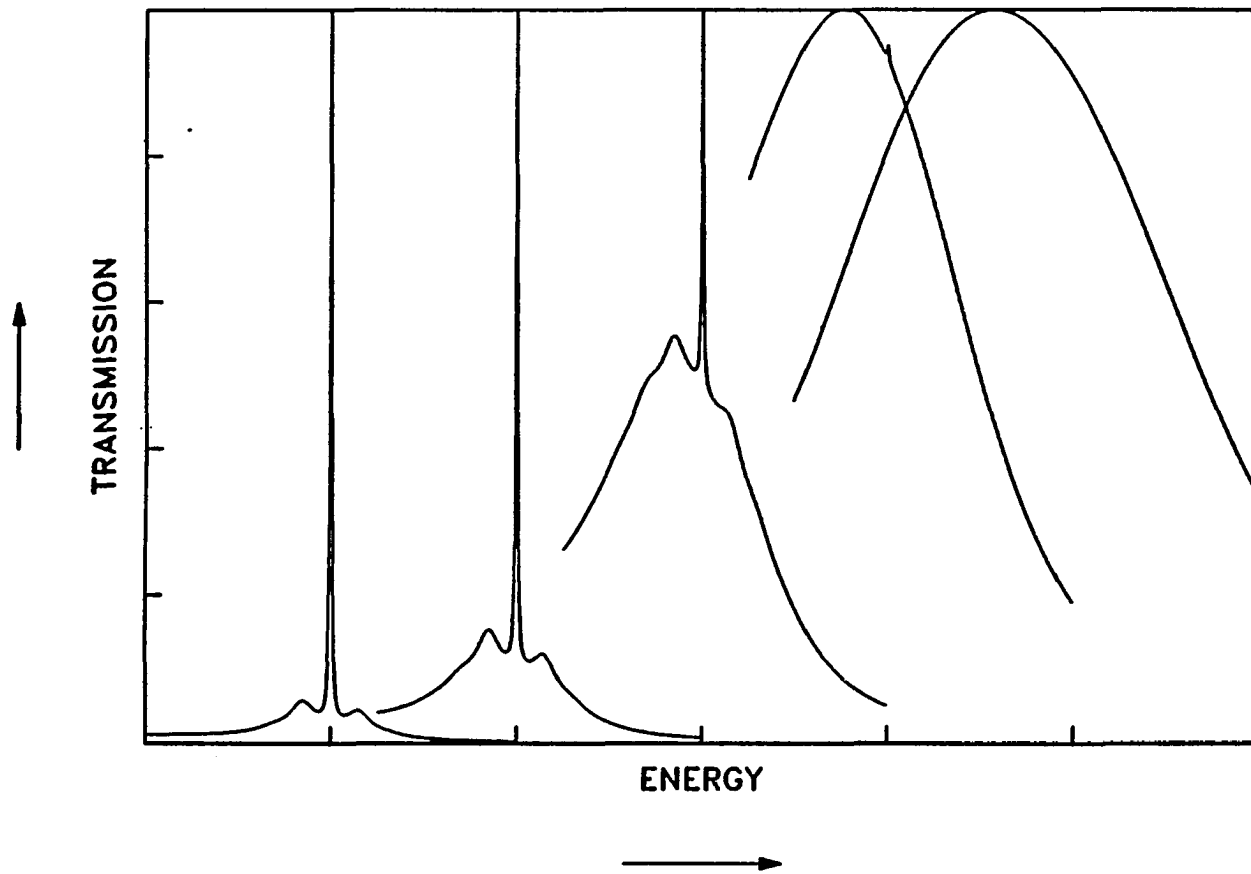


Figure 3. Hole profiles calculated according to Eqn. 25 with $\Gamma = \omega_m = 30$, $\gamma = 1$, $\Gamma_{inh} = 300$, and $\omega_B = v_m + 200$. From left to right the values of S are 0.5, 1., 2., 4., 8. The hole profiles are artificially displaced from each other for ease of inspection.

and the inhomogeneous distribution width, Γ_{inh} . For both Fig. 2 and Fig. 3, $\Gamma_{inh}=300$ was used. In order to display the holes on a single coordinate system, the distribution maxima were taken as $\nu_m = 0, 200, 400, 600,$ and 800 corresponding to $S=0.5, 1.0, 2.0, 4.0, 8.0,$ respectively. The corresponding burn frequencies were $\omega_B = \nu_m$ for Fig. 2, and $\omega_B = \nu_m + 200$ for Fig. 3. Comparison of Fig. 1 and Fig. 2 reveals several interesting features. First, while the single line shapes show phonon absorption primarily to the high energy side of the zero-phonon line, the hole spectra have phonon wings to both higher and lower energy. As shown in Fig. 2, the holes burnt at $\omega_B = \nu_m$ have a phonon structure that is nearly symmetric about the zero-phonon hole. For holes burnt with $\omega_B > \nu_m$ (the distribution maximum) the phonon wings are skewed toward ν_m , as shown in Fig. 3. Skewing in the opposite direction occurs for $\omega_B < \nu_m$. The influence of the position of the excitation frequency within the homogeneous distribution has previously been noted by Kikas [23], with regard to line narrowed spectra in which only a low energy phonon band occurs.

There are a number of reports which experimentally confirm the presence of both high and low energy phonon holes [5,24,25]. The low energy phonon wings are understood to originate primarily from the burning of zero-phonon features of sites at energies lower than ω_B , which have been excited through phonon absorption. The higher energy phonon hole consists of the phonon wings of sites which absorb through their zero-phonon line plus a contribution from the tails of the phonon wings of lower energy sites. This summing of the tails of lower energy sites is responsible for the slight asymmetry which is revealed by close examination of the holes of Fig. 2. Figure 3 of ref. 25 is an example of nearly symmetric high- and low-energy phonon holes. The preponderance of published hole spectra in which

the low energy phonon hole is predominant indicates that these holes were burnt at energies higher than the energy of the peak of the site distribution function.

The ratio of zero-phonon hole to the total hole intensity is (from Eqn. 25) e^{-2S} at $\omega_B = \nu_m$. This is in contrast with the corresponding ratio for the single-site absorption given above: e^{-S} . For the hole spectra this ratio is not constant but varies with the position of ω_B within the inhomogeneous distribution. From Eqn. 25 it can be seen that all the frequency terms in the denominators disappear for $r=r'=0$ when $\Lambda = \omega_B = \nu_m$. This produces the zero-phonon hole at ω_B . However, when $\omega_B \neq \nu_m$, these terms do not disappear and cause a reduction in the intensity of the zero-phonon hole relative to the total hole intensity. This effect is most easily seen by comparing the hole shapes for $S=4$ in Fig. 2 with the corresponding hole in Fig. 3, in which the zero-phonon hole is noticeably less intense. It should be emphasized that this decrease of the zero-phonon hole intensity is readily seen in the computed spectra where the spectra are all normalized to unity. Experimentally, the effect may be partly obscured by the variation in hole depth due to differences in absorption through out the inhomogeneous profile.

Note in Fig. 2 and 3, that for $S=8$ no zero-phonon hole is detectable. For this S -value the zero-phonon feature would carry e^{-16} of the total intensity, i.e., $1 \cdot 10^{-7}$. Certainly, such a weak feature would be impossible to detect experimentally. Comparison of Fig. 2 with Fig. 3 for $S=8$ shows that the hole has broadened considerably as the burn frequency shifts from ν_m to $\nu_m + 200$. This broadening is due to there being two dominate features in the hole spectrum: one which occurs at ν_m and the other which occurs at ν_B . The large number of absorbers at ν_m will make a major contribution to the hole spectrum even when these absorbers are only being excited through phonon side-band absorption. The more strongly absorbing

molecules with zero-phonon absorption at ν_B will make a strong contribution to the hole shape. As these two contributions separate from each other the hole appears to widen until the separation is approximately equal to the widths of the two features. Since the widths will be on the order of Γ_{inh} , separate features may not be discernible until $\omega_B = \nu_m \pm 300$, or greater. Experimentally, such large shifts may be into a very weakly absorbing region, producing negligible holes.

Comparison of Calculated and Experimental Profiles for Primary Electron Donor States

On the basis of the hole-burning results (see Introduction) of Maslov et al. [8] on P700 of a PSI and Boxer et al. [10,12] and Meech et al. [11,13] on P870 and P960 of Rb. sphaeroides and Rps. viridis, one would conclude that the two primary electron donor states of the bacterial systems differ in a very substantive way from P700. Again, Maslov and coworkers observed only a sharp zero-phonon hole coincident with ω_B which is two orders of magnitude sharper than the approx. 400 cm^{-1} wide holes observed for P870 and P960. The hole-burning studies of Boxer and coworkers on P870 and P960 are more extensive than those of Meech and coworkers and show that there is an interesting dependence of the broad hole profile on ω_B (see Introduction and below). The later more detailed studies of Gillie and coworkers [9] on P700 of enriched PSI particles from spinach revealed that the hole profile is comprised of a weak but sharp (approx. 0.05 cm^{-1}) hole superimposed on an intense broad hole whose width is comparable to those observed for P870 and P960. With this work it would appear that the differences between the hole-burning characteristics of P870 (P960) and P700 may not be so great.

In what follows it will be shown that the hole-burning and complementary characteristics, such as the Stokes shift and thermal broadening, of the three primary electron donor states are consistent with strong linear electron-phonon coupling and a significant site inhomogeneous broadening contribution to the low temperature absorption profile. At this point, the absence of a sharp zero-phonon hole in the spectra of P870 and P960 should only be viewed as consistent with strong electron-phonon coupling and site inhomogeneous broadening. The calculations indicate that under optimum experimental conditions the zero-phonon hole may be observable. In the same vein, it is the presence of the broad intense hole in the spectra of P700 which is, at this time, more important than the observation of the weak zero-phonon hole. It will be seen that the variations in the parameters of Eqn. 25 required to account for the principal differences in the hole spectra for the three primary electron donor states are not, in any profound sense, different.

P870 and P960

Previously we have shown that the P870 hole-burning data [10,11] for Rb. sphaeroides can be explained by Eqn. 25 [17] with the appropriate choice of the parameters S , ω_m , Γ_{inh} , Γ , γ , and ν_m . In this subsection we present a more detailed comparison of the experimental results with the calculated hole shapes for P870 and P960 of Rps. viridis. Ideally, hole burning, Stokes shift and thermal broadening data (associated with the absorption and fluorescence origin profiles) should suffice to fix the values of most of the above parameters. We proceed to discuss the determination of these parameters and the difficulties associated therewith when a zero-phonon hole coincident with the ω_B is not observable (as is the case for P870 and P960).

For holes burnt on the low-energy side of the absorption profile, Eqn. 25 shows that the broad hole maximum will occur near the maximum, ν_m , of the zero-phonon site distribution function. When $\omega_B = \nu_m$, the broad hole maximum will coincide with ω_B . The displacement between the absorption profile and ν_m is approx. $S\omega_m$. Furthermore, the Stokes shift is approx. $2S\omega_m$ so that one has an important check on the value of $S\omega_m$ determined from hole burning.

Calculations with Eqn. 25 also show that slight variations in the position of the broad hole maximum with variations in ω_B will be observable when $\Gamma_{inh} \gtrsim S\omega_m$. These variations are observed for P870 [10] but not for P960 [12]. Thus, it would appear that $\Gamma_{inh}(P960) < \Gamma_{inh}(P870)$. We return to this point shortly when the thermal broadening data are discussed.

When phonon structure is not observable in the absorption or hole spectra, thermal broadening data can be used to determine the mean phonon frequency ω_m . The linear electron-phonon coupling contribution to the width of the absorption profile is [19]

$$\tilde{\Gamma}(T) = \left(S \omega_m^2 \coth \frac{\hbar\omega_m}{2kT} \right)^{1/2} \quad (28)$$

Use of Eqn. 28 to determine ω_m is complicated by the fact that Γ_{inh} is also a contributor to the absorption linewidth, Γ_{abs} . When the absorption profile is assumed to be a Gaussian, the method of moments [18, 19] yields

$$\Gamma_{abs}(T) = (\tilde{\Gamma}(T)^2 + \Gamma_{inh}^2)^{1/2} \quad (29)$$

for the T-dependent absorption linewidth. However, the assumption of a Gaussian is not sufficiently accurate because of the asymmetries associated with the P870 and P960 absorption profiles. Calculations with Eqn. 26 yield the relationship

$$\Gamma_{\text{abs}}(T) \sim \tilde{\Gamma}(T) + \Gamma_{\text{inh}} \quad (30)$$

The thermal broadening data for the P870 and P960 absorption profiles are consistent with Eqn. 30. In Fig. 4 is shown the absorption spectra for the reaction center of *Rb. sphaeroides* and *Rps. viridis* in an ethylene glycol/water glass at 1.6 K. For this solvent, the P870 and P960 absorption bands are particularly well separated from their respective bacteriochlorophyll monomer absorption at 800 and 835 nm, respectively. Thus, accurate thermal broadening studies on the primary electron donor states are possible. The results of such a study are shown in Fig. 5. Aside from an approx. 210 cm^{-1} offset, the thermal broadenings for P870 and P960 are identical within experimental error. The same behavior has been observed by Holten and Kirmaier (unpublished data, Department of Chemistry, Washington University) who employed poly(vinyl alcohol) and gelatin films as low-temperature matrices. Although solvent perturbations on the width and position of the primary electron donor state absorption profile exist, it is generally the case that the width of P870 is substantially greater than that for P960. From Fig. 5 we can conclude that $\Gamma_{\text{inh}}(\text{P870}) \sim \Gamma_{\text{inh}}(\text{P960}) + 210$. However, in order to analyze the data of Fig. 5 with Eqn. 28 so that ω_m can be determined, a value for $\Gamma_{\text{inh}}(\text{P960})$ is required. As $\Gamma_{\text{inh}}(\text{P960})$ increases, ω_m decreases. Our determination of $\Gamma_{\text{inh}}(\text{P960})$ will rest on the quality of fit of Eqn. 25 to the hole burning data. However, we note that the linear electron-phonon coupling of chlorophylls is weak [26] as has recently been

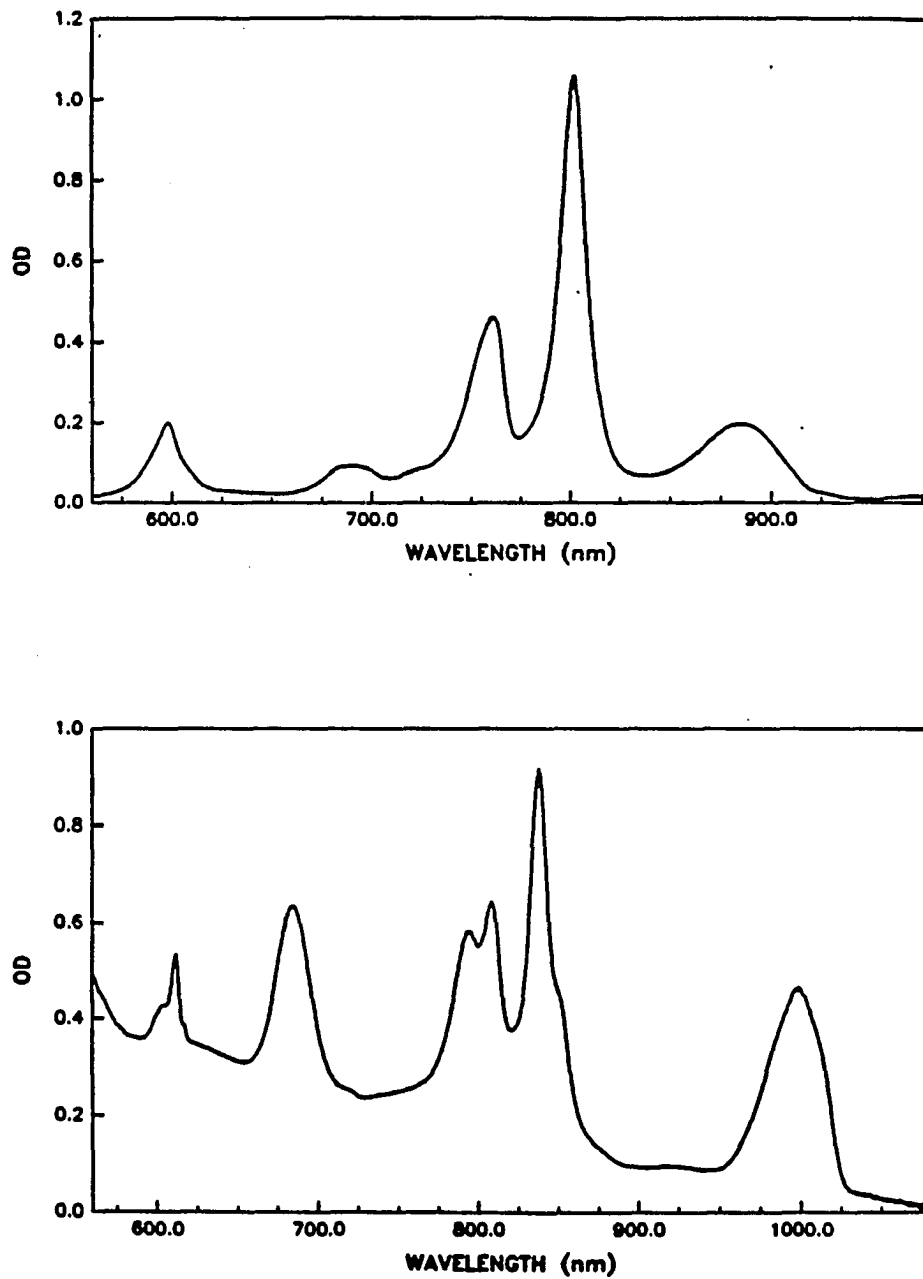


Figure 4. Absorption spectra of reaction center preparations from (A) *Rb. sphaeroides* and (B) *Rps. viridis*, both in ethylene glycol/ water glass at 1.6 K.

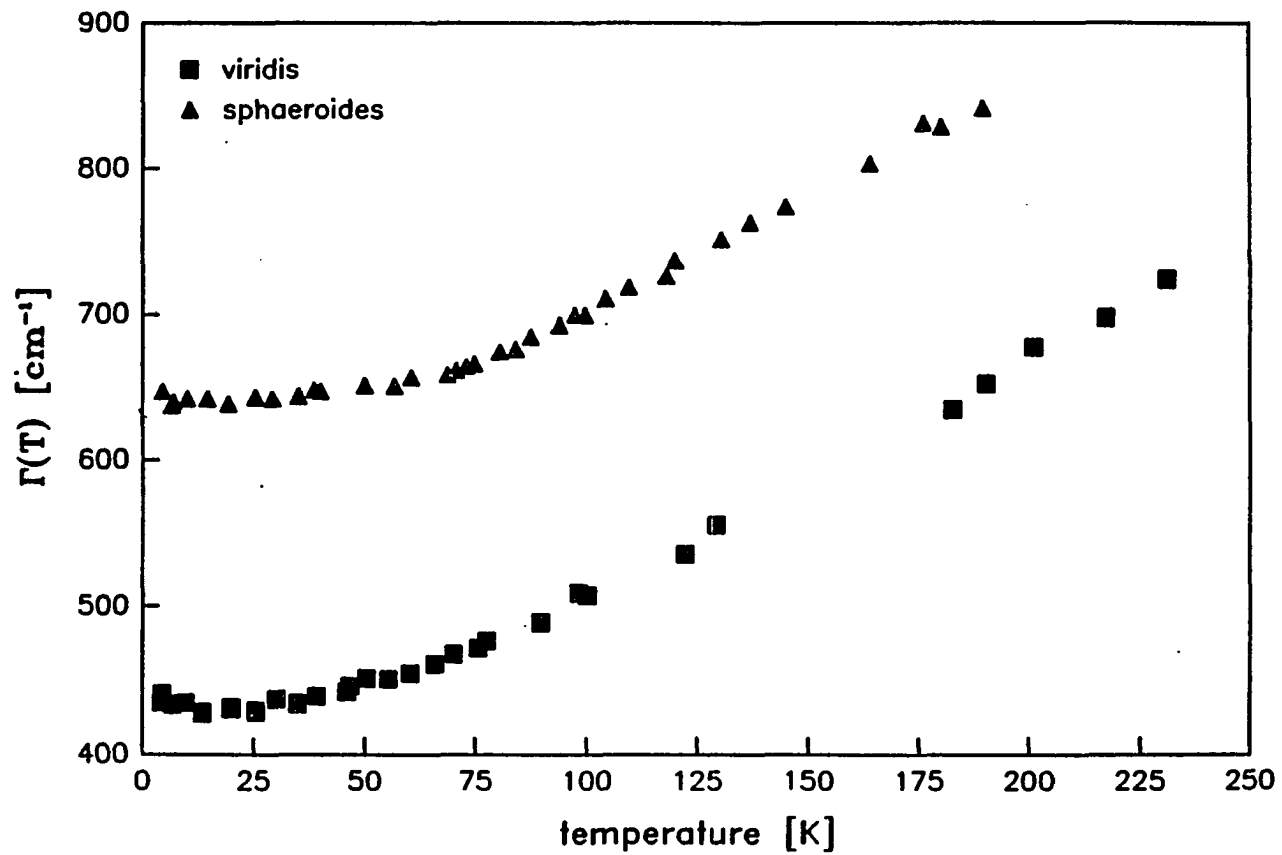


Figure 5. Thermal broadening of the P870 and P960 PED bands of *Rb. sphaeroides* and *Rps. viridis* in an ethylene glycol/water glass. Γ corresponds to the full-width at half-maximum.

determined for the core antenna complex C670 of PSI [14]. Thus, the widths of B800 and B835 in Fig. 4a and b as well as those for bacteriopheophytin monomer serve as rough guide for Γ_{inh} (P960). Of course, each of these 'monomer' bands is contributed to by two identical pigments associated with the L and M protein arms of the reaction center [27,28]. Inequivalent protein interactions for *Rps. viridis* are sufficient to produce a splitting of the bacteriopheophytin b band at 800 nm (Fig. 4b). Moreover, the Q_y states of the pigments in the reaction center are to a modest extent mixed by excitonic interactions [29]. Nevertheless from the 'monomer' transitions in Fig. 4a and b, Γ_{inh} values in the range 150-350 cm^{-1} can be estimated. This range is consistent with the Γ_{inh} values for C670 and P700 of PSI, see following subsection.

Reasonable fits with Eqn. 25 to the hole-burning data of Boxer and coworkers on P870 [10] and P960 [12] are obtained for the parameter values given in Table I. The calculated curves for P870 are shown in Fig. 6 where the burn frequencies are given relative to $\nu_m \equiv 0$ (maximum of the site distribution function) and chosen to be similar to the burn frequencies used in the experiment. For $S=4$, the zero-phonon hole carries only 0.03% of the total hole intensity for $\omega_B \sim \nu_m \equiv 0$. It is discernible for the $\omega_B=0$ and -100 cm^{-1} curves, but is less so for the $\omega_B > 0$ curves because of the diminishing contribution from zero-phonon transitions to the absorption relative to that from multi-phonon as ω_B increases past ν_m . The signal to noise and resolution of the experiments in refs. 10, 12 would preclude observation of the weak zero-phonon hole. On the other hand, for S as small as 2, a zero-phonon hole would be easily detectable for the γ given in Table I. In Fig. 6, the displacements between the broad hole maximum and ω_B and the increase in the broad hole width with increasing ω_B are consistent with the experimental data [10,12]. As discussed in

Table I. Parameters used to calculate hole spectra for the various reaction center^a

	Γ_{inh}	Γ	γ	S	ω_m
P960	150	40	1.0	4.5	80
P870	350	50	2.5	4.5	80
P700	300	30	0.06	5.5	30
C670	200	40	0.03	<0.9	30

^aFor comparison, values for the core antenna complex C670 of PSI are also included.

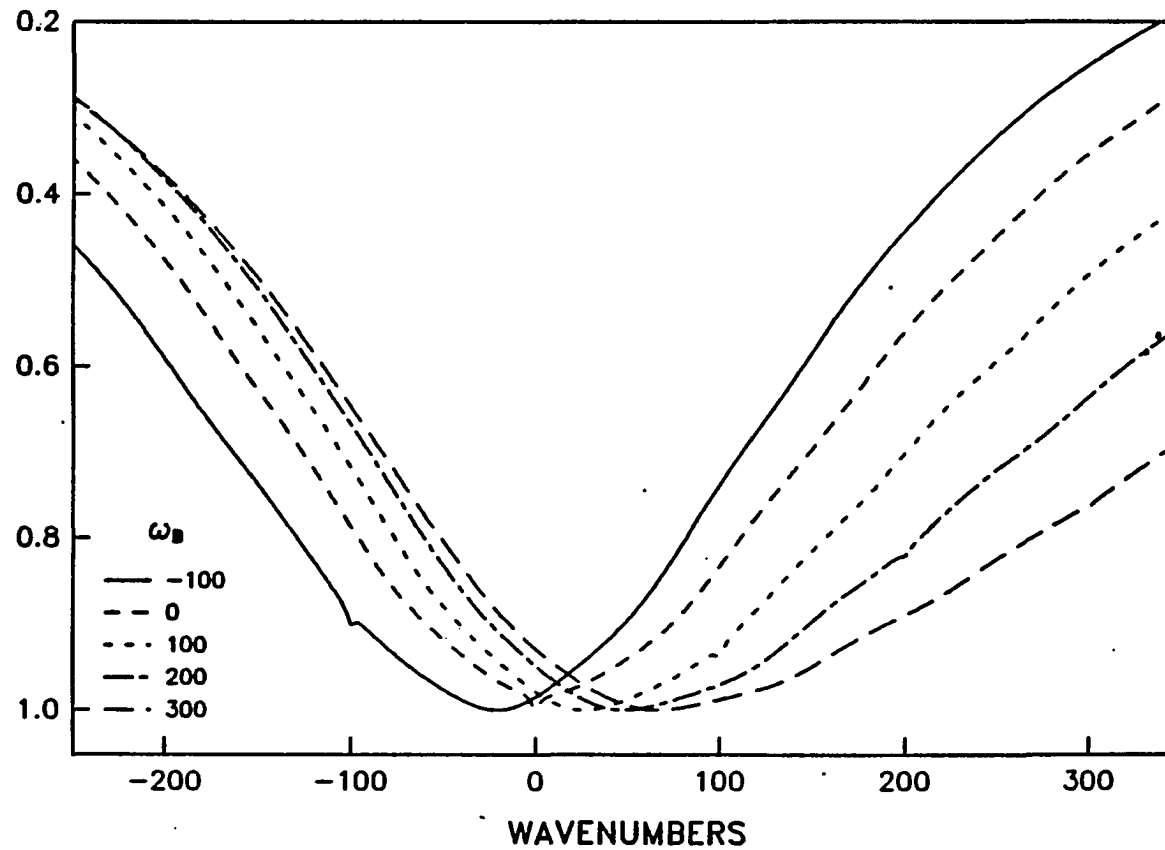


Figure 6. Hole spectra of P870 calculated according to Eqn. 25 with the parameters given in Table I.

ref. 17, the broadening and shifting of the holes in Rb.sphaeroides is due to the superposition of two broad holes. One of these holes is due to burning of the large number of sites at ν_m which contribute through phonon absorption even when ω_B is quite remote from ν_m . This hole does not shift. The other hole is coincident with ω_B and therefore changes with changes in ω_B . The contribution of these two terms is easily seen in the calculations when ω_B is shifted more than Γ_{inh} from ν_m . This effect is evident in Fig. 3 of ref. 17. The effect is much more difficult to see experimentally, due to overlapping absorptions when ω_B is shifted to higher energy of ν_m and due to very weak absorption when shifted to lower energy.

To what extent are the parameter values in Table I for P870 consistent with the various types of experimental data? First, the differences between the hole spectra of P870 and P960 (see below) are accounted for by a value of Γ_{inh} (P870) which is substantially greater than the value for Γ_{inh} (P960) (as required by the data of Fig. 4 and those of Holten and Kirmaier (unpublished data)). Second, the measured Stokes shift for P870 is approx. 500 cm^{-1} [18,27] which should be compared with $2S\omega_m \sim 640 \text{ cm}^{-1}$ (from Table I). The agreement is reasonable considering the experimental uncertainties. Furthermore, 500 cm^{-1} would be a lower limit for $2S\omega_m$ if the P870 fluorescence is not thermally relaxed with respect to phonons or if small depressions in phonon mode frequencies occur in the excited state. Third, for Γ_{inh} (P870) $\sim 350 \text{ cm}^{-1}$, the thermal broadening data of Fig. 5 are well accounted for by Eqn. 28 with $\omega_m = 108 \text{ cm}^{-1}$. This frequency (mean) is associated with the ground electronic state. In setting $\omega_m = 80 \text{ cm}^{-1}$ a frequency depression of $\sim 20\%$ is assumed for the excited electronic state. Fourth, no direct measurement of the one-phonon profile width, Γ , is possible due to the large Huang-Rhys factor S . However, a value of $\Gamma \sim 40 \text{ cm}^{-1}$ has recently been measured for C670 of PSI [14].

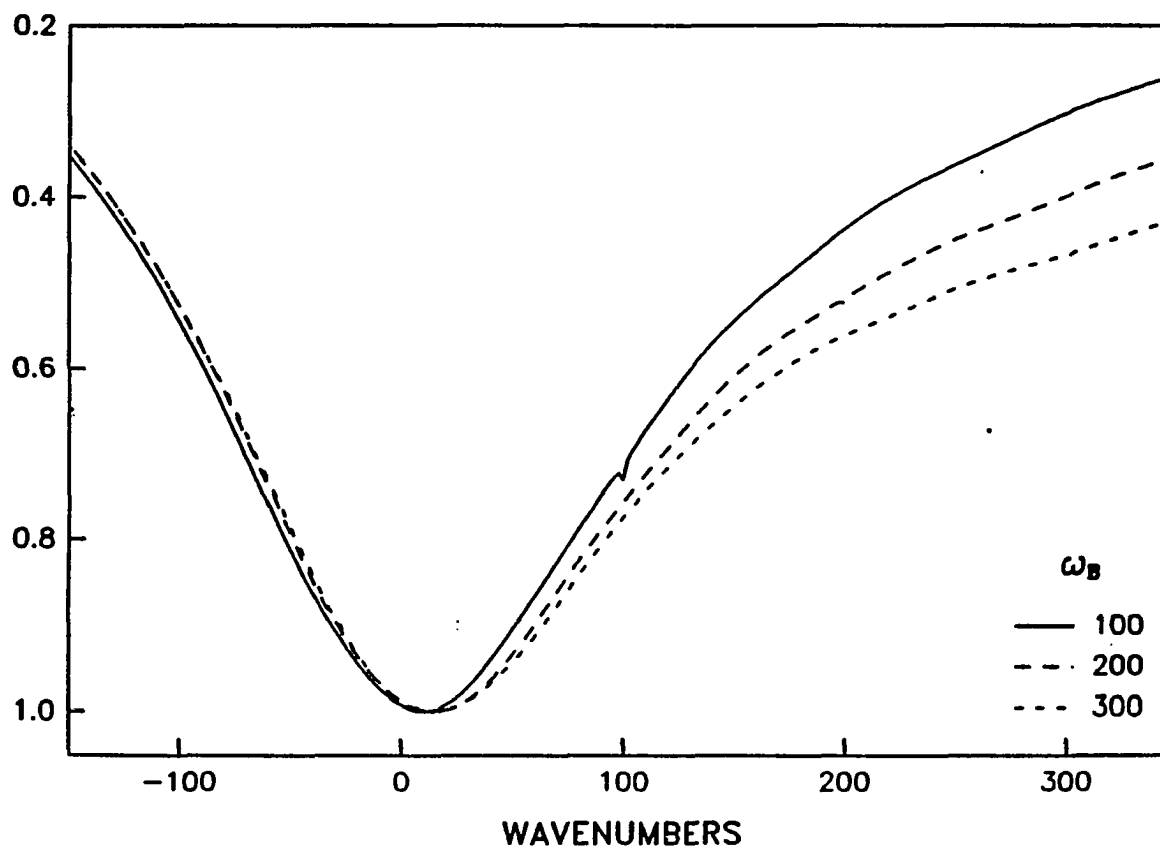


Figure 7. Hole spectra for P960 calculated according to Eqn. 25 with the parameters given in Table I.

Furthermore, fluorescence-line-narrowed spectra of aromatic molecules imbedded in low T glasses typically exhibit Γ values in the range 20-50 cm^{-1} . The calculated spectra of Fig. 6 are only slightly altered by decreasing Γ from 50 to 30 cm^{-1} . At 30 cm^{-1} phonon sideband progression structure, not noticeable in the experimental data, begins to appear. There is also a slight decrease in the hole width.

We turn now to P960 of Rps. viridis which also exhibits broad holes whose widths are similar to those observed for P870. However, the shifting of the hole maximum and variation of the holewidth with ω_m appear to be absent for P960. This can be understood if $\Gamma_{\text{inh}}(\text{P960})$ is significantly less than $\Gamma_{\text{inh}}(\text{P870})$ as required by Fig. 5. Given the similarity [28,30] in the reaction center structure for Rb. sphaeroides and Rps. viridis, the identical thermal broadening characteristics for P870 and P960 (vide supra) are reasonable. The calculated hole spectra for P960 obtained with the parameter values given in Table I are shown in Fig. 7. The values for S and ω_m are the same as those used for P870 but $\Gamma_{\text{inh}}(\text{P960})$ is reduced to 150 cm^{-1} . Note that with $\Gamma=40 \text{ cm}^{-1}$ some phonon progression structure is evident on the high-energy side of the holes. Increasing Γ to approx. 50 cm^{-1} smears out this structure while only increasing the holewidth 10-20 cm^{-1} . Figure 7 shows that the broad hole maximum is essentially insensitive to variations in ω_B as observed [12]. Furthermore and very importantly, the holes are nearly identical on the low-energy side while exhibiting deviations in the high-energy side which is also in accord with the experimental spectra [12]. Figure 7 indicates that under the appropriate conditions (high signal-to-noise ratio, $\omega_B \sim \nu_m \equiv 0$ and adequately high burn and reading resolutions) that a weak zero-phonon hole for P960 should be observable. Although the agreement between these calculations and the data of ref. 12 is perhaps less satisfying than the agreement of the experimental and calculated P870 data, the

main trends of ref. 12 are observed. At least in part, the deviation between calculated and experimental hole is attributable to requiring that the zero-phonon hole be absent from the calculated holes in agreement with experimental results. This was done while at the same time doing the calculations at a higher resolution than actually used in the experiments. In ref. 12 and 13 laser linewidths of approx. 2 cm^{-1} were used. These linewidths would result in an effective value for γ of approx. 4 cm^{-1} , rather than the value of 1 cm^{-1} used in the calculations which is consistent with the lifetime of P960.

P700 of PSI

An example of a broad hole burned spectrum for P700 of enriched (approx. 35:1) PSI particles from spinach chloroplasts is shown in Fig. 8 [9]. Superimposed on the broad hole is a weak but sharp zero-phonon hole coincident with ω_B . Such profiles have been observed for $700 < \lambda_B < 720 \text{ nm}$. Recent very high resolution (approx. 0.002 cm^{-1}) measurements have shown that the zero-phonon holewidths is approx. 0.05 cm^{-1} [14], which is a factor of 2 narrower than the value reported in ref. 9 where the read resolution used was lower. The implications of the zero-phonon holewidth are considered later. In Fig. 8 the increase in absorption at $\sim 14540 \text{ cm}^{-1}$ is most likely due to electrochromic shifts of the core antenna chlorophyll absorptions resulting from the reaction center charge separation process [31,32]. The presence of the intense broad hole whose width is comparable to those observed for P870 and P960 immediately indicates that the linear electron-phonon coupling for P700 is also very strong. Unfortunately, theoretical calculations cannot be guided by temperature-dependent absorption and fluorescence data for P700 due to spectral interference from the core antenna state C670. Reliable P700 Stokes

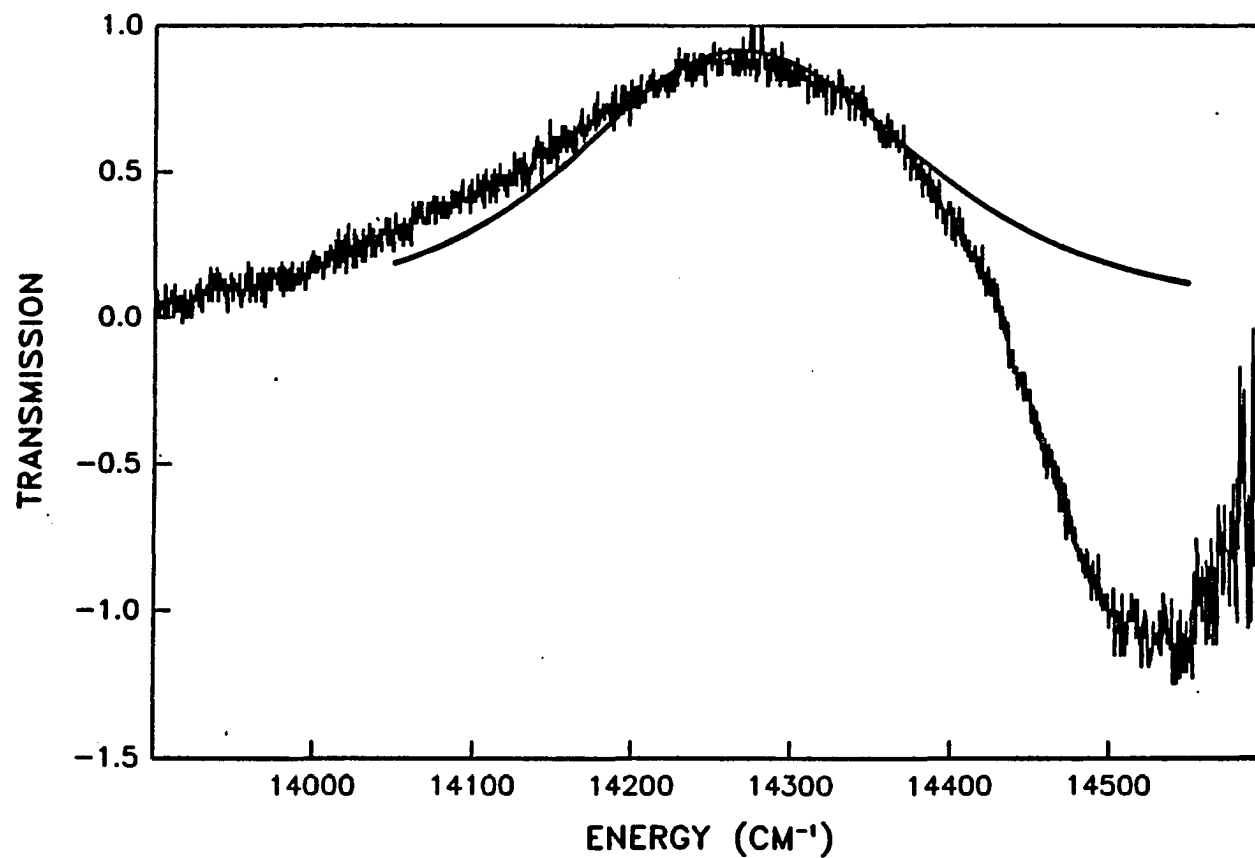


Figure 8. Calculated and experimental hole spectra for P700. The calculated spectrum has been shifted 30 cm^{-1} to lower energy so that the zero-phonon holes of both spectra can be seen. The experimental hole was produced by burning for 10 min with $100 \mu\text{W}/\text{cm}^2$ at 14284 cm^{-1} .

shift data are also not available. Nevertheless, reasonable agreement with the P700 due hole burning data [9] was achieved with Eqn. 25 for $S=7$, $\omega_m=30 \text{ cm}^{-1}$, $\Gamma=30 \text{ cm}^{-1}$, $\Gamma_{inh}=300 \text{ cm}^{-1}$, and $\gamma=0.06 \text{ cm}^{-1}$ [9].

As discussed earlier, Eqn. 25 predicts that the intensity ratio of the zero-phonon to phonon hole is given by e^{-2S} . In ref. 9 the expression e^{-S} was inadvertently used which yielded $S=7.1$ from the measured ratio of 1:1200. Utilization of the correct expression obviously yields $S=3.5$. This value with the other parameters fixed at values used in ref. 9 yields hole spectra with phonon progressional structure which should be (but is not) observable under experimental conditions of ref. 9. At this time we are reticent to change the values of $\omega_m=30 \text{ cm}^{-1}$ and $\Gamma\sim 30 \text{ cm}^{-1}$, since a direct measurement of the one-phonon profile for C670 (albeit a different state) yields these values within experimental uncertainty. The value of $\Gamma_{inh}\sim 300 \text{ cm}^{-1}$ will also be maintained, since the C670 absorption profile, which exhibits barely but, nevertheless, discernible structure due to chlorophyll a pigments in different environments, can be fit with Gaussian profiles with widths of $\sim 300 \text{ cm}^{-1}$ [33]. With these parameters set, the experimental P700 hole profile can be fit for $S\sim 5$ or 6 (Table I) (Fig. 8). This increase in S beyond the value of 4 is not unreasonable since Eqn. 25 is only valid for the short burn time limit (where experimental measurements are difficult to make). Thus, the value of S determined with e^{-2S} and the data must be viewed as a lower limit [14]. With the parameter values of Table I, the calculated spectrum is in reasonable agreement with the experimental spectrum.

DISCUSSION

The theoretical approach taken here satisfactorily accounts for the principal characteristics of the photochemical hole spectra of the P700, P870, and P960 primary electron donor states. The calculations indicate that the linear electron-phonon coupling for all three state is very strong ($S \gg 1$) and that the site inhomogeneous broadening contribution to the absorption profile is large, Table I. For P870 and P960, the interplay between hole burning, thermal broadening, and Stokes shift data for determining of S , ω_m , and Γ_{inh} were essential. The interrelationships between these types of data were not taken into account in the earliest interpretations of the hole-burning data [10-13].

As improved and more complete data sets become available the values for S , ω_m , and Γ_{inh} given in Table I will undergo refinement but not to the extent which would negate the two principal conclusions stated above. Of possible concern is that the value of $\omega_m = 80 \text{ cm}^{-1}$ for P870 and P960 was determined primarily from the thermal broadening data for ethylene glycol/water glass while the hole burning experiments of Boxer and coworkers [10,12] were performed using poly(vinyl alcohol) (PVOH) films. However, the thermal absorption broadening characteristics of P870 and P960 in gelatin and PVOH films are (Holten and Kirmaier, unpublished data, Department of Chemistry, Washington University) are very similar to those shown in Fig. 5. This, even though the absorption peak positions and residual low T widths exhibit a measurable dependence on the host (e.g., $\Gamma_{abs}(P960) = 494 \text{ cm}^{-1}$ in gelatin, $\Gamma_{abs}(P870) \sim 600 \text{ cm}^{-1}$ in PVOH). The dependence of $\Gamma_{abs}(0 \text{ K})$ on host solvent indicates a dependence of Γ_{inh} on host due to solvent perturbation of the special pair. To our knowledge, however, a correlation between the magnitude of

Γ_{inh} and the nature (strength) of the electron-phonon coupling has not been observed for any molecular system. Therefore, the conclusions that ω_m is insensitive to the host and that ω_m is determined by the special pair-protein complex are reasonable. A related question is why Γ_{inh} (P870) appears generally to be greater than Γ_{inh} (P960) for a given host. The answer may involve solvent penetration, since the special pair of *Rps. viridis* is 'capped' by cytochrome c [28], whereas this is not the case for *Rb. sphaeroides*[30]. If so, the disparity in Γ_{inh} is of no biological significance although it should be noted that a consideration of the energetic inequivalence of the two monomers of the special pair is necessary for the interpretation of data which speak to excitonic effects of the special pair. That is, in addition to the inequivalence resulting from interactions with the protein environment a contribution from solvent may be necessary. On the other hand, the disparity in Γ_{inh} may be a consequence of a varying degree of intrinsic disorder in the isolated reaction center of the two bacterial systems.

The values of 50 and 40 cm^{-1} for Γ of P870 and P960, Table I, deserve some comment. They cover a reasonable range based on the fluorescence line-narrowed and hole-burned spectra of a large number of chromophores imbedded in glass and polymer hosts and the direct measurement of $\Gamma \sim 40 \text{ cm}^{-1}$ for C670 [14] (Table I). However, little significance should be attached to the difference in Γ between P870 and P960, since the value of Γ for P960 can be increased to approx. 50 cm^{-1} without significantly affecting the calculated hole spectra (increasing Γ leads to slight additional hole broadening).

Before discussing the P700 results it is appropriate to consider the underlying assumptions of the theory. First, it is based on the linear coupling approximation. Second, the one-phonon profile is characterized by a single maximum (mean

phonon frequency, ω_m). Third, the r-phonon profiles are described as Lorentzians with a width $\Gamma_r = r^{1/2}\Gamma$ for $r \geq 1$. The Lorentzian assumption is made so that a physically transparent analytic hole shape can be obtained. Even though r-phonon profiles are probably more accurately described by an asymmetric Gaussian (tailing more slowly on the high energy side), the essential characteristics for the case of coupling to the continuum of phonons, such as the dependence of the broad hole maximum and width on ω_B , are not significantly affected by utilization of Lorentzians. The employment of the Gaussian relationship $\Gamma_r = r^{1/2}\Gamma$ with a Lorentzian serves to mimic a Gaussian behavior for the width of the 2- and higher-phonon profiles. On the other hand, the theory is also valid for the case where the one-phonon profile is associated with a pseudo-localized mode at ω_m . Now Γ is determined by the distribution in values of ω_m (from disorder) and a homogeneous contribution from harmonic relaxation of the pseudolocal model into the continuum of bath phonons [20]. When the latter is dominant, a Lorentzian for the one-phonon profile would be appropriate. The second assumption is consistent with the majority of one-phonon profiles observed in the fluorescence line-narrowed and hole-burned spectra of molecules imbedded in glasses and polymers and the one-phonon profile observed for C670 [14]. Nevertheless, the theory is readily modified to take into account a multi-peaked one-phonon profile. We have done this and performed calculations with a bimodal distribution (ω_{m1}, ω_{m2}). The total Huang-Rhys factor S is $S_1 + S_2$ with a contribution from both components. As expected (because of the additional adjustable parameters), better agreement is obtained especially for P960. However, until independent confirmation of bimodal structure is obtained, it would be premature to present these results. The first assumption means that the quadratic electron-phonon coupling, which defines the changes in phonon frequencies upon

pigment excitation, has been neglected. Provided these are not large ($\leq 20\%$), Eqn. 25 is still accurate. However, the quadratic coupling can contribute to the thermal broadening of the absorption (fluorescence) profiles [18,19]. In the harmonic approximation it alone governs the temperature dependence of the absorption maximum [18,19]. We have performed detailed studies of the lineshift for both P870 and P960 (ethylene glycol/water glass). Both absorption bands exhibit a significant blue shift with increasing temperature which is adequately fit by the quadratic coupling expression $\omega_1^2(\delta_1^2-1)(4\omega_1)^{-1}\coth(\hbar\omega_1/2kT)$, where ω_1 is the ground-state phonon frequency [18] and where $\delta_1=\omega_1'/\omega_1$, with ω_1' the frequency for the excited electronic state. It is found that $\omega_1=84$ and 124 cm^{-1} for P870 and P960, respectively. These values are in reasonable agreement with those obtainable from the data of Holten and Kirmaier (unpublished data) on P870 and P960 in a gelatin film. We note first that it is difficult to understand how low-frequency modes could undergo such dramatic increases in frequency. Second, our calculations show that the thermal broadening from the sequence structure from such modes combined with a contribution from the linear electron-phonon coupling are inconsistent with the thermal broadening data. We conclude, therefore, that the thermal lineshifts of P870 and P960 arise from the anharmonic terms which affect the thermal expansivity of the reaction center but do not contribute significantly to the thermal broadening. We note that the lineshifts associated with the bacteriochlorophyll and the bacteriopheophytin monomer absorption bands, Fig. 4a and b, are negligible between 4 and $\sim 200\text{ K}$ (limit of our experiments). This suggests the special pair geometry may have a significant dependence on the thermal expansivity.

We consider next the results for P700 and C670 (Table I). For C670 the direct observation of the one-phonon profile building on the zero-phonon establish that the

linear coupling is weak ($S < 0.9$) [14]. The implication of this for excitation transport from the core antenna to P700 is discussed elsewhere [14]. More important for this paper is that direct measurement of $\omega_m \sim 30$ and $\Gamma \sim 40 \text{ cm}^{-1}$ for C670 was possible. The $\omega_m = \Gamma = 30 \text{ cm}^{-1}$ values for P700 were used in our earlier calculations [9], which preceded the C670 studies. In view of the C670 results, these values for P700 are preserved in this paper, although it should be emphasized that ω_m for C670 and P700 could, in principle, be different. The lack of reliable Stokes shift and thermal broadening data for P700 is unfortunate, since, as emphasized earlier, they provide a valuable check on the ω_m value. With ω_m and Γ fixed, the determination of S for P700 was dictated by the observation of a zero-phonon hole and its weak intensity relative to the broad hole whose width is comparable to those observed for P870 and P960. The sharpness of the zero-phonon hole (approx. 0.05 cm^{-1} [14]) means that S cannot be reduced as low as 4, since for this value it would be too intense (peak height) in comparison with the experimental spectra. Maslov et al. [8] have noted that the zero-phonon hole for Chlamydomonas reinhardtii cannot be burned when the burning is preceded by white light bleach of P700 at low temperature. This suggested that the sharp hole is associated with electron transfer from P700 [8]. Nevertheless, one cannot exclude the possibility that the sharp hole is not due to P700 but rather long-wavelength absorbing chlorophyll a species which are strongly coupled to the reaction center. The reason for mentioning this is that the zero-phonon holewidth provides a lower limit for electron transfer from P700 to A_0 (primary acceptor of PSI) of approx. 200 psec [14]. In view of the time-domain studies [34,35] of the T-dependence of electron transfer from P870, this result is surprising. These studies show that the transfer time decreases by a factor of approx. 2 in going from room temperature (where the value is approx. 5 psec) to

cryogenic temperatures. Recent time domain studies have yielded values of 10 psec [36] and 2.8 psec [37] for P700 at room temperature. However, care must be taken when comparing the time domain and hole-burning data. The zero-phonon holewidth could reflect the dynamics of the zero-point level of P700, whereas the states initially prepared in the time domain experiments form a multi-phononic distribution. Provided that (i) thermalization of protein baths phonons is not completely prior to electron transfer and (ii) the nuclear barrier associated with electron transfer is larger than typical phonon frequencies (approx. 30 cm^{-1}), the low temperature hole burning result can be qualitatively understood. However, the preliminary results of our very recent hole-burning experiments following chemical and white light bleaching of P700 indicate that the sharp zero-phonon hole is not associated with P700 that is photoactive at liquid helium temperature (in contradiction with results of Maslov et al. [8]). More extensive experiments of this type are in progress. The recent bleaching experiments do confirm that the broad intense hole is due to photoactive P700 so that our conclusion that P700 is characterized by strong electron-phonon coupling is unaltered.

As noted in the Introduction, the nature of the phonons which are active in the primary electron donor state absorption (hole burning) is not known. Two possibilities are: spatially delocalized modes associated with the protein complex and highly localized modes associated with the special pair (e.g., intra-dimer monomer ... monomer stretch). We tentatively favor the former, since for P870 approx. 80 cm^{-1} phonons have been implicated as the key Franck-Condon nuclear tunneling modes associated with electron transfer to the bacteriopheophytin monomer as well as in the subsequent reduction of the quinone [15]. In addition, approx. 30 cm^{-1} phonons have been observed for the chlorophyll a monomers of

C670 [14] and have been implicated as the key acceptor modes for excitation transport from C670 to P700 [14]. Thus, low-frequency phonons also appear to be active in processes involving pigment monomers. Of course, for the special pair the distinction between protein and dimer modes can be artificial if dynamical mixing is significant (due to their comparable frequencies).

The question of why the linear electron-phonon coupling is strong for P700, P870, and P960, but weak for C670 (and chlorophyllic monomers in matrices [26]) is very important. High-resolution optical data on a large number of molecular crystals have shown that Huang-Rhys factors as large or greater than approx. 4 generally exist only for excited states which possess significant charge-transfer character, e.g., the charge-transfer state of π -molecular donor-acceptor complexes [38]. This was the basis for an earlier conclusion [17] that the primary electron donor states P870 and P960 possess significant charge-transfer character in addition to neutral excitonic character. Significant charge-transfer character is consistent with the theoretical findings of Parson et al. [39] and Warshel and Parson [40] who consider mixing of the pure charge-transfer states of the dimer with the neutral excitonic state. Since then, this conclusion has been supported by Stark results which revealed that the permanent excited state dipole moment of P870 [41,42] is large (7-8 D) and roughly parallel to the Mg...Mg axis of the special pair. Since it is difficult to conceive of a way in which a monomer can support significant charge-transfer character for its Q_y state, it has been suggested that P700 is also a special pair [9], a point of continuing controversy (ref. 43 and references therein).

Finally, we comment on the differences between the interpretation put forth here for the primary electron donor state hole profile and that of Meech et al. [13]. The interpretation initially favored by Boxer and coworkers [10] is similar to that

presented in ref. 13. Within this qualitative model the large holewidths (approx. 400 cm^{-1}) for P870 and P960 is ascribed to homogeneous broadening resulting from an ultra-fast (approx. 25 fsec) charge-separation process which precedes electron transfer to the bacteriopheophytin. The initially prepared primary electron donor state is viewed as a neutral excitonic state that decays primarily into an intra-dimer charge-transfer state. Subsequent to this, evolution to an interdimer state involving a BChl monomer is postulated to occur. Electron-phonon (vibration) coupling and inhomogeneous broadening were not taken into account and calculated hole spectra were not presented [13]. Very recently [44] Won and Friesner have taken both of these effects into account in a model in which the initially prepared state (P870 and P960) is viewed as a mixed state with significant charge-transfer character (within the adiabatic Born-Oppenheimer approximation). Thus there are definite similarities between their model and ours [17] which we have considered in detail here. However, a major difference stems from the fact that Won and Friesner assume that the electron-phonon (and vibration) coupling is weak which means that the absence of a sharp zero-phonon hole in their calculated spectra for P960 is due to breakdown of the Born-Oppenheimer approximation associated with ultra-fast decay of the primary electron donor state into charge-separated states of the reaction center. It is at this time not clear whether the parameter values chosen by Won and Friesner for their multi-parameter model are consistent with the thermal broadening and Stokes shift data for P960. Within our model, ultra-fast decay of the primary electron donor state need not be invoked to account for the data, since (within the Born-Oppenheimer approximation) the primary electron donor state's significant charge-transfer character leads directly to strong linear electron-phonon coupling which renders the sharp zero-phonon holes very weak. We are not aware of any

optical spectra for charge-transfer states of π -molecular systems that do not clearly indicate strong electron-phonon coupling. In our model the primary electron donor state is dirty in the sense that the absorption profile is determined by transitions to a wide distribution of mixed exciton-phonon levels. The primary electron donor state possesses significant charge-transfer character which leads to a large permanent dipole and its associated strong linear electron-phonon coupling. We can note that Warshel and Parson [40] conclude that charge-transfer character can arise from mixing of the neutral excitonic and charge-transfer states of the special pair itself.

CONCLUSIONS

A theory for spectral hole burning has been developed that is valid for arbitrarily strong linear electron-phonon coupling and large site inhomogeneous line broadening. The Condon approximation is employed for the phonons which is known to be accurate for strongly allowed optical transitions, such as those of the photosynthetic pigments. The model calculations show that detailed studies of the hole profile dependence on the burn frequency (ω_B) can determine the site inhomogeneous line broadening (Γ_{inh}), the center of gravity of the zero-phonon site excitation energy distribution function relative to the absorption maximum, the Huang-Rhys factor (S) and effective phonon frequency (ω_m). For the case of strong linear coupling, the connection between hole burning and thermal broadening data for the absorbing state has been given.

The theory successfully accounts for the gross and many fine features of the hole spectra for the primary electron donor states P870, P960, and P700. The unifying picture which emerges is that the primary electron donor states are characterized by strong linear coupling ($S \geq 4$) and large Γ_{inh} . It had been suggested earlier [9] that the strong coupling states possess a significant charge-transfer character. Such character is supported by the recent Stark measurements [41]. The hole burning data suggests that P700, like P870 and P960, is a special pair. The large Γ_{inh} contribution to a primary electron donor state absorption profile reflects the distribution of zero-phonon transition frequencies associated with an ensemble of spatially separated reaction center. Thus, there is no direct connection between Γ_{inh} and an average value for the energetic inequivalence (δE) between the Q_y states of the monomers of a special pair. Nevertheless, it is known that protein

interactions render the two monomers inequivalent [45]. The value of Γ_{inh} serves as an indicator for the magnitude of δE . For the interpretation of data which speak to excitonic resonance effects within a special pair, a consideration of the magnitudes of δE , the excitonic resonance matrix element, and the homogeneous linewidth of the Q_y state is necessary.

The results presented here, together with the hole burning data for C670 [14] and those from temperature-dependent time domain studies on the primary and secondary [15] electron-transfer processes of the reaction center of Rb.sphaeroides should be viewed as a whole. In doing so it becomes apparent that the linear electron-phonon coupling may play an important role in the early events of photosynthesis. These include population of the primary electron donor state by excitation transport from the antenna or by direct optical excitation, and the primary electron-transfer from the primary electron donor state. Detailed quantum-mechanical transport theories which take into account strong linear coupling will need to address also the question of the distribution of pigment-state energies due to protein inhomogeneity. It is interesting to note that a large distribution width for the energy gap associated with a donor \Rightarrow acceptor transport process is effectively compensated for by a large Huang-Rhys factor. An example of such a process would be the final trapping step in excitation transport from the antenna to primary electron donor state.

Finally, it appears that spectral hole burning is powerful and generally applicable technique for probing the excited state structure and dynamics of photosynthetic system. Very recently, hole burning and fluorescence line narrowing have been successfully applied by Avarmaa and Jaaniso [46] to the antenna chlorophyll of etiolated leaves. There would appear to be no reason why hole

burning cannot be applied to a variety of pigment-protein complexes which have not been studied, e.g., PSII of green plants. In view of the recent calculations of Scherer and Fischer [47,48] and Warshel et al. [49] on the electronic structure and electron-transfer dynamics of the reaction center of *Rps. viridis* it would also appear to be profitable to perform more extensive hole-burning experiments in the region of the P960 absorption (also P870). These calculations indicate that the absorbing charge-separated states involving the special pair, the BChl monomer and bacteriopheophytin may be located in the near energetic vicinity of the primary electron donor state.

REFERENCES

1. Kharlamov, B. M.; Personov, R. I.; Bykovskaya, L. A. *Opt. Commun.* 1974, 1, 191.
2. Kharlamov, B. M.; Personov, R. I.; Bykovskaya, L. A. *Opt. Spectrosc.* 195, 39, 137.
3. Gorokhovskii, A. A.; Karli, R. K.; Rebane, L. A. *JETP Lett.* 1974, 20, 216.
4. Small, G. J. In Spectroscopy and Excitation Dynamics of Condensed Molecular Systems; Agranovich, V. M., Hochstrasser, R. M., Eds.; Elsevier/North Holland: Amsterdam, 1983, p 515.
5. Friedrich, J.; Haarer, H. In Optical Spectroscopy of Glasses; Zschokke, I., Ed.; Reidel: Dordrecht, 1986, p 149.
6. Rebane, L. A.; Gorokhovskii, A. A.; Kikas, J. V. *Appl. Phys.* 1982, B29, 235.
7. Hayes, J. M.; Jankowiak, R.; Small, G. J. In Persistent Spectral Hole-Burning: Science and Application; Moerner, W. E., Ed.; Springer-Verlag: West Berlin, 1988, p 153.
8. Maslov, V. G.; Chunaev, A. S.; Tugarinov, V. V. *Mol. Biol.* 1981, 15, 788.
9. Gillie, J. K.; Fearey, B. L.; Hayes, J. M.; Small, G. J.; Golbeck, J. H. *Chem. Phys. Lett.* 1987, 134, 316.
10. Boxer, S. G.; Lockhart, D. J.; Middendorf, T. R. *Chem. Phys. Lett.* 1986, 121, 476.
11. Meech, S. R.; Hoff, A. J.; Wiersma, D. A. *Chem. Phys. Lett.* 1985, 121, 287.
12. Boxer, S. G.; Middendorf, T. R.; Lockhart, D. J. *FEBS Lett.* 1986, 200, 237.
13. Meech, S. R.; Hoff, A. J.; Wiersma, D. A. *Proc. Natl. Acad. Sci. USA* 1986, 83, 9464.

14. Gillie, J. K.; Hayes, J. M.; Small, G. J.; Golbeck, J. H. *J. Phys. Chem.* 1987, 91, 5524.
15. Bixon, M.; Jortner, J. *J. Phys. Chem.* 1986, 90, 3795.
16. Parson, W. W.; Woodbury, N. W. T.; Becker, M.; Kirmaier, C.; Holten, D. In Antennas and Reaction Centers of Photosynthetic Bacteria; Michel-Beyerle, M. E., Ed.; Springer-Verlag: Berlin, 1985, p 278.
17. Hayes, J. M.; Small, G. J. *J. Phys. Chem.* 1986, 90, 4928.
18. Scherer, P. O. J.; Fischer, S. F.; Hürber, J. K. H.; Michel-Beyerle, M. E. In Antennas and Reaction Centers of Photosynthetic Bacteria; Michel-Beyerle, M. E., Ed.; Springer-Verlag: Berlin, 1985, p 131.
19. Pryce, M. H. L. In Phonons in Perfect Lattices and Lattices with Point Defects; Stenenson, R. W. H., Ed.; Oliver and Boyd: London, 1965, p 403.
20. Rebane, K. K. Impurity Spectra of Solids; Plenum: New York, 1970.
21. Personov, R. I. In Spectroscopy and Excitation Dynamics of Condensed Molecular Systems; Agranovich, V. M., Hochstrasser, R. M., Eds.; Elsevier/North Holland: Amsterdam, 1983, p 515.
22. Huang, K.; Rhys, A. *Proc. Roy. Soc.* 1951, A208, 352.
23. Kikas, J. *Chem. Phys. Lett.* 1978, 57, 511.
24. Kharlomov, B. M.; Bykovskaya, L. A.; Personov, R. I. *Chem. Phys. Lett.* 1977, 50, 407.
25. Hayes, J. M.; Fearey, B. L.; Carter, T. P.; Small, G. J. *Int. Rev. Phys. Chem.* 1986, 5, 175.
26. Carter, T. P.; Small, G. J. *Chem. Phys. Lett.* 1985, 120, 178.

27. Woodbury, N. W. T.; Parson, W. W. *Biochim. Biophys. Acta* 1984, 767, 345.
28. Deisenhofer, J.; Epp, O.; Miki, K.; Huber, R.; Michel, H. *Nature* 1985, 318, 618.
29. Knapp, E. W.; Scherer, P. O. J.; Fischer, S. F. *Biochim. Biophys. Acta* 1986, 852, 295.
30. Chang, C. H.; Tiede, D.; Tang, J.; Smith, U.; Norris, J.; Schiffer, M. *FEBS Lett.* 1986, 205, 82.
31. Sétif, P.; Mathis, P.; Vängård, T. *Biochim. Biophys. Acta* 1972, 767, 404.
32. Schaffernicht, H.; Junge, W. *Photochem. Photobiol.* 1981, 34, 223.
33. Ikegami, I.; Itoh, S. *Biochim. Biophys. Acta* 1986, 851, 75.
34. Martin, J. L.; Breton, J.; Hoff, A. J.; Antonetti, A. *Proc. Natl. Acad. Sci. USA* 1986, 83, 957.
35. Wasielewski, M. R.; Teide, D. M. *FEBS Lett.* 1986, 204, 368.
36. Fenton, S. M.; Pellin, M. J.; Govindjee; Kaufman, K. J. *FEBS Lett.* 1976, 100, 1.
37. Owens, T. G.; Webb, S. P.; Mets, L.; Alberte, R. S.; Fleming, G. R. *Proc. Natl. Acad. Sci. USA* 1987, 84, 1532.
38. Brillante, A.; Philpott, M. R. *J. Phys. Chem.* 1980, 72, 4019.
39. Parson, W. W.; Scherz, A.; Warshel, A. In Antennas and Reaction Centers of Photosynthetic Bacteria; Michel-Beyerle, M. E., Ed.; Springer-Verlag: Berlin, 1985, p 122.
40. Warshel, A.; Parson, W. W. *J. Amer. Chem. Soc.* 1987, 109, 6143.
41. Lockhart, D. J.; Boxer, S. G. *Biochemistry*, 1987, 26, 664.

42. Scherer, P. O. J.; Fischer, S. F. Chem. Phys. Lett. 1986, 131, 153.
43. Rutherford, A. W.; Heathcote, P. Photosyn. Res. 1985, 6, 295.
44. Won, Y.; Friesner, R. A. Proc. Natl. Acad. Sci. USA 1987, 84, 5511.
45. Tiede, D. M. Biochemistry 1987, 26, 397.
46. Avarmaa, R. A.; Jaaniso, R. H. Proceedings of Modern Methods of Laser Spectroscopy of Molecules in Low-Temperature Media, Tallin, USSR.
47. Fischer, S. F.; Scherer, P. O. J. Chem. Phys. Lett. 1987, 115, 151.
48. Scherer, P. O. J.; Fischer, S. F. Chem. Phys. Lett. 1987, 141, 179.
49. Warshel, A.; Creighton, S.; Parson, W. W. J. Phys. Chem. 1988, 92, 2696.

ADDITIONAL RESULTS

The application of spectral hole burning to the photosynthetic reaction centers of green plant and purple bacteria has provided new information about the primary electron donor (PED) states. For example, structured transient hole burned spectra exhibiting four holes are obtained for the PED state P960 [40,41] and P870 [50] of Rps. viridis and Rb. sphaeroides, respectively. The hole spectrum for P960 and P870 is comprised of several relatively broad holes including a vibronic hole of $\sim 130 \text{ cm}^{-1}$ that builds on the lowest energy hole denoted as X. Hole X and its associated ZPH (coincident with λ_B) can be confidently assigned to the origin transition of the PED state of Rps. viridis and Rb. sphaeroides. The widths of the ZPH yield decay times that correlate well with those determined for P870* and P960* at 10 K by ultra-fast spectroscopy [24,51]. Observation of a zero-phonon hole supports the theory of Hayes and coworkers [38,39] since the theory of Won and Friesner [42-44] does not allow such observation.

The hole spectra for P680 [52], the primary electron donor of PSII, is also structured and consist of a zero-phonon hole (5 cm^{-1} width) and a broad ($\sim 130 \text{ cm}^{-1}$ width) hole. It bears resemblance to the hole burned spectrum of $|X\rangle^*$ for P960. The zero-phonon width yields a decay time of 1.9 psec at 4.2 K, consistent with 3 psec determined using femtosecond transient absorption at room temperature [53].

A zero-phonon hole (width $\sim 0.29 \text{ cm}^{-1}$) superimposed on a broad hole ($\sim 300 \text{ cm}^{-1}$) was reported for P700 of PSI [54]. The zero-phonon hole width corrected for instrument resolution yielded a decay time of ~ 90 psec and 1.6 K. This is inconsistent with the room temperature value of <10 psec [55-58] (assuming that the T-dependence for PSI is similar to that for P960 and P870), since the low

temperature decay time for P960 and P870 is known to decrease by 2X when cooled to cryogenic temperatures [51]. It has already been suggested on the basis of chemical and white light bleaching of P700 that the narrow hole is not associated with P700 that is active at liquid He temperatures [46].

This section reports new persistent photochemical hole burn profiles for P700 of PSI. The hole profiles at 1.6 K for a wide range of burn wavelengths (λ_B) are broad (FWHM $\sim 310 \text{ cm}^{-1}$) and for the 45:1 enriched particles studied exhibit no sharp zero-phonon hole feature coincident with λ_B . The λ_B -dependent hole profiles are analyzed using the theory of Hayes and Small [38] for hole burning in the presence of arbitrarily strong linear electron-phonon coupling. A Huang-Rhys factor S in the range 4-6 and a corresponding mean phonon frequency in the range $35\text{-}40 \text{ cm}^{-1}$ together with an inhomogeneous line broadening of $\sim 100 \text{ cm}^{-1}$ are found to provide good agreement with experiment. The zero-point level of P700* is determined to lie at $\sim 710 \text{ nm}$ at 1.6 K while the absorption maximum lies at $\sim 702 \text{ nm}$.

The hole burning was performed using a Ar^+ pumped ring dye laser with the laser dye LD688. The laser linewidth is $\sim 0.002 \text{ cm}^{-1}$. The enriched ($\sim 45:1$ Chl a:P700) Photosystem I particle from spinach chloroplast is dissolved in a glycerol: water mixture to which 1 mM ascorbic acid has been added. The solvent is buffered to $\text{pH} \sim 8.3$. A computer controlled double beam spectrometer operating at resolution of $\sim 0.2 \text{ cm}^{-1}$ was used for hole reading. The samples were held in the dark at room temperature for a few minutes before being quickly cooled (< 10 minutes) to 4.2 K. All the experiments were done at 1.6 K.

At 1.6 K the 45:1 PSI particles exhibit a principal absorption maximum near 670 nm due to Chl a of the core antenna complex and a distinct but weak shoulder

located near 700 nm, which represents P700, upper curve of Fig. 1. The three lower absorbance spectra correspond to burns of 1, 5 and 10 min with $I_B = 5 \mu\text{W}/\text{cm}^2$ and $\lambda_B = 701.8 \text{ nm}$. No ZPH could be observed coincident with this λ_B -value or several other values in the range between 701 and 715 nm. Under comparable burning conditions and read resolution, the earlier studied 35:1 particles exhibited a readily discernible, albeit weak, ZPH coincident with λ_B . From Fig. 2 it is apparent that the P700 hole is broad (ΔOD spectra are shown later).

The increase in absorption to higher energy of $\sim 700 \text{ nm}$ seen in the upper spectrum of Fig. 1 is due to the onset of the Chl a antenna absorption. Figure 2 shows a series of hole burned spectra obtained with $\lambda_B = 693.2 \text{ nm}$ (the upper spectrum is the pre-burn spectrum). At this wavelength absorption by the core antenna complex is dominant but there is some absorption due to the high energy side of the P700 absorption profile. The second and third curves of Fig. 2 are the hole burned spectra obtained with $I_B = 5 \mu\text{W}/\text{cm}^2$ for burn times of 1 and 10 min. Although not apparent from the figure, a weak ZPH is observed for the 10 min burn. The lowest spectrum of Fig. 2 was obtained after an additional 5 min burn with $I_B = 2 \text{ W}/\text{cm}^2$ and clearly shows a ZPH coincident with λ_B . The ZPH is ascribed to NPHB of the antenna Chl a [46,47] and not P700 since the ZPH could not be observed for λ_B -values selective for P700. Although excitation transport within the core antenna complex is significantly slower at 1.6 K than at room T, the quantum efficiency for excitation trapping by P700 is still close to unity [47]. On the other hand, the NPHB quantum efficiency for the antenna Chl a is significantly less than unity [59,60]. This explains why the ZPH develops at higher burn fluences than the P700 hole.

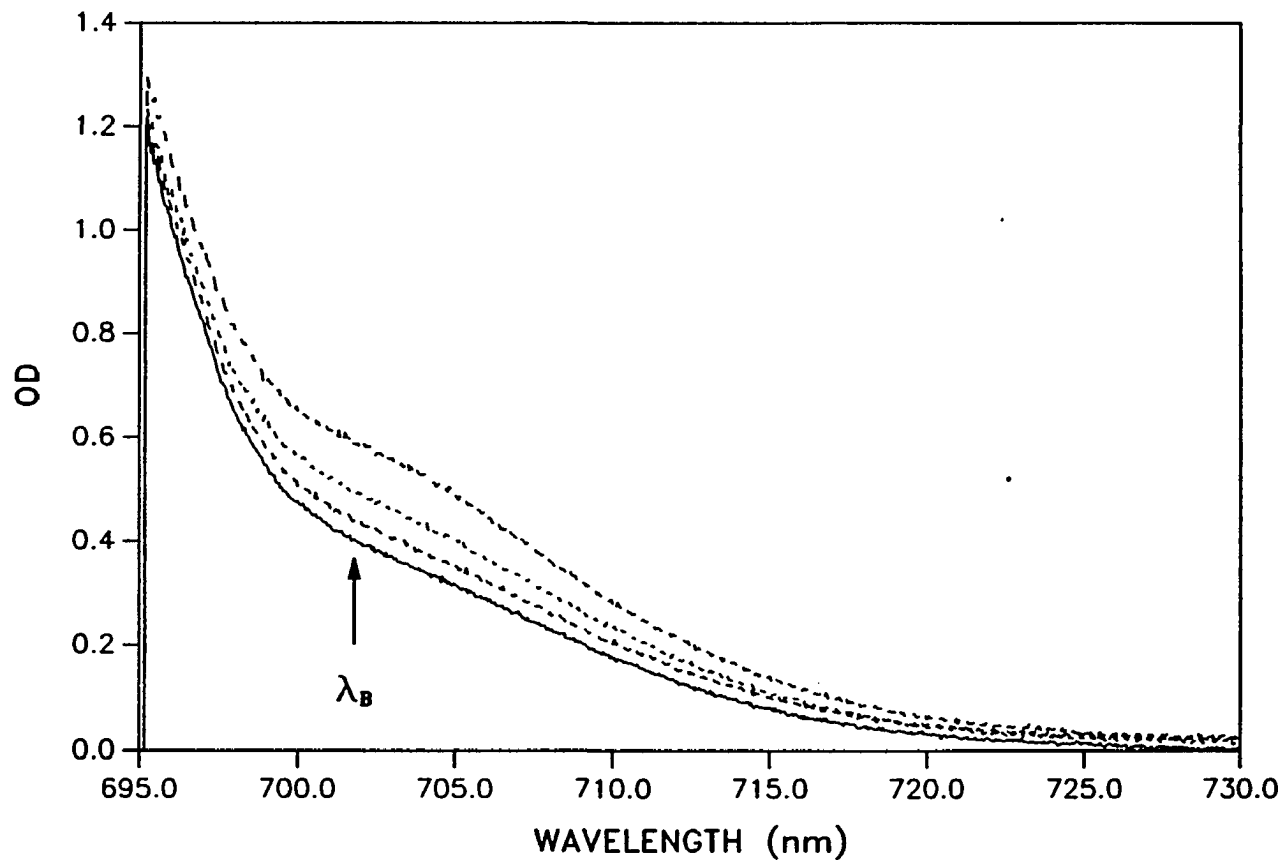


Figure 1. Burn time dependence of the P700 bleaching at 1.6 K for 45:1 PSI particles, $\lambda_B = 701.8$ nm, $T = 1.6$ K. The top curve is the preburn spectrum. Burn times (second to fourth) are 1, 5, 10 min with burn intensity $I_B = 5 \mu\text{W}/\text{cm}^2$.

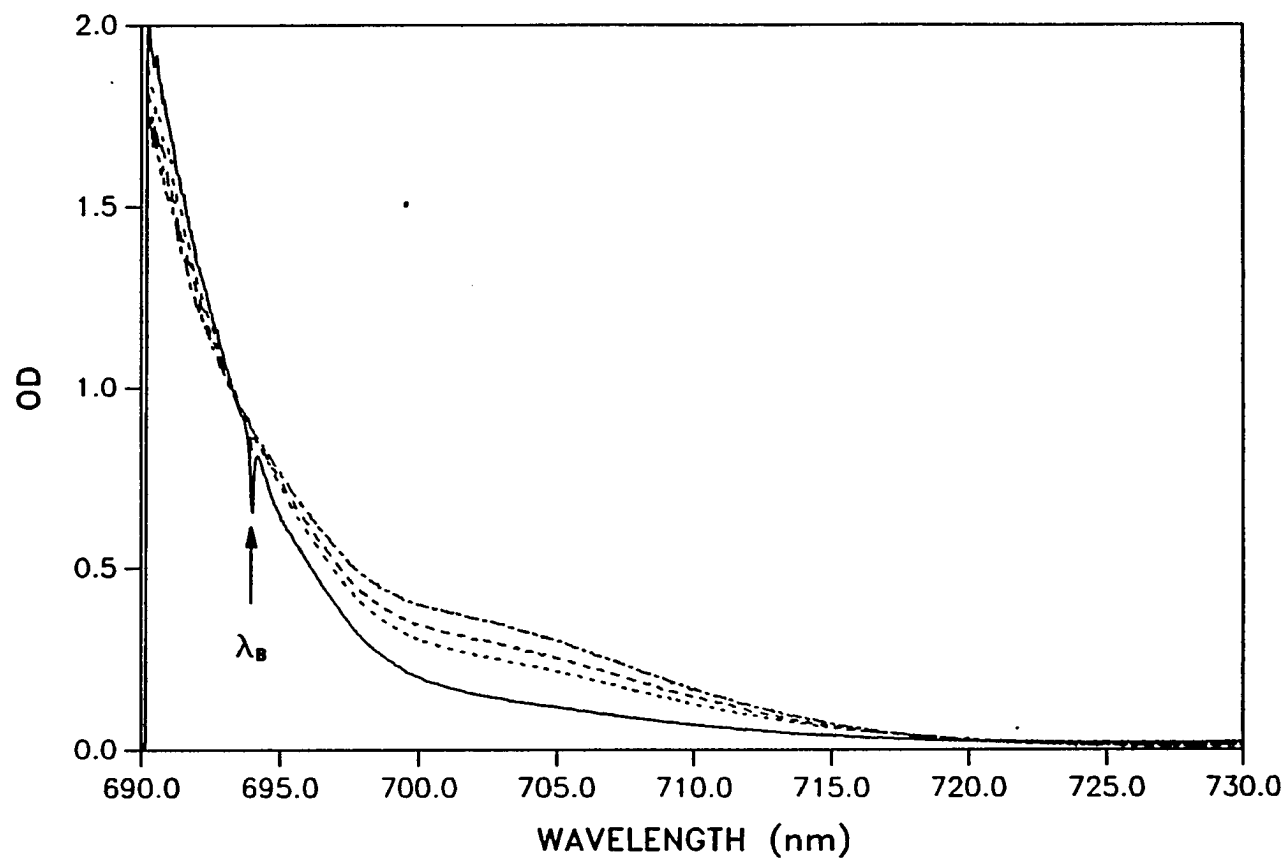


Figure 2. Burn time dependence of the P700 bleaching for 45:1 particles, $\lambda_B = 693.2 \text{ nm}$, $T = 1.6 \text{ K}$. The upper spectrum is the preburn spectrum. Burn times for the second and third spectra are 1 and 10 min, respectively, with $I_B = 5 \mu\text{W/cm}^2$. The lowest spectrum was obtained by an additional 5 min burn with $I_B = 2 \text{ W/cm}^2$. The ZPH is ascribed to NPHB of the antenna Chl *a*, see text.

Figure 3 shows the ΔOD hole burned spectrum obtained with $\lambda_B = 680.5$ nm, which is close to the maximum of the antenna Chl a absorption at 670 nm. At 680.5 nm the P700 absorption is negligible. The saturated ZPH at λ_B , due to NPHB of antenna Chl a, is intense and accompanied by the real- and pseudo-PSBH (displaced by $\omega_m \sim 20$ cm⁻¹) [46,47]. The broad positive going feature at ~ 675 nm is the anti-hole associated with NPHB [47]. The increase in noise in the vicinity of the anti-hole is due to the high O.D. near the absorption maximum. The broad P700 hole, produced by trapping of the antenna excitation, is also evident in the figure with a maximum near 702 nm.

The P700 ΔOD hole profiles obtained for $\lambda_B = 715.0$ and 706.5 nm are shown in Fig. 4 and the profile for $\lambda_B = 702.6$ nm in Fig. 5. The absorption by the antenna Chl a at these wavelengths is weak in comparison to P700. The maxima of the P700 holes for $\lambda_B = 715.0, 706.5$ and 702.6 nm are located at 705, 703 and 702 nm, respectively, and again, no sharp ZPH is observed coincident with λ_B . The solid curves are fits to the spectra obtained using the theory of Hayes and Small [38] (see also Paper II of this section).

Application of the theory to the hole profiles of P700 is more difficult than for the other PED states, e.g., P680, since resolved phonon structure and the ZPH are not observed. Furthermore, the Stokes shift associated with the P700 emission ($\sim 2S\omega_m$) is not known. However, we can determine that $S \gtrsim 4.5$. Otherwise, a ZPH coincident with ω_B should have been observed (given the signal/noise ratio of our spectra) for $\gamma = 1$ cm⁻¹. This value of γ corresponds to the lifetime of P700 determined at ice temperature [58]. If this lifetime were to decrease by a factor of about 2 in the low temperature limit, which is a possibility given the data for P870 [24,51], P960 [51] and P680 [52,53], a value of S closer to 4 would preclude

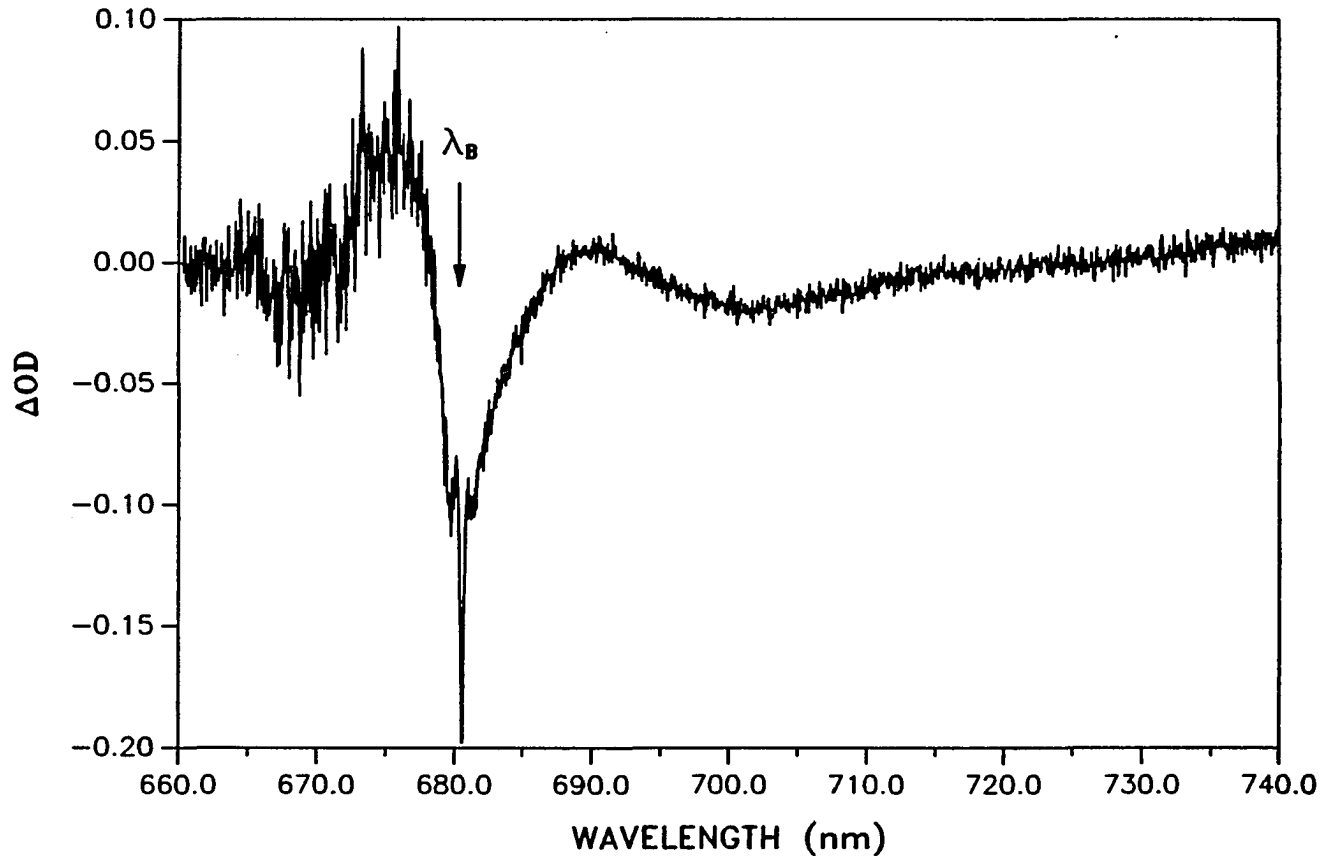


Figure 3. Difference absorbance (ΔOD) hole burned spectrum of P700 for 45:1 particles, $\lambda_B = 680.5$ nm, $T = 1.6$ K. Excitation was for 10 min with $I_B = 50 \mu W/cm^2$. The ZPH at λ_B and phonon sideband holes displaced from λ_B by $\sim 20 \text{ cm}^{-1}$ are due to NPHB, see text. The broad hole centered at ~ 702 nm is due to bleaching of the P700 absorption profile. For the spectrum shown here, saturation of the ZPH and phonon sideband holes gives the false impression that the linear electron-phonon coupling is stronger than reported earlier for antenna Chl *a* [see Section II]. The increase in noise in the anti-hole region near 675 nm is due to the high O.D. of the sample near the absorption maximum (~ 670 nm).

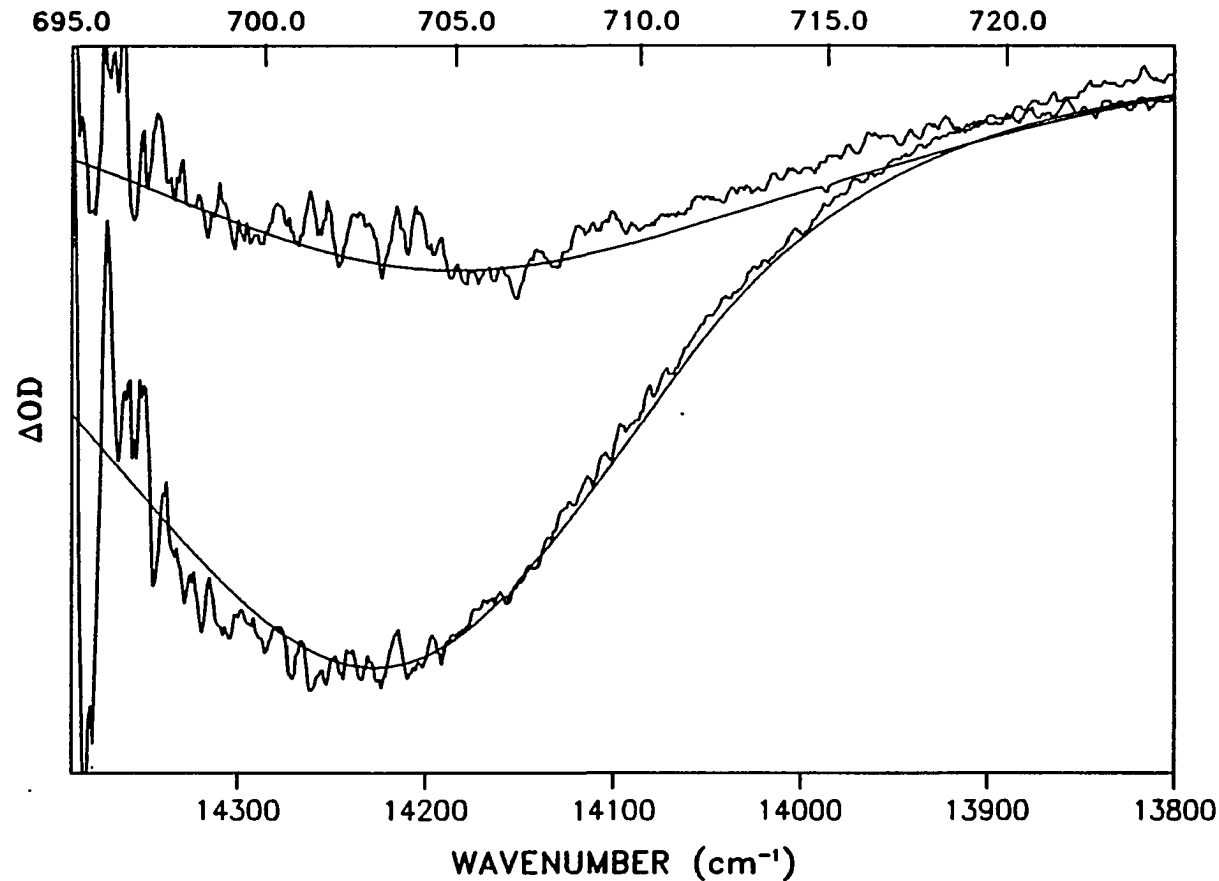


Figure 4. Difference absorbance hole burned spectra of P700 for 45:1 particles, $\lambda_B = 715.0$ nm and $= 706.2$ nm (top to bottom, respectively), $T = 1.6$ K. The ΔOD scale is 0.2. Burn time was 30 sec with $I_B = 10$ $\mu W/cm^2$. The solid lines are computed fits with $S = 4.5$, $\omega_m = 45$ cm^{-1} , $\Gamma_I = 1$ cm^{-1} , $\gamma = 1$ cm^{-1} , and $\nu_m = 14085$ cm^{-1} . The calculated spectrum for $\lambda_B = 715$ nm exhibits a very weak ZPH which could not be expected to be observable given the signal to noise ratio of the experimental spectrum. The top ordinate scale is wavelength (nm).

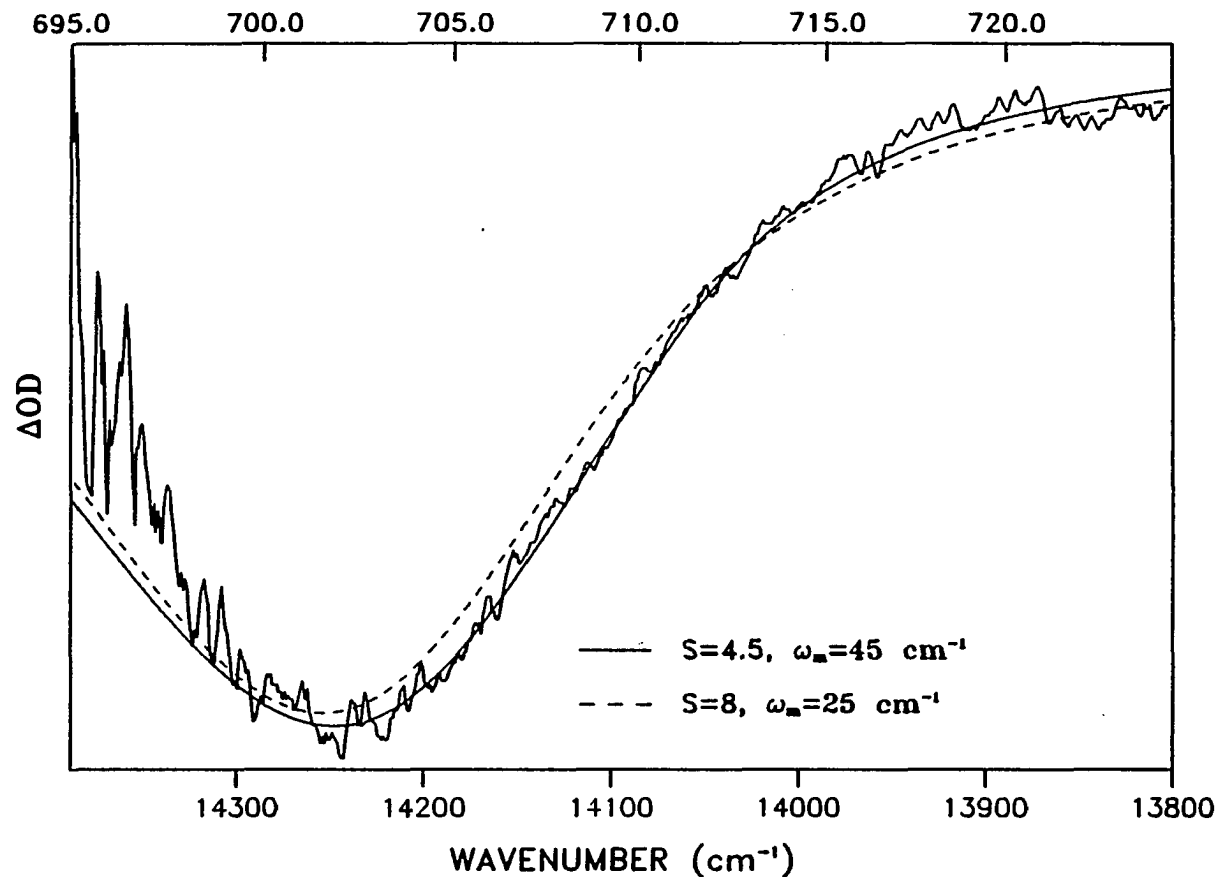


Figure 5. Difference absorbance hole burned spectrum of P700 for 45:1 particles, $\lambda_B = 702.6$ nm, $T = 1.6$ K. The ΔOD scale is 0.2. Burn time was 30 sec with $I_B = 10 \mu W/cm^2$. The solid and broken lines are computed fits with $S = 4.5$ and $\omega_m = 45 \text{ cm}^{-1}$ (—) or $S = 8$ and $\omega_m = 25 \text{ cm}^{-1}$ (---). See Fig. 5 caption for other parameter values. The top ordinate scale is wavelength (nm).

observation of the ZPH in our spectra for PSI-45. In our earlier work with PSI-35 particles [54] a value of $S = 5.5$ was used to fit the hole spectra of P700 because the observed ZPH with a width of only $\sim 0.05 \text{ cm}^{-1}$ was assumed to be due to P700. The present and other [39,46] studies indicate that it is not, *vide infra*.

The modest λ_B -dependence of the P700 hole profile maxima shown here, as well as that measured from $\lambda_B = 708.2, 701.8$ and 693.2 nm spectra, indicate that $\Gamma_I < S\omega_m$. The hole maxima for these three λ_B values are located at 703, 702 and 701 nm, respectively. One is constrained in the choice of the center (ν_m) of the zero-phonon transition frequency by the observed λ_B -dependence [38,39] and the requirement that the calculated absorption spectrum must provide agreement with the observed spectrum. The calculated hole profiles in Figs. 4 and 5 for $S = 4.5$, $\omega_m = 45 \text{ cm}^{-1}$, $\Gamma_I = 100 \text{ cm}^{-1}$, $\Gamma = 60 \text{ cm}^{-1}$ and $\nu_m = 14085 \text{ cm}^{-1}$ (710 nm) provide reasonable agreement with the observed profiles. The deviations on the high energy side of the hole maxima are the result of the appearance of an increase in absorption (with a maximum near 690 nm [54,61,62]) which has been attributed to an electrochromic shift of the Chl a in the near proximity of the RC [61,62]. Thus, the quality of fit of the theoretical profiles can only be judged on the basis of the region of the experimental profiles in the vicinity of the hole maximum and to lower energy of the maximum. The P700 absorption spectrum calculated with the above parameter values is shown in Fig. 6. The calculated profile exhibits a maximum at 701.5 nm and a width of 350 cm^{-1} . From the theory one expects [39] that the calculated absorption width should be given roughly by $S\omega_m + \Gamma_I$ (300 cm^{-1} in this case).

Chemical and white light bleaching experiments on PSI-35 particles discussed by Gillie and coworkers [46] and Hayes and coworkers [39] had indicated that the

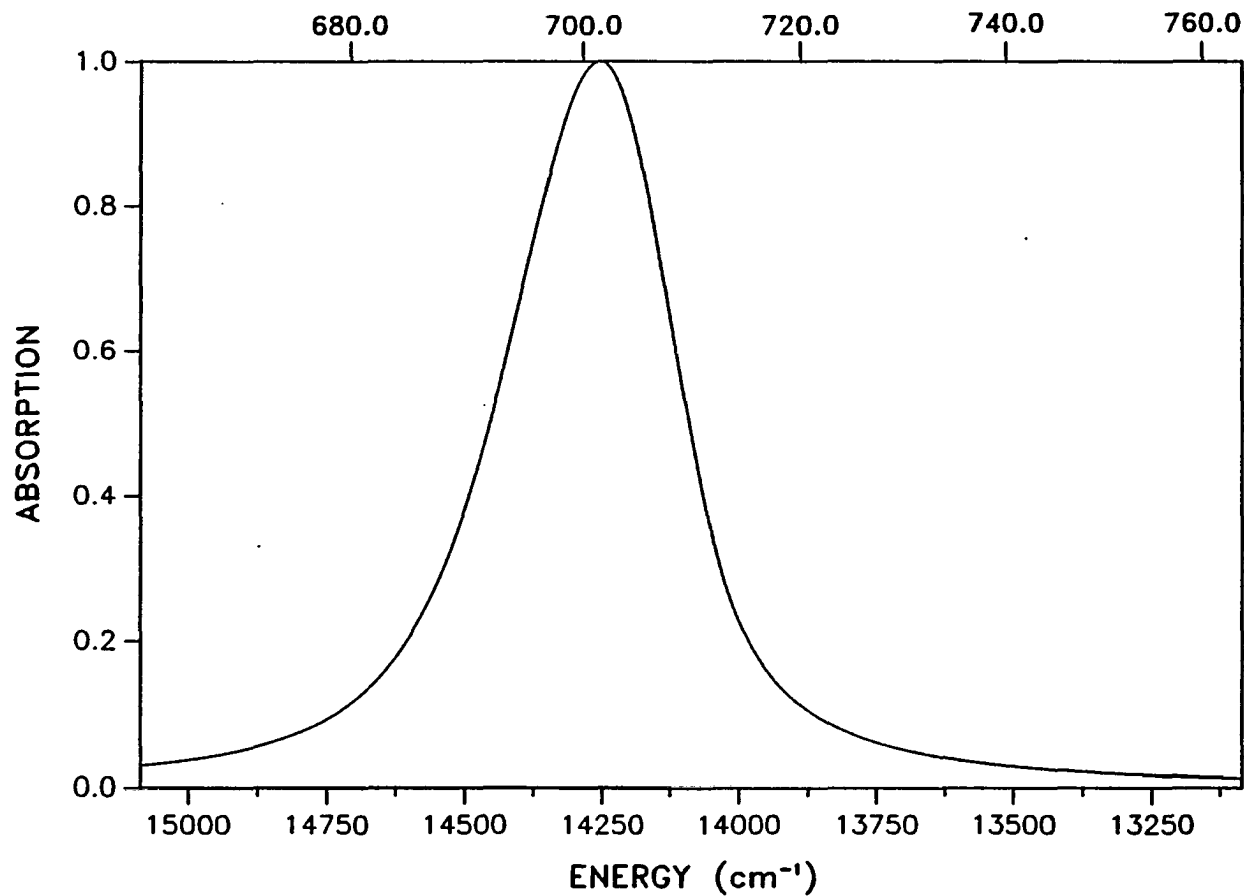


Figure 6. Calculated absorption profile for P700 at 1.6 K. The parameters used were $S = 4.5$, $\omega_m = 45 \text{ cm}^{-1}$, $\Gamma_I = 100 \text{ cm}^{-1}$, $\gamma = 60 \text{ cm}^{-1}$, $\gamma = 1 \text{ cm}^{-1}$, and $\nu_m = 14085 \text{ cm}^{-1}$ (710 nm).

sharp ZPH reported earlier [54] for P700 of PSI-35 particles is not due to photoactive P700. The present results for PSI-45 particles confirm this. With the enrichment procedure described by Golbeck [63] we have found that an enrichment of $\sim 35:1$ is more difficult to attain than an enrichment of $\sim 45:1$. This suggests, perhaps, that the $35:1$ particles could be subject to a higher probability for damage than the $45:1$ particles. The sharp but weak ZPH reported for the $35:1$ particles could be due to inactive P700 or antenna Chl a perturbed by the isolation procedure. In any event, a hole width of 0.05 cm^{-1} [46] translates to a minimum depopulation decay time for P700 at 1.6 K of 210 psec, which is difficult to reconcile in view of the measured decay times at room T [58,64,65] and the fact that the decay rates for P870* [24,51], P960 [51] and P680* [52,53] increase as the temperature is decreased from room T.

Turning now to the application of the theory to the ΔOD spectra shown in Figs. 4 and 5 it can be seen that the parameter values $S = 4.5$, $\omega_m = 45 \text{ cm}^{-1}$, $\Gamma = 60 \text{ cm}^{-1}$, $\Gamma_I = 100 \text{ cm}^{-1}$ and $\nu_m = 14085 \text{ cm}^{-1}$ provide reasonable fits to the observed profiles. In fitting to the spectra, Γ was held constant at 60 cm^{-1} , a value that is about twice that observed for the antenna Chl a [47]. The increase in Γ was scaled according to the ratio of the ω_m value utilized for P700 to that observed for the antenna Chl a. We hasten to add that the comparable theoretical fits to the P700 hole profiles could be achieved using two or more mean phonon frequencies. However "multi-phonon" fits are not justified at this time since the underlying structure for P700 has not been observed. It was found that the λ_B -dependence of the hole maximum could not be accounted for if ν_m ($\lambda = 710 \text{ nm}$) was varied by more than $\pm 2 \text{ nm}$ from 710 nm. The fitting of the λ_B -dependence also depends quite sensitively on the ratio $S\omega_m/\Gamma_I$ as one would expect since in the limit $S\omega_m \gg$

Γ_I there should be no λ_B -dependence [39]. Comparable fits to the hole spectra can be obtained by increasing Γ_I somewhat (e.g., to 120 cm^{-1} as determined for P680 [52]) provided $S\omega_m$ is appropriately increased. This is also true if S is increased and ω_m decreased proportionately (for a fixed Γ_I). However, it was found that the goodness of fit to the low energy side of the hole profiles worsens if S is increased too much above 4.5, e.g., to 8 (Fig. 5). Our many calculations (only a few of which are shown here) indicate that S and ω_m values in the ranges 4-6 and $50\text{-}35 \text{ cm}^{-1}$ and $\Gamma_I \sim 100 \text{ cm}^{-1}$ can adequately account for the observed hole profiles. The calculated absorption spectrum in Fig. 6 is difficult to compare with experiment because of the interference by the low energy tail of the antenna Chl a, see upper curve of Fig. 1. However, since the linear electron-phonon coupling is strong (i.e., the homogeneous contribution to the P700 absorption is large) the photochemical hole burning can produce a bleach that essentially encompasses the entire absorption profile. In particular, for λ_B significantly to the blue of 710 nm (center of the zero-phonon excitation frequency distribution), e.g., 702.6 nm as in Fig. 5, or located in the antenna Chl a absorption origin (Fig. 3) the hole should be a faithful representation of the P700 absorption profile at 1.6 K. The calculated absorption spectrum is in good agreement with the two hole burned spectra just mentioned. Thus, we conclude that P700 exhibits a maximum at $\sim 702 \text{ nm}$ and a FWHM of 350 cm^{-1} at 1.6 K. Approximately 30 and 70% of this width is due to inhomogeneous broadening (from linear electron-phonon coupling), respectively.

From the results presented here for P700 it is apparent that the P700 hole spectra are significantly different from those for the other PED states P680, P870 and P960. Although here appear to be significant differences [20,66] between the interactions of the special pair and amino acid residues in Rps. viridis and Rb.

sphaeroides the similarity in their cofactor structures [67] is sufficient to yield very similar hole spectra for P960 and P870. The hole spectra for P700 show no evidence of any structure (akin to that associated with the $\sim 130 \text{ cm}^{-1}$ mode of P870 and P960) even though the P700 hole profile and calculated absorption profile are about 100 cm^{-1} narrower than the overall hole widths and absorption widths of P870 and P960. This, together with the fact that $\Gamma_{\text{I}} \sim 100 \text{ cm}^{-1}$ for P700, is telling in the sense that if a mode analogous to the 130 cm^{-1} is active in the P700 hole profile, the fact that it cannot be resolved means that its frequency is considerably reduced. We cannot distinguish between this possibility or the possibility that such a progression forming mode does not exist. The existence of the special pair for P700 is still being debated but evidence for its existence appears to be mounting. Assuming that it does exist, the above remarks and the absence of the ZPH for P700 indicate that its geometric and electronic structure of its excited state may be quite different from those for the purple bacteria. The absence of the ZPH for P700 indicates that $S \geq 4.5$ and, therefore, that the coupling of P700^* with low frequency phonons is stronger than for P870^* , P960^* and P680^* whose S -values are close to 2. The strong linear electron-phonon coupling for P700^* suggests that it may possess significant charge-transfer character as is the case for P870^* [69-71] and P960^* [69,71,72].

CONCLUSIONS

Spectral hole burning studies performed by this group have demonstrated that the hole burning characteristics for the PED states P960, P870, P680, and P700 are similar and defined by strong electron-phonon coupling and significant site inhomogeneous broadening. The exact description of the PED states, neutral exciton with significant intra-dimer charge transfer character or admixtures of P^{*} and a charge transfer between P and other reaction center pigments, is left unresolved. A dimer structure for P700 is indicated.

REFERENCES

1. Deisenhofer, J.; Epp, O.; Miki, K.; Huber, H. *J. Mol. Biol.* 1984, 180, 385.
2. Deisenhofer, J.; Epp, O.; Miki, K.; Huber, R.; Michel, H. *Nature* 1985, 318, 618.
3. Michel, H.; Epp, O.; Deisenhofer, J. *EMBO J.* 1986, 5, 2445.
4. Michel, H.; Deisenhofer, J. *Chemica Scripta* 1987, 27B, 173.
5. Allen, J. R.; Feher, G.; Yeates, T. O.; Rees, D.C.; Deisenhofer, J.; Michel, H.; Huber, R. *Proc. Natl. Acad. Sci. USA* 1986, 83, 8589.
6. Chang, C. H.; Teide, D.; Tang, J.; Smith, U.; Norris, J.; Schiffer, M. *FEBS Lett.* 1986, 205, 82.
7. Kirmaier, C.; Holten, D. *Photosynth. Res.* 1987, 13, 225.
8. Budil, D. E.; Gast, P.; Chang, C. H.; Schiffer, M.; Norris, J. *Ann. Rev. Phys. Chem.* 1987, 38, 561.
9. Michel-Beyerle, M. E.; Plato, M.; Deisenhofer, J.; Michel, H.; Bixon, M.; Jortner, J. *Biochim. Biophys. Acta* 1988, 932, 52.
10. Parson, W. W.; Scherz, A.; Warshel, A. In Antenna and Reaction Centers of Photosynthetic Bacteria: Michel-Beyerle, M. E., Ed.; Springer-Verlag: Berlin, 1985, p 122.
11. McElroy, J. D.; Mauzerall, D. C.; Feher, G. *Biochim. Biophys. Acta* 1972, 267, 363.
12. Norris, J. R.; Uphaus, R. A.; Crespi, H. L.; Katz, J. J. *Proc. Natl. Acad. Sci. USA* 1971, 68, 625.
13. Warshel, A.; Parson, W. W. *J. Amer. Chem. Soc.* 1987, 109, 6143; *J. Amer. Chem. Soc.* 1987, 109, 6152.

14. Zinth, W.; Knapp, E. W.; Fischer, S. F.; Kaiser, W.; Deisenhofer, J.; Michel, H. *Chem. Phys. Lett.* 1985, 119, 1.
15. Knapp, E. W.; Scherer, P. O. J.; Fischer, S. F. *Biochim. Biophys. Acta* 1986, 852, 295.
16. Scherer, P. O. J.; Fischer, S. F. *Biochim. Biophys. Acta* 1987, 891, 157.
17. Rackovsky, S.; Scher, H. *Biochim. Biophys. Acta* 1982, 681, 152.
18. Scherer, P. O. J.; Fischer, S. F. *Chem. Phys. Lett.* 1987, 141, 179.
19. Warshel, A.; Creighton, S.; Parson, W. W. *J. Phys. Chem.* 1988, 92, 2696.
20. Yeates, T. O.; Komiya, H.; Chirino, A.; Rees, D. D.; Allen, J. P.; Feher, G. *Proc. Natl. Acad. Sci. USA* 1988, 85, 7993.
21. Teide, D. M.; Kellog, E.; Breton, J. *Biochim. Biophys. Acta* 1987, 892, 294.
22. Creighton, S.; Hwang, J. K.; Warshel, A.; Parson, W. W.; Norris, J. *Biochemistry* 1988, 27, 774.
23. Robert, B.; Lutz, M. *Biochemistry* 1988, 27, 5108.
24. Martin, J. L.; Breton, J.; Hoff, A. J.; Migus, A.; Antonetti, A. *Proc. Natl. Acad. Sci. USA* 1986, 83, 957.
25. Breton, J.; Martin, J. L.; Migus, A.; Antonetti, A.; Orszag, A. *Proc. Natl. Acad. Sci. USA* 1986, 83, 5121.
26. Holten, D.; Hoganson, C.; Windsor, M. W.; Schenck, C. C.; Parson, W. W.; Migus, A.; Fork, R. L.; Shank, C. V. *Biochim. Biophys. Acta* 1980, 952, 461.
27. Kirmaier, C.; Holten, D.; Parson, W. W. *FEBS Lett.* 1985, 185, 76.
28. Hopfield, J. J. *Proc. Natl. Acad. Sci. USA* 1974, 71, 3640.

29. Marcus, R. A. Chem. Phys. Lett. 1987, 133, 471.
30. Bixon, M.; Jortner, J.; Michel-Beyerle, M. E.; Ogrodnik, A.; Lersch, W. Chem. Phys. Lett. 1987, 140, 626.
31. Plato, M.; Möbius, K.; Michel-Beyerle, M. E.; Bixon, M.; Jortner, J. J. Amer. Chem. Soc. 1988, 110, 7279.
32. Marcus, R. A. Chem. Phys. Lett. 1988, 133, 471.
33. Won, Y.; Friesner, R. A. Biochim. Biophys. Acta 1988, 935, 9.
34. Boxer, S. G.; Lockhart, D. J.; Middendorf, T. R. Chem. Phys. Lett. 1985, 121, 476.
35. Boxer, S. G.; Middendorf, T. R.; Lockhart, D. J. FEBS Lett. 1986, 200, 237.
36. Meech, S. R.; Hoff, A. J.; Weirisma, D. A. Chem. Phys. Lett. 1985, 121, 287.
37. Meech, S. R.; Hoff, A. J.; Weirisma, D. A. Proc. Natl. Acad. Sci. USA 1986, 83, 9464.
38. Hayes, J. M.; Small, G. J. J. Phys. Chem. 1986, 90, 4928.
39. Hayes, J. M.; Gillie, J. K.; Tang, D.; Small, G. J. Biochim. Biophys. Acta 1988, 932, 287.
40. Tang, D.; Jankowiak, R.; Gillie, J. K.; Small, G. J.; Tiede, D. M. J. Phys. Chem. 1988, 92, 4012
41. Tang, D.; Jankowiak, R.; Small, G. J.; Tiede, D. M. Chem. Phys. 1989, 131, 99.
42. Won, Y.; Friesner, R. A. Proc. Natl. Acad. Sci. USA 1987, 84, 5511.
43. Won, Y.; Friesner, R. A. In Structure of Bacterial Reaction Centers: X-ray Crystallography and Optical Spectroscopy with Polarized Light; Breton, J., Verméglio, A., Eds.; Plenum: New York, 1988, p 341.

44. Won, Y.; Freisner, R. A. *J. Phys. Chem.* 1988, 92, 2208; *J. Phys. Chem.* 1988, 92, 2214.
45. Small, G. J. In Spectroscopy and Excitation Dynamics of Condensed Molecular Systems; Agranovich, V. M., Hochstrasser, R. M., Eds.; North-Holland: Amsterdam, 1983, p 515.
46. Gillie, J. K.; Hayes, J. M.; Small, G. J.; Golbeck, J. H. *J. Chem. Phys.* 1987, 91, 5524.
47. Gillie, J. K.; Small, G. J.; Golbeck, J. H. *J. Phys. Chem.* 1989, 93, 1620.
48. Renge, I.; Muring, K.; Avarmaa, R. *J. Lumin.* 1987, 37, 207.
49. Maslov, V. G.; Chunaev, A. S.; Tugarinov, V. V. *Mol. Biol.* 1981, 15, 788.
50. Tang, D.; Johnson, S. G.; Jankowiak, R.; Hayes, J. M.; Small, G. J.; Tiede, D. M. *J. Phys. Chem.*, submitted.
51. Breton, J.; Martin, J. -L.; Fleming, G. R.; Lambry, J. -C. *Biochemistry* 1988, 27, 8276.
52. Jankowiak, R.; Tang, D.; Small, G. J.; Seibert, M. *J. Phys. Chem.* 1989, 93, 1649.55.
53. Wasielewski, M. R.; Johnson, D. G.; Seibert, M.; Govindjee *Proc. Natl. Acad. Sci. USA* 1989, 86, 524.
54. Gillie, J. K.; Fearey, B. L.; Hayes, J. M.; Small, G. J.; Golbeck, J. H. *Chem. Phys. Lett.* 1987, 134, 316.
55. Shuvalov, V. A.; Klevanik, A. V.; Kryulov, A. V.; Ke, B. *FEBS Lett.* 1979, 107, 313.
56. Shuvalov, V. A.; Ke, B.; Dolan, E. *FEBS Lett.* 1979, 100, 5.

57. Shuvalov, V. A.; Nuijjs, A. M.; van Gorkum, H. J.; Smit, H. W. J.; Duysens, L. N. M. *Biochim. Biophys. Acta* 1986, 850, 319.
58. Owens, T. G.; Webb, S. P.; Mets, L.; Alberte, R. S.; Fleming, G. R. *Proc. Natl. Acad. Sci. USA* 1987, 84, 1532.
59. Jankowiak, R.; Small, G. J. *Science* 1987, 237, 618.
60. Jankowiak, R.; Shu, L.; Kenney, M. J.; Small, G. J. *J. Lumin.* 1987, 36, 293.
61. Schaffernicht, H.; Junge, W. *Photochem. Photobiol.* 1981, 34, 223.
62. Sétif, P.; Mathis, P.; Vänngård, T. *Biochim. Biophys. Acta* 1984, 767, 404.
63. Golbeck, J. H. In Methods in Enzymology: San Pietro, A., Ed.; Academic: New York, 1980, p 129.
64. Fenton, J. M.; Pellin, M. J.; Govindjee; Kaufmann K. J. *FEBS Lett.* 1979, 100, 1.
65. Wasielewski, M. R.; Fenton, J. M.; Govindjee *Photosyn. Res.* 1987, 12, 181.
66. Allen, J. P.; Feher, G.; Yeates, T. O.; Komiya, H.; Rees, D. C. *Proc. Natl. Acad. Sci. USA* 1988, 85, 8487.
67. Allen, J. P.; Feher, G.; Yeates, T. O.; Komiya, H.; Rees, D. C. *Proc. Natl. Acad. Sci. USA* 1987, 84, 5730; *Proc. Natl. Acad. Sci. USA* 1987, 84, 6162.
68. Golbeck, J. H. *Biochim. Biophys. Acta* 1987, 895, 167.
69. Braun, H. P.; Michel-Beyerle, M. E.; Breton, J.; Buchanan, S.; Michel, H. *FEBS Lett.* 1987, 221, 221.
70. Lockhart, D. J.; Boxer, S. G. *Biochemistry* 1987, 26, 664.
71. Lockhart, D. J.; Boxer, S. G. *Proc. Natl. Acad. Sci. USA* 1988, 85, 107.

72. Lösche, M.; Feher, G.; Okamura, M. Y. Proc. Natl. Acad. Sci. USA 1987, 84, 7537.

SECTION II.

NONPHOTOCHEMICAL HOLE BURNING OF THE ANTENNA
COMPLEXES OF PHOTOSYSTEM I

SECTION II: NONPHOTOCHEMICAL HOLE BURNING OF THE ANTENNA COMPLEXES OF PHOTOSYSTEM I

INTRODUCTION

The majority of the chlorophyll in the photosynthetic thylakoid membrane act to collect, harvest, solar energy and transport that energy to the reaction center. Because of its overlap with the solar irradiance spectrum, limited at high energy by O_2 absorption and at low energy by H_2O overtone absorption, the first excited state Q_y transition of chlorophyll plays an important role in efficient solar energy collection. How energy deposited in the Q_y transition is transferred from spatially distant Chl to the reaction center has been extensively studied using fluorescence [1-11], picosecond absorption recovery [12-15], singlet-singlet annihilation [16-20], and spectral hole burning [21-25]. This subject has been extensively reviewed [26-31].

This section will discuss the dynamics of excitation energy transport (EET) in the light harvesting chlorophyll protein complex (LHCPI) associated with Photosystem I. In particular, results from nonphotochemical hole burning (NPHB) on the core antenna complex and LHCPI are presented to explore these questions: How are the pigments arranged in their protein environment? Is the excitation localized or delocalized within LHCPI? What roles do intramolecular vibrations and low frequency protein vibrations (phonons) play in mediating EET?

Discussions on the nature of EET in photosynthetic units (PSU) began in 1938 when Franck and Teller drew analogies to EET in crystals. "The coupling between particles in the crystals and the resonance caused by the identity of the crystal cells

has the consequence that excitation energy will be transferred from one cell to another" [32]. Franck and Teller outlined the work of Frenkel [33] and Peierls [34] that suggested the concept of excitation waves, called excitons, within crystals. Franck and Teller concluded, however, that "the existence of a PSU is improbable." The existence of the PSU has been demonstrated [35-38]. Robinson [39] gave a succinct review of the progress made in understanding EET and trapping in photosynthesis up to 1966.

Franck and Teller [32] assumed a one-dimensional PSU which is probably the main source of the error in their analysis [39]. This assumption leads to a transfer time of $\tau=0.01$ psec which is too fast for efficient trapping at the RC [32]. Bay and Pearlstein [40,41] extended the theories to two dimensional arrays. In either case, the theories have assumed that the Chls in the antenna proteins are arranged in a regular lattice array and the exciton migration is believed to be diffusive, i.e., a noncoherent random walk through the lattice. The Chls interact in the conventional Förster dipole-dipole mechanism. It is important to understand the conditions by which exciton motion becomes incoherent, i.e., a random walk.

Mathematically, a delocalized exciton is described when the eigenfunctions for the excited state are written as superposition of excitations on the individual crystal cells [33,34]. The coefficients are made to vary sinusiodally as a function of the coordinate of the cell [33,34]. For one-dimensional excitons, the stationary states of the system Hamiltonian are

$$|k\rangle = N^{-1/2} \sum_n e^{ik \cdot r_n} |n\rangle \quad (1)$$

where N is the number of independent identical molecules. The states are characterized by the exciton wavevector \underline{k} [42].

In large molecules the electronic transitions are coupled to intramolecular vibrations and lattice vibrations (phonons). If the exciton-phonon interaction (or lattice coupling energy) is comparable with or larger than the exciton bandwidth, the system is said to be a strong exciton scatterer [33,34]. If we consider propagation of an exciton wavepacket with a well-defined \underline{k} , the scattering processes act to change the \underline{k} -state directionality, hence the exciton loses memory of the initially prepared \underline{k} -state. For band transport, phonons scatter the exciton (labeled by the wavevector \underline{k}) between different \underline{k} -states. For hopping transport, phonons scatter the nearly localized exciton states (labeled by the site index \underline{n}) [43]. The exciton wavepacket is said to take a random walk.

However, if the exciton-phonon coupling is weak, no change in the \underline{k} -state description occurs and the exciton moves as a perfect wave through the system [43]. This is often referred to as "coherent" transport.

The coherent process only applies on the time scale in which the \underline{k} -states have a well defined relationship. A criterion for coherent exciton migration (CEM) relates the \underline{k} -state lifetime, $\tau(k_0)$, to the exciton mean free path, $l(k_0)$, and the group velocity, $V_g(t)$ by [42,44]

$$l(k_0) = \tau(k_0) V_g(t). \quad (2)$$

The exciton defined by a wavevector with a mean value about k_0 is coherent if $\tau(k_0)$ is greater than the intramolecular transfer time given by $\langle \tau \rangle = a / \langle V_g(t) \rangle$ with a being the lattice spacing [42]. The group velocity can be calculated from the nearest-neighbor interaction and distance. Physically, we see that the exciton remains in a particular \underline{k} -state (wavelike) for $\tau(k_0)$ until it is modulated sufficiently via scattering processes to alter the \underline{k} -state description [43]. The mean free path is

the distance traveled before the \underline{k} -state description is altered. Prerequisites for CEM in organic crystals are low temperatures and high quality strain-free crystals [45]. For 1,2,4,5-tetrachlorobenzene, $l(k) = 300$ to 10^4 Å and $\tau(k) = 10^{-7}$ sec [44,46]. Determining $l(k)$ and $\tau(k)$ for photosynthetic systems is difficult. Recent NPHB experiments on the antenna system of *P. aestuarii* show that the exciton-phonon coupling is weak [47] which could suggest that CEM might occur in the light harvesting complexes of PSUs. Other descriptions of EET can be envisioned, i.e., polariton formation and migration [45,48] (the reader is referred to a special issue of Chemical Physics [see ref. 45] for discussions of EET in solids).

When discussing the problems of EET, one must be careful of the terminology. The coherent or noncoherent transfer limit is defined as above. If the excitation is localized, it is associated with a particular site. Excitation into a strongly excitonic system is necessarily delocalized since the exciton wavefunction is a superposition of the wavefunctions of the interacting molecules. No spatial transfer is needed within a subunit, in this case, since the prepared state involves all the molecules in the subunit.

Our understanding of EET in antenna systems has been greatly enhanced with the mathematical descriptions given by Knox [26,49-51], Paillotin [52-55], and Pearlstein [31,40,41,56]. These models describe the nature of the EET as random hops between Chls arranged in a regular lattice array. The conditions for this description were described earlier. This description of EET is preferred because the mathematics is simplified. In the Pearlstein model the excitation executes a random walk until it reaches a trap, a reaction center in this case. At this point it may undergo photochemical conversion or reenter the antenna to continue its random walk. The interaction between Chls is described by the Förster [57] dipole-dipole

interaction mechanism and falls off as $1/R^6$ where R is the distance between molecules. The Chls are weakly interacting. References [26,28,29,39,41,58] are good reviews of the details of the theories.

The random walk is said to be "diffusion limited" if the photoconversion rate at the trap is faster than the time required for the excitation to reach the trap for the first time (first passage time). If the photoconversion is slower then the kinetics are "trap limited" [41].

Pearlstein [41] proposed a means of experimentally determining the first passage time. The mean lifetime of the excitation, M_o , is given by

$$M_o = [1 + (F_D/F_T)(N-1)]k_p^{-1} + \{ [1 - p_o(0)](N-1)[(qF_T)^{-1} - (qF_A)^{-1}] + [-f_{oo} + \sum_i f_{oi}p_i(0)]NF_A^{-1} \} \quad (3)$$

where N is the Chl array size; F_T, F_D are the Förster rate constants for trapping and detrapping; F_A is the reversible Förster rate constant for hopping between nearest-neighbor antenna Chl; k_p is the photoconversion rate constant; p_i is the probability of finding the excitation on molecule i , with p_o the probability that it resides on the reaction center; q is the lattice coordination number; f_{ij} 's are lattice parameters that depend on N and the lattice structure.

In the case where the probability of exciting the RC and antenna is unknown, Eqn. 3 becomes

$$M_o = [1 + (F_D/F_T)(N-1)]k_p^{-1} + (1/F_A) \{ (F_A/F_T) + [q\alpha N^2]/(N-1)^2 - 1 \} * (N-1)(1-PRC) \quad (4)$$

where $p_0(0)=p_{RC}$ and $p_i(0)=(1-p_{RC})/(N-1)$ for all $i \neq 0$ and $\alpha = -f_{00}$. Excitation of the reaction center at various wavelengths should selectively excite different fractions of reaction centers. M_0 could be measured using time resolved fluorescence providing the excitation is at wavelengths at which no accessory pigments are excited. (Pearlstein defines proximal pigments as all antenna pigments which have the lowest $S_0 - S_1$ transition energy and therefore the excitons migrate directly to the RC's. All other pigments are accessory pigments.) At each excitation wavelength the fractional optical density, p_{RC} , due to RC absorbance must be determined [41]. A plot of M_0 vs. $(1-p_{RC})$ should be linear and the slope gives τ_{FPPT} (first passage time) from which a single site transfer time (SST) can be calculated. The estimate of the SST is only as good as the calculated Förster rate constants.

If it is assumed that all sites, individual antenna Chl's and RC's, are equally likely to be excited at $t=0$, then the rate equation is written [41]

$$M_0 = [1 + (F_D/F_T)(N-1)]k_p^{-1} + [1/qF_T - 1/qF_A][(N-1)^2/N] + \alpha N/F_A. \quad (5)$$

If only the RC is excited the rate equation becomes

$$M_0 = [1 + (F_D/F_T)(N-1)]k_p^{-1}. \quad (6)$$

Owens et al. [4,5] took the approach outlined in Eqn. 5 to test the predictions of Pearlstein's model. Their experiments monitored the temporal characteristics of the fluorescence from PSI particles with varying sizes of antennas. For excitation

between 630 and 670 nm the fluorescence lifetime varied linearly with the size of the antenna. The analysis yielded a first passage time of ~20 psec with a SST of 0.21 psec. The excitation makes an average 2.4 reaction center visits before photoconversion and the excitation migration is diffusion limited.

Other researchers [26,31,49-54,59-63] have expanded the random walk model to test a variety of effects which might influence the efficiency of light harvesting. Seely [60] showed that spectral variety (spectral forms of Chl proteins that absorb at successively lower energy) can increase the trapping rate 4 to 5 times over that expected for a single wavelength absorbing Chl protein. This is achieved by enhancing the Förster overlap integral. Proper orientation of the electronic transition dipoles may introduce a similar factor of 4 to 5 times. It had already been suggested that if the longest wavelength absorbing form surrounds the RC, the trapping would be faster than if the surrounding Chls consist of a homogeneously absorbing protein complex [64,65]. This is the basis for the "funnel" model for the antenna.

Altmann and coworkers performed Monte Carlo calculations to study the effect of chlorophyll concentration and chlorophyll-trap ratio on the trapping rate in a two-dimensional random lattice [66]. They assumed the excitation undergoes a Förster type random walk migration. The calculated chlorophyll fluorescence lifetime agrees with in vivo results and is consistent with trapping upon first arrival at the trapping center.

Paillotin [52-53] used a Pauli master equation to describe the fluorescence quantum yield and fluorescence temporal decay of photosynthetic systems. Paillotin showed that the rate determining step in exciton capture is charge separation at the RC and that pigment heterogeneity promotes trapping at the RC (funnel effect).

Shipmann [61] using a Pauli master equation approach, incorporated Monte Carlo techniques to vary Chl position and orientation within regions determined by freeze-fractured photosynthetic membranes. Shipmann included variables such as Chl concentration, depth of trap, and the R_0 Förster parameter to study antenna fluorescence lifetime, detrapping rates, and other factors. Two important conclusions are: 1) the fluorescence polarization is lost in <30 psec, and 2) the funnel effect is not required for efficient trapping of excitation at the RC since this would enhance both trapping and detrapping. He explains that the real purpose of absorption heterogeneity is to regulate the excitation flow from one photosystem to another within the thylakoid membrane [61]. Absorption and time resolved excitation and emission spectra of the core antenna complex of PSI show that the excitation is homogeneously distributed among all the spectral forms [5]. On this basis, Owens and coworkers [5] recently concluded that the funnel model does not apply to the core antenna protein of PSI.

Den Hollander et al. [16,17] expanded the master equation approach of Paillotin to discuss energy transfer, trapping, loss, and annihilation in a photosynthetic system. Their Monte Carlo calculations support the use of the random walk master equation model provided the densities of the excitations and RCs in a particular domain are small. They calculated the total fluorescence yields and the total fraction of RCs closed after the light pulse. These formulations were applied to data obtained by picosecond laser excitation of the purple bacteria Rhodospirillum rubrum and Rhodopseudomonas capsulata at various excitation intensities. The random walk approach is consistent with the data and yields a ratio of energy transfer between neighboring antenna molecules of $k_h = (1-2) \times 10^{12} \text{ s}^{-1}$ for R. rubrum and $k_h = 4 \times 10^{11} \text{ s}^{-1}$ for Rps. capsulata.

Kubzmauskas et al. [63] suggested that in some bacterial photosynthetic cases the approximation of infinitely high rate constant for trapping at the RC [41,60,62] is invalid and added a time limit of energy capture by the RCs. Their analysis incorporates a globular (subunit) structure of photosynthetic systems [63] into the master equation. In this approach the energy transfer within subunits is by coherent excitons and by incoherent excitons between subunits. Scherz and Parson [67] used a model involving strong ($\sim 730 \text{ cm}^{-1}$) exciton interactions within BChl dimers and weak ($\sim 35 \text{ cm}^{-1}$) between dimers to explain absorption and circular dichroism spectra obtained by Rafferty for the B800-850 complex of *Rb. sphaeroides* [68].

Other experimental evidence suggest that the Chls (BChls) in antenna systems are not arranged in a regular array lattice. The pigment-protein antenna complex for purple bacteria is postulated to be organized in large lakes which surround a network of B875 antenna that connect the RCs [69-71]. For the antenna pigments B800-850 of purple bacteria a "supramolecular" organization is proposed [71]. The Zuber model for B850 consist of "cyclic unit structure" of antenna BChl pairs in C_6 symmetry or possibly groups of 4 BChl in C_3 symmetry [72]. The model is consistent with the Scherz and Parsons model described earlier. The Kramer model [73] gives a basic structural unit consisting of four BChl 850, two BChl 800, and three carotenoid molecules. Although not perfect, the three models all give reasonable agreement with the available spectral data. Pearlstein [31] gives a current review.

The crystal structure of the antenna protein of *P. aestuarii*, a green photosynthetic bacteria, defines the basic structure to be a trimer of subunits [74,75]. Each subunit contains seven BChl a molecules. Analysis of the absorption and circular dichroism spectrum by Pearlstein [76] shows that the system possesses

strong excitonic coupling ($\sim 250 \text{ cm}^{-1}$) for BChl within the subunit. Recently, the time dependent absorption depolarization of the Q_x electronic transition in the P. aestuarii antenna protein complex at a time resolution of 1.5 psec was obtained [15]. Causgrove et al. [15] found that substantial residual polarization persist at long times. This is a consequence of the nonrandom orientation of the protein chromophores. Their interpretation is that excitons created within the tightly coupled BChls of a subunit hop (random walk) by a Förster mechanism between subunits.

Long time residual fluorescence polarization reported by Fetisova and coworkers for the green bacteria Chlorobium limicola and Chloroflexus aurantiacus, suggest that there is local ordering of the transition dipoles [6], possibly similar to P. aestuarii. "In this case the excitation energy transfer within BChl antenna may be described as that between those clusters with parallel transition moments: each cluster may be considered as a single large 'molecule' which (as a whole) may serve as a donor or acceptor molecule in hopping-type excitation transfer" [6]. The proteins function to hold the BChl in precise alignment to optimize EET.

The three dimensional structure of the light harvesting chlorophyll a/bprotein complex determined at 30 Å resolution using electron microscopy in negative stain gives a trimer of monomer Chls as the basic unit [77,78]. Pump-probe depolarization studies on the Chl a antenna complex of Photosystem I also gave a substantial residual polarization similar to that obtained on P. aestuarii [15]. This suggest that some form of local ordering also exist for this protein complex. The hop time between subunits is ~ 10 psec. This data is important since the crystal structure for green plant photosynthetic antenna systems has yet to be determined.

The discussion so far has centered on whether or not a subunit structure or regular array structure gives the best description of the photosynthetic antenna pigment-protein complexes. Final answer to this question awaits structure determination.

One final point to be mentioned before discussing multiphonon excitation energy transport theories, concerns the flow of excitation between PSI and PSII in green thylakoid membranes. The puddle model describes a PSU in which a given RC and its associated antenna system constitute a isolated PSU. Excitation created within a PSU cannot be transferred to another PSU. In the lake model [28], the RC resides in a lake of antenna pigment complexes and the excitations can migrate from RC to RC via antenna pigment complexes until it is captured or decays. The connected PSU model proposed by Joliot and Joliot [79] allows for partial connectivity between PSUs so that the excitation can migrate from a PSU with a closed RC to a neighboring PSU. The bipartate and tripartate models of Butler [80] attempt to account for energy distribution and fluorescence in PSII. Since these are kinetic models, the structural details of the antenna are not considered.

Recall that the analysis of Owens and coworkers [4,5] for the lifetime dependence of the fluorescence yielded a single site transfer time of ~ 0.2 psec at room temperature. NPHB experiments on C670 and PSI-200 antenna complexes indicate that the excitation depopulation lifetime at 1.6 K is ~ 300 psec. If these two values represent the same process, then nearly three orders of magnitude change occurs in going from room temperature down to 1.6 K. A tenfold decrease in EET between room temperature and 4 K is found for the B800-850 of Rb. sphaeroides using singlet-singlet annihilation techniques [19]. We turn now to multiphonon EET theory because the Förster rate equations does not explicitly describe the

temperature dependence of the rate. The temperature dependence is implied for the Förster expressions in the overlap integral, i.e. the overlap of the absorption spectrum of the acceptor and fluorescence spectrum of the donor changes as the temperature changes. Multiphonon EET theory also enjoys the freedom to address the subunit or regular array question since no assumptions about the antenna structure are made during the derivation.

Multiphonon excitation energy transport theory has its historical development in understanding non-radiative decay processes of ions and molecules in solids [56,81-86]. The classical limits (high temperature) were first developed to describe electron transfer reactions in solution at an electrode surface [87-89]. Semiclassical [90] and quantum calculations were applied by researchers [91-93] studying the temperature behavior of the DeVault and Chance cytochrome c reaction [94,95] and photosynthetic antenna systems [96]. Currently, the effort in this area has focussed on the nature of the excited states, and electron transfer processes in the reaction centers of purple photosynthetic bacteria [97-100].

The nonadiabatic microscopic rate equation for energy transport can be written in terms of the Fermi Golden Rule expression [101,102] :

$$W_{av-b} = \frac{2\pi}{\hbar} \sum_w |V_{av,bw}|^2 \delta(E_{bw} - E_{av}) \quad (7)$$

Conceptually, this is written as a nonradiative decay process between a donor and acceptor. The summation is over all available system phonon and intramolecular modes. V is the matrix coupling element that includes the electron energy, lattice vibrations and the interaction between the electron and the lattice [84,85]. The δ

function insures the overlap of the initial and final states. This is the starting point for the classical and quantum mechanical treatment. We have assumed at this point that the microscopic rate W_{av-b} for energy transport is slow compared to medium-induced vibrational relaxation (VR) and vibrational excitation [102]. The VR time scale for optical phonons have been experimentally determined with typical values being $\tau_{VR}^{-1} \sim 5 \times 10^{-12}$ sec [103,104].

In the Condon approximation, the purely electronic coupling term can be separated from the vibrational term so that the matrix coupling element can be written

$$|V_{av,bw}|^2 = V^2 |\langle av|bw \rangle|^2 \quad (8)$$

which upon substitution into Eqn. 7 yields

$$W_{av-b} = \frac{2\pi}{\hbar} V^2 \sum_w |\langle av|bw \rangle|^2 \delta(E_{bw} - E_{av}). \quad (9)$$

We have assumed in the Condon approximation a separation of time scales so that the transition is vertical, i.e. the coordinates of the system do not change as quickly as the rate of the transfer process.

The macroscopic rate for energy transport can be written as the thermal average of the microscopic rates [95,102] so that

$$W_{a-b} = \sum_v p_v W_{av-b} \quad (10)$$

where the thermal occupation p_v is

$$p_v = \exp(-E_{av}/k_b T) / Z_1 \quad (11)$$

and

$$Z_1 = \sum_v \exp(-E_{av}/k_b T) \quad (12)$$

is the partition function of the donor manifold. The rate constant is then given as

$$W_{a-b} = \frac{2\pi}{\hbar} V^2 F \quad (13)$$

where F is the thermally averaged Franck-Condon factor

$$F = \sum_v \sum_w p_v |\langle av | bw \rangle|^2 \delta(E_{bw} - E_{av}). \quad (14)$$

It is this term that contains the thermal dependence.

The major problem in obtaining a tractable and physically understandable rate equation is performing the double summation in the F term. The problem is more difficult than presented in Eqns. 13 and 14 if one considers diagonal energy disorder [85,105,106]. Equation 14 was originally solved for the case in which all the modes available to the system have a common frequency by Huang and Rhys in 1950 [107]. A solution to the multi-frequency problem was first outlined by Kubo [83] and expanded by Kubo and Toyozawa [84]. Dogonadze et al. calculated the probability of the transitions between two multi-dimensional parabolic terms [108]. A simplified derivation of Kubo's result is given by DeVault [95] and Englman [81] and will not be given here.

The expressions written in terms of generating functions are

$$W_{a-b} = \frac{2\pi}{\hbar} V^2 \frac{1}{2\pi\hbar} \int_{-\infty}^{\infty} f(t) \exp(-i\Delta Et/\hbar) dt \quad (15)$$

with

$$f(t) = \exp\{-G + G_+(t) + G_-(t)\} \quad (16)$$

$$G_+(t) = \sum_{\mathbf{k}} S_{\mathbf{k}} (\bar{n}_{\mathbf{k}} + 1) \exp(i\omega_{\mathbf{k}}t) \quad (17)$$

$$G_-(t) = \sum_{\mathbf{k}} S_{\mathbf{k}} \bar{n}_{\mathbf{k}} \exp(-i\omega_{\mathbf{k}}t) \quad (18)$$

$$G = G_+(0) + G_-(0). \quad (19)$$

$F(t)$ describes the time evolution of the system and the summation is over all \mathbf{k} system modes. G_+ and G_- represent the absorption and emission, respectively, of one quantum of vibrational energy. G gives the initial condition of the system. $S_{\mathbf{k}}$ is the coupling strength (electron-phonon or electron-vibrational) and is generally written in reduced coordinates

$$S_{\mathbf{k}} = \frac{1}{2} \Delta_{\mathbf{k}}^2 \quad (20)$$

with Δ being the dimensionless nuclear coordinate [81,102]. $\bar{n}_{\mathbf{k}}$ is the thermal occupation

$$\bar{n}_{\mathbf{k}} = [\exp(\hbar\omega_{\mathbf{k}}/k_bT) - 1]^{-1} \quad (21)$$

with $\hbar\omega_k$ the mode frequency.

The term $\exp\{G_+(t) + G_-(t)\}$ can be written as

$$\exp\left\{\sum_k S_k [\bar{n}_k(\bar{n}_k+1)]^{1/2} \left[\left(\frac{\bar{n}_k+1}{\bar{n}_k}\right)^{1/2} \exp(i\omega_k t) + \left(\frac{\bar{n}_k}{\bar{n}_k+1}\right)^{1/2} \exp(-i\omega_k t) \right]\right\} \quad (22)$$

which can be expressed as [95,102]

$$\prod_k \left\{ \sum_{m_k=-\infty}^{\infty} \left(\frac{\bar{n}_k+1}{\bar{n}_k}\right)^{m_k/2} I_{m_k} \left\{ 2S_k [\bar{n}_k(\bar{n}_k+1)] \right\}^{1/2} \exp(m_k i\omega_k t) \right\} \quad (23)$$

where I_{m_k} is the modified Bessel function and m_k is the net change in quantum number for the oscillator mode k .

If we consider just the single mode case the rate equation becomes

$$W_{a-b} = \frac{2\pi}{\hbar} V^2 \left(\frac{1}{2\pi\hbar}\right) \exp(-G) (2\bar{n}+1) \left(\frac{\bar{n}+1}{\bar{n}}\right)^{p/2} I_p \{ 2S[\bar{n}(\bar{n}+1)] \}^{1/2} \times \int_{-\infty}^{\infty} dt \exp\{i(p\omega - \Delta E/\hbar)t\} \quad (24)$$

which simplifies to

$$W_{a-b} = \frac{2\pi}{\hbar\omega} V^2 \exp[-S(2\bar{n}+1)] \left(\frac{\bar{n}+1}{\bar{n}}\right)^{p/2} I_p \{ 2S[\bar{n}(\bar{n}+1)] \}^{1/2} \quad (25)$$

where $p = \Delta E / \hbar \omega$ with ΔE the energy difference between the donor and acceptor and $\hbar \omega_s$ the frequency of the relevant mode. In this case, p is the number of quanta that will be necessary to account for the energy mismatch and thus assures energy overlap of the donor and acceptor states.

In the low temperature limit $\bar{n} \rightarrow 0$ so that

$$W_{a-b} = \left(\frac{2\pi}{\hbar^2 \omega_s} \right) V^2 e^{-S} \frac{S^p}{p!} \quad (26)$$

In the high temperature limit I_p can be expressed as a asymptotic expression [109]

$$I_p = (2\pi Z)^{-1/2} \exp(Z - p^2/2Z). \quad (27)$$

Substituting Eqn. 27 and

$$\frac{\bar{n}+1}{\bar{n}} = \exp(\hbar \omega / k_b T) \quad (28)$$

into Eqn. 25 with the appropriate high temperature limiting values [95]

$$2S[\bar{n}(\bar{n}+1)]^{1/2} - S(2\bar{n}+1) \rightarrow -S\hbar \omega / k_b T \quad (29)$$

and

$$2S[\bar{n}(\bar{n}+1)]^{1/2} \rightarrow 2Sk_b T / \hbar \omega \quad (30)$$

gives the exact expression

$$W = \frac{2\pi}{\hbar} V^2 \left(\frac{1}{4\pi S\hbar\omega k_b T} \right)^{1/2} \exp\left(-\frac{(\Delta E - S\hbar\omega)^2}{4S\hbar\omega k_b T}\right) \quad (31)$$

for the single mode case. An alternate derivation of this result is given by Jortner [91]. If we let $\lambda = S\hbar\omega$ then the high temperature result is written as

$$W = \frac{2\pi}{\hbar} V^2 \left(\frac{1}{4\pi\lambda k_b T} \right)^{1/2} \exp\left(-\frac{(\Delta E - \lambda)^2}{4\lambda k_b T}\right) \quad (32)$$

which is Marcus's result [88,89] with λ defined as the reorganization energy.

The multi-frequency equations can be calculated by carrying the summation terms of Eqns. 22 and 23. Both Jortner [91] and Sarai [92] have utilized a two mode formulation for inclusion of a low frequency protein mode (soft mode) and intramolecular vibration (hard mode) to explain the temperature dependence of the cytochrome c electron transfer reaction.

This section includes two papers that report results of NPHB on the light harvesting chlorophyll complex of PSI. The first paper gives results for the core antenna complex C670 in which a pseudo-phonon sideband hole and vibronic satellite holes are reported for the first time in a pigment-protein complex. The second paper reports a more in depth study done on the "native" PSI particle that contains its natural complement of Chl proteins. Multiphonon EET theory is used to account for the temperature dependence of the EET and explore possible structure models for the antenna complex.

PAPER I. HOLE BURNING SPECTROSCOPY OF A
CORE ANTENNA COMPLEX

**Hole Burning Spectroscopy of a Core
Antenna Complex**

J. K. Gillie, J. M. Hayes, G. J. Small, and J. H. Golbeck

Journal of Physical Chemistry 1988, 91, 5524

INTRODUCTION

The importance of the electron-phonon coupling, associated with low-frequency protein modes, for electron-transfer (ET) and electronic excitation transport (EET) in the photosynthetic unit poses an interesting problem. Recently, such coupling (strong) has been argued, on theoretical grounds, to be very important for certain optical excitation and ET processes of photosynthetic reaction centers (RC). Bixon and Jortner conclude, for example, that in the RC of photosynthetic bacteria the quinone reduction and its back charge recombination with the radical cation of the primary electron donor (PED) are governed (from a nuclear tunneling point of view) by protein modes of $\sim 100 \text{ cm}^{-1}$ in energy [1]. The role of the intramolecular modes of the donor and acceptor was judged to be unimportant [1]. Hayes, Gillie, and co-workers [2-4] have demonstrated that the recent hole burning data of the PED states P870, P960, and P700 of *Rb. sphaeroides* [5,6], *Rps. viridis* [7,8], and Photosystem I [3], can be quantitatively understood in terms of strong linear electron-phonon coupling and inhomogeneous line broadening (Γ_I) from pigment site inhomogeneity. That is, the absorption profiles of P870, P960, and P700 are dictated by a large Huang-Rhys factor S (long phonon progression) and Γ_I . An alternate interpretation [5,6,8] is that the broad ($\sim 400 \text{ cm}^{-1}$) hole observed for P870 and P960 results from an ultra-fast ($\sim 25 \text{ fsec}$) charge separation process within the special pair (a BChl dimer) prior electron transfer to the bacteriopheophytin. The optically excited PED state is viewed as a neutral pair excitonic state and electron-phonon coupling is neglected. This model, however, cannot account for the dependence of the hole profiles on the laser burn frequency (ω_B) and the thermal broadening data associated with the PED state [2,4]. In the model of Hayes and

Small [2] phononic (by analogy with vibronic) transitions determine its absorption profile.

The key parameters of the theory for hole burning in the presence of arbitrarily strong electron-phonon coupling are S , Γ_I , the mean phonon frequency ω_m , and the width of the one phonon profile Γ [2-4]. The values of the parameters for the three aforementioned PED states are given in Table 1 since they are germane to this paper. The Stokes shift and Franck-Condon factor for the zero-phonon transition associated with the PED states are, to a reasonable approximation, given by $2S\omega_m$ and $\exp(-S)$, respectively. It was noted [2,3] that the large value of S for the PED states means that the optically excited PED state possesses substantial charge-transfer character [9]. The same conclusion was more recently reached by Lockhart and Boxer [10] based on Stark measurements on P870.

In this paper we report the first application of hole burning to an antenna (core) protein complex, C670 of Photosystem I. These data are used to determine the importance of protein phonons for EET from the antenna complex to the PED state of the RC. The importance of site inhomogeneity to EET within the antenna complex at low temperatures is also considered. A vibronic (and phononic) satellite hole spectrum of an antenna complex, which represents the first high-resolution optical spectrum of an antenna complex, is presented and discussed. Finally, new high-resolution photochemical hole burning data are given for the P700 absorption region.

Table I. Electron-Phonon Coupling Parameters^a

	C670	P700	P870	P960
Γ_I, cm^{-1}	~200	~300	~350	~150
S	<0.9	5-6	4-5	4-5
ω_m, cm^{-1}	30	30	80	80
Γ, cm^{-1}	~40	30	50	40

^aData for C670 from this work. Other data from ref. 4. Γ_I , site inhomogeneous line broadening contribution to absorption profile at helium temperature; ω_m , mean phonon frequency; Γ , full-width half-maximum of the one-phonon profile.

EXPERIMENTAL

Enriched (~35:1 Chl *a*:P700) Photosystem I particles from spinach chloroplasts were isolated following the procedure of Golbeck [11] and dissolved in a buffered (pH 8.3) glycerol:water glass-forming solvent containing 1 mM ascorbic acid. A typical absorption spectrum showing a distinct P700 shoulder at 1.6K is given in reference 3. For the hole burning, the optical density (OD) at the burn frequency ω_B was adjusted to < 0.5 . A Coherent 699-21 dye laser (line width $\sim 0.002 \text{ cm}^{-1}$) was used for burning with intensity of $\lesssim 4 \mu\text{W}/\text{cm}^2$ (see Fig. 3 caption) for the high-resolution hole-widths studies. In these studies the read scans were performed in the transmission mode with the ring laser as the probe source (intensity set four orders of magnitude lower than the burn intensity). Moderate resolution ($\sim 0.2 \text{ cm}^{-1}$) hole reading was performed with a double beam spectrometer [12]. The laser dyes used for the C670 and P700 experiments were DCM and LD688.

RESULTS AND DISCUSSION

Figure 1 shows a persistent hole spectrum for C670 obtained for $\lambda_B = 670.48$ nm, $T_B = 1.6$ K, and at moderate resolution. The spectrum is dominated by a zero-phonon hole coincident with λ_B . The inset of Fig. 2 shows this hole burned to saturated [13]. The change in OD associated with the saturated hole is 17%. No intramolecular vibronic satellite holes to lower wavelength of λ_B are discernible (not surprising since the ODs of the the vibronic transitions, e.g., at $\lambda = 625$ nm, are ≤ 0.1). However, the broad but weak depression in OD identified by the arrow to the right of λ_B in Fig. 1 is a phonon sideband hole with a frequency of ~ 30 cm^{-1} . This hole is very similar to that shown in the inset of Fig. 2. We have, therefore, the first direct observation of a phonon sideband transition in a photosynthetic unit. The integrated area of the zero-phonon hole divided by the total intensity is given approximately by $\exp(-2S)$, where S is the the Huang-Rhys factor for C670 [2-4]. From the inset of Fig. 2 we obtain a value of $S \sim 0.9$ which corresponds to weak coupling. However, burn-time-dependent spectra are required for an accurate determination of S [14]. Since the coupling is weak, this means that the value of S determined from Fig. 2, when the zero-phonon hole is saturated, serves as a upper limit [14]. Since the fractional contribution of zero-phonon transition to the OD at ω_B in Fig. 1 is $\sim \exp(-S)$, one can estimate (from the inset of Fig. 1) that $\sim 40\%$ of the zero-phonon transitions are burnt at saturation for $S \sim 0.9$. Saturated hole depths rarely correspond to an OD change of greater than $\sim 50\%$ [15,16].

It can be concluded, therefore, that the linear electron-phonon coupling for C670 is weak in contrast with P700 where it is strong [3]. The implication of this for nonadiabatic EET [17-19] from C670 to P700 is interesting. It is protein modes

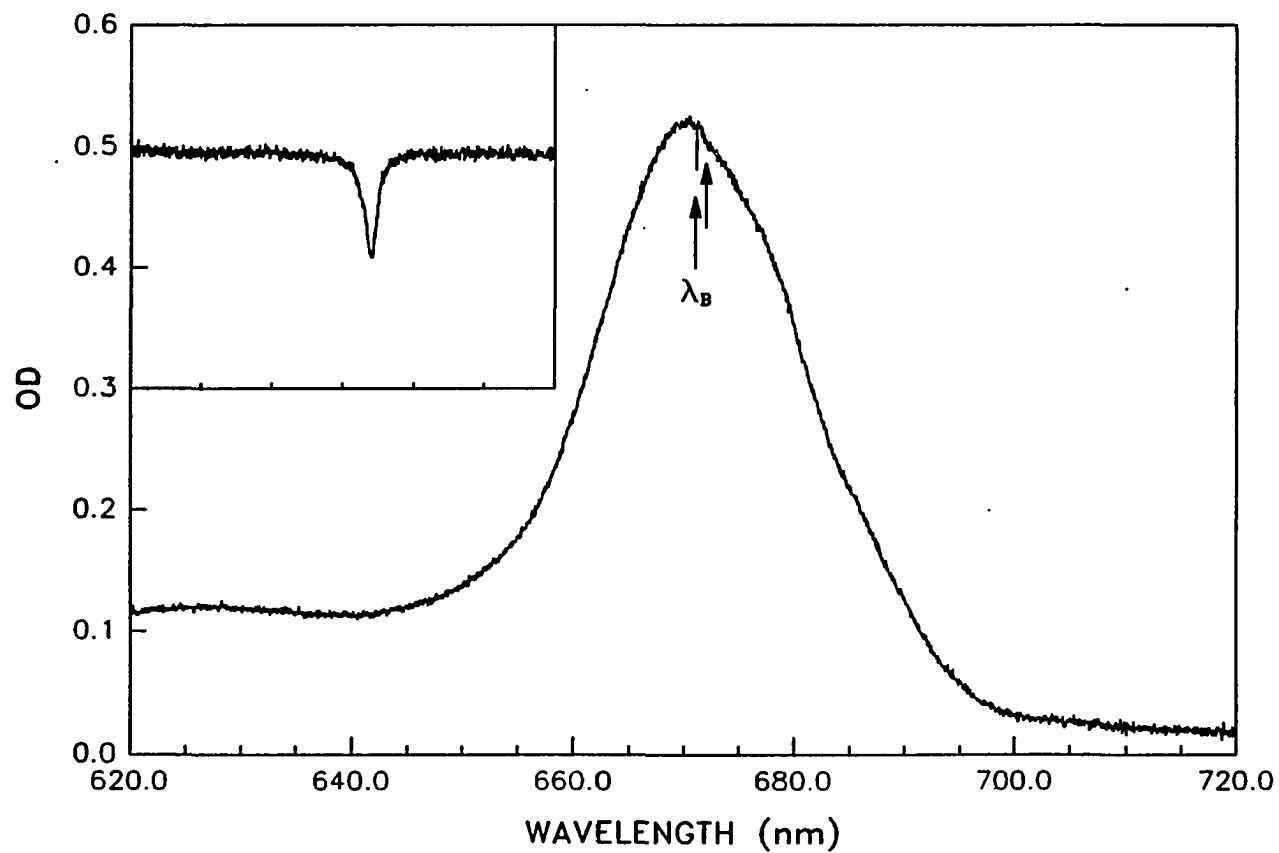


Figure 1. Hole burned spectrum for the PSI core antenna complex at 1.6 K. The burn wavelength $\lambda_B = 670.48$ nm. The arrow on the right locates the broad phonon sideband hole displaced by $\sim 30 \text{ cm}^{-1}$ from the zero-phonon hole. Inset shows a 3 Å scan recorded with a smaller step-size but same OD scale.

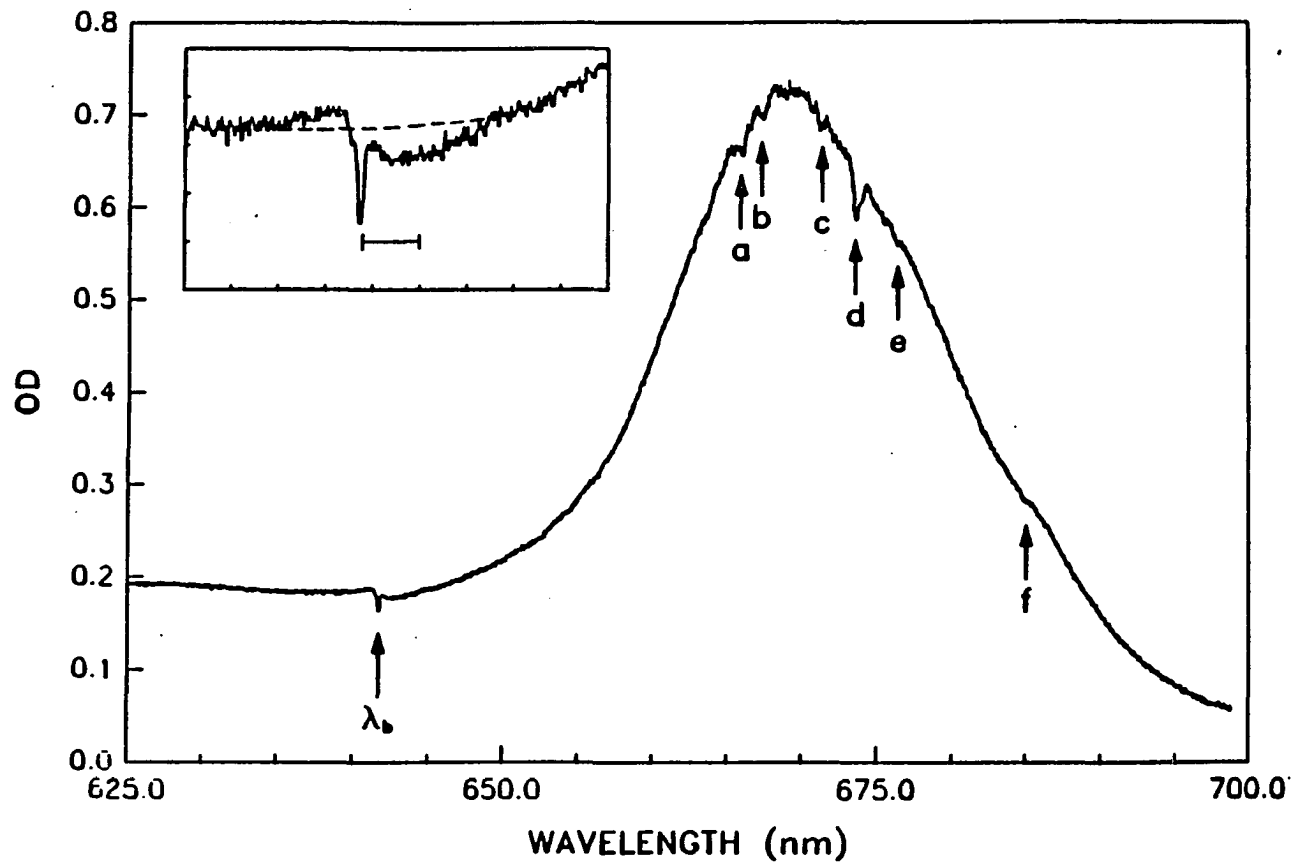


Figure 2. Vibronic and phononic hole structure of the PSI core antenna complex (C670) at 1.6 K. The burn wavelength is $\lambda_B = 641.45$ nm. Features a-f are vibronic satellite holes (see text). The inset spectrum shows the phonon sideband hole and anti-hole with the dashed line indicating the baseline prior to burning. The energy interval |—| just below the zero-phonon hole is 30 cm^{-1} . The ordinate scale for the inset is in OD units.

of frequency $\sim 30 \text{ cm}^{-1}$ are primary acceptor modes in the EET process. We note that protein modes associated with the strong electron-phonon coupling of P700 were identified as having a frequency that is also $\sim 30 \text{ cm}^{-1}$ [3].

The hole burning of C670 has been observed not to be affected by bleaching of P700 prior to burning of C670. Thus, the hole burning mechanism appears to be unrelated to irreversible charge separation in the RC of Photosystem I (i.e., the result of an electrochromic shift of antenna Chl *a* due to charge separation within the RC). We suggest, therefore, that the hole burning mechanism in nonphotochemical due to phonon-assisted tunneling between different configuration of the glasslike antenna protein complex. The antihole to the left of the zero-phonon hole in the inset of Fig. 2 is consistent with this mechanism. This mechanism is very common for topologically disordered pigment hosts in glasses and polymers [15,16,20]. The site inhomogeneous line broadening for C670 is discussed below.

The hole burned spectrum of Fig. 2 was obtained for a burn wavelength $\lambda_B = 641.45 \text{ nm}$ which is on the low E tail of the first vibronic transition ($\lambda \sim 625 \text{ nm}$) associated with C670. The vibronic satellite holes observed in the C670 absorption profile are analogous to those which have been observed [12,20] for laser dyes in polymer films (as just one example). Such structure is well understood. Thus, the displacement in cm^{-1} of features a-f measured relative to ω_B represent excited state vibrational frequencies of Chl *a*. The values obtained are 580, 601, 741, 802, and 986 cm^{-1} . Closer inspection of the satellite features reveals additional bands at 518, 676, 747 cm^{-1} . Except for the feature at 802 cm^{-1} , these frequencies agree extremely well ($\pm 2 \text{ cm}^{-1}$) with those determined from high-resolution studies of monoligated Chl *a* imbedded in a low temperature matrix [21]. By shifting λ_B to

lower values, it should be possible to determine the entire vibronic spectrum of Chl a in the antenna complex [20]. Such experiments are planned.

A zero-phonon hole coincident with ω_B can be produced over a wide range of ω_B values lying within the C670 absorption profile, traces A-C of Fig. 3. The λ_B values are 660.2, 670.3, and 678.1 nm, respectively. Thus, C670 possess significant site inhomogeneous line broadening ($\Gamma_I \gtrsim 200 \text{ cm}^{-1}$) since the results of Fig. 2 confirm that C670 is due to Chl a [22]. The hole widths corresponding to traces are 0.047, 0.036, and 0.032 cm^{-1} . These widths provide a lower limit for the depopulation lifetime (T_1) through the relation $T_1 = (\pi c \Delta\nu)^{-1}$, where $\Delta\nu$ is the hole width in cm^{-1} and c is the speed of light. The lifetimes corresponding to $\lambda_B = 660.2, 670.3, \text{ and } 768.1 \text{ nm}$ are 220, 290, 340 psec. The T_1 lifetimes may be longer if pure dephasing and/or spectral diffusion are contributing to the hole width [23]. Recently, Owens and coworkers [24] have used a random hopping model and picosecond fluorescence decay data for C670 to conclude that the single site EET time for Chl a is ~ 0.1 psec at room temperature. If the single site transfer (SST) occurred as rapidly at 1.6 K, the zero-phonon hole width would be $\sim 100 \text{ cm}^{-1}$. However, the time domain and hole burning results are not necessarily in disagreement. A marked lengthening of the SST time may be expected at very low temperatures relative to room temperature for a host medium which exhibits significant disorder (as mirrored by a large Γ_I) [25], as is the case for C670 in the core antenna complex. At a temperature of 1.6 K, EET is "downhill" from donor Chl a to acceptor Chl a and most involve phonon emission (for energy conservation) since $\Gamma_I \sim 200 \text{ cm}^{-1} \gg$ the energy uncertainty of the donor (acceptor) zero-point state due to total dephasing. For weak electron-phonon coupling ($S < 1$), an order of magnitude estimate for the lengthening factor of the SST time is 10-100. We note

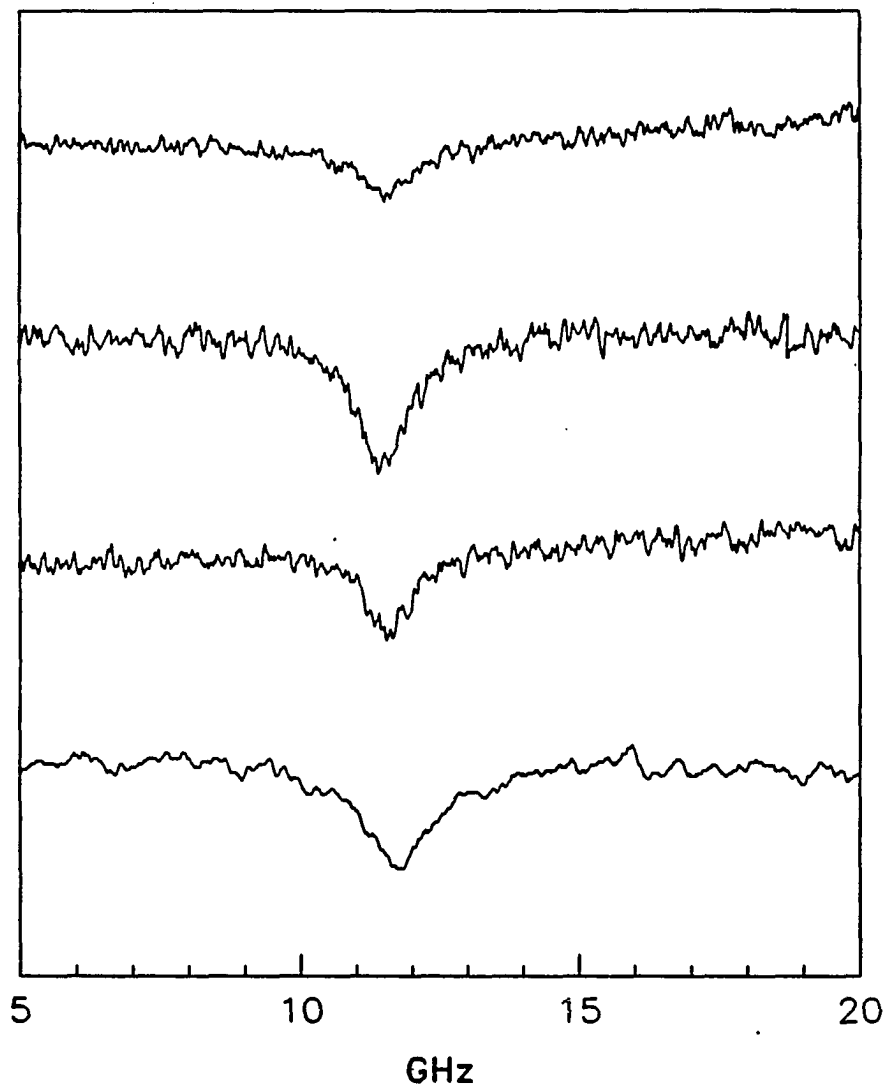


Figure 3. High resolution scans of holes burned in C670 (A-C) and P700 (D), 1.6 K. Burn wavelengths and percent ΔOD change are (A) 659.2 nm, 7.3%, (B) 670.3 nm, 9.7%, (C) 678.1 nm, 9.6% and (D) 709.6 nm, < 10%. Burn intensities were $4 \mu\text{W}/\text{cm}^2$ for A-C and $0.2 \mu\text{W}/\text{cm}^2$ for D. $30 \text{ GHz} = 1 \text{ cm}^{-1}$.

that for EET in an inhomogeneous medium the SST should increase as λ_B decreases [25]. This trend is exhibited by traces A-C of Fig. 3. In consideration of the above discussion it should be noted that the random hopping model for EET may be an oversimplification. It is conceivable that the core antenna protein structure could impart a degree of delocalized-exciton character to EET. The nature and spatial extent of exciton delocalization would be important in understanding the relationship between the frequency and the time domain data.

Earlier hole burning studies on P700 established that the hole profile is comprised of a weak but sharp zero-phonon hole (coincident with λ_B) superimposed on a broad intense hole [3]. An example of the former is shown in trace D of Fig. 3. If, as in reference 3, the zero-phonon hole width is taken to provide a lower limit for the ET time of P700, a value of 210 psec is obtained from Fig. 3. Very recently, however, we have performed hole burning following both chemical and white light bleaching of the P700 absorption and find that the broad hole is not formed while the sharp hole is. Thus, the possibility exist that only the former can be associated with P700 that is photoactive at helium temperatures. A lower limit of 210 psec for the ET time presents interpretive difficulties since recent room temperature time domain picosecond measurements yield a lifetime of ~ 10 (reference 26) and 2.8 (reference 24) psec. These values are within about a factor of two of those determined for P870 and P960 from time domain experiments [27,28]. Time domain studies have shown that the lifetime of P870 due to ET decreases by about a factor of two in going from room temperature to 8K and that the ET rate is constant for $T \lesssim 50$ K [29]. These results are in accord with earlier extensive T-dependent studies by Woodbury et al. [30].

REFERENCES

1. Bixon, M.; Jortner, J. *J. Phys. Chem.* 1986, 90, 3795.
2. Hayes, J. M.; Small, G. J. *J. Phys. Chem.* 1986, 90, 4928.
3. Gillie, J. K.; Fearey, B. L.; Hayes, J. M.; Small, G. J.; Golbeck, J. H. *Chem. Phys. Lett.* 1987, 134, 316.
4. Hayes, J. M.; Gillie, J. K.; Tang, D.; Small, G. J. *Biochim. Biophys. Acta*, 1988, 932, 287.
5. Boxer, S. G.; Middendorf, T. R.; Lockhart, D. L. *Chem. Phys. Lett.* 1986, 123, 476.
6. Meech, S. R.; Hoff, A. J.; Wiersma, D. A. *Chem. Phys. Lett.* 1985, 121, 287.
7. Boxer, S. G.; Middendorf, T. R.; Lockhart, D. J. *FEBS Lett.* 1986, 200, 237.
8. Meech, S. R.; Hoff, A. J.; Wiersma, D. A. *Proc. Natl. Acad. Sci. U.S.A.* 1986, 83, 9464.
9. Parson, W. W.; Scherz, A.; Warshel, A. In Antennas and Reaction Centers of Photosynthetic Bacteria, Michel-Beyerle, M. E., Ed.; Springer-Verlag: Berlin, 1985; Springer Series in Chemical Physics, Vol. 42, p 122.
10. Lockhart, D. J.; Boxer, S. G. *Biochemistry* 1987, 26, 664.
11. Golbeck, J. H. In Methods in Enzymology, San Pietro, A., Ed.; Academic: New York, 1980; Vol.69, p 129.
12. Fearey, B. L.; Carter, T. P.; Small, G. J. *J. Phys. Chem.* 1983, 87, 3600.
13. Maximum hole depth.
14. Friedrich, J.; Swalen, J. D.; Haarer, D. *J. Phys. Chem.* 1980, 73, 705.

15. Small, G. J. In Spectroscopy and Excitation Dynamics of Condensed Molecular Systems, Agranovich, V. M., Hochstrasser, R. M. Eds.; North Holland: Amsterdam, 1983, p 515.
16. Hayes, J. M.; Jankowiak, R.; Small, G. J. In Persistent Spectral Hole-Burning: Science and Applications, Moerner, W. E., Ed.; Springer-Verlag: West Berlin, 1988, p 153..
17. Förster, T. *Naturwissenschaften* 1946, 33,166.
18. Dexter, D. L. *J. Chem. Phys.* 1953, 21, 836.
19. Kubo, R.; Toyozawa, Y. *Prog. Theor. Phys.* 1966, 13, 160.
20. Hayes, J. M.; Fearey, B. L.; Carter, T. P.; Small, G. J. *Int. Rev. Phys. Chem.* 1986, 5, 175.
21. Rebane, K. K.; Avarmaa, R. A. *Chem. Phys.* 1982, 68, 191.
22. Shoulders to lower energy of 670 nm in Fig. 1 indicate that in the core antenna complex there is more than one type of protein environment for Chl a.
23. See reference 19 and references therein.
24. Owens, T. G.; Webb, S. P.; Mets, L.; Alberte, R. S.; Fleming, G. R. *Biophysics*, submitted for publication.
25. Rockwitz, K. D.; Bässler, H. *Chem. Phys.* 1982, 70, 307.
26. Fenton, J. M.; Pellin, M. J.; Govindjee; Kaufmann, K. J. *FEBS Lett.* 1979, 100, 1.
27. Martin, J. L.; Breton, J.; Hoff, A. J.; Migus, A.; Antonetti, A. *Proc. Natl. Acad. Sci. U.S.A.* 1986, 83, 958.
28. Wasielewski, M. R.; Tiede, D. M. *FEBS Lett.* 1986, 204, 368.

29. Breton, J.; Fleming, G. R.; Martin, J. L., private communication, Service of Biology, Dept. of Biology, CEN Saclay, France.
30. Woodbury, N. W.; Becker, M.; Middenhoff, D.; Parsons, W. W. *Biochemistry* 1985, 24, 7516.

**PAPER II. NONPHOTOCHEMICAL HOLE BURNING OF THE NATIVE
ANTENNA COMPLEX OF PHOTOSYSTEM I (PSI-200)**

**Nonphotochemical Hole Burning of the Native Antenna
Complex of Photosystem I (PSI-200)**

J. K. Gillie, G. J. Small, J. H. Golbeck

Journal of Physical Chemistry 1989, 93, 1620

INTRODUCTION

Because of its importance in electronic excitation transfer and charge separation in the photosynthetic unit, the lowest excited singlet (Q_y) state of chlorophyllic molecules has been the subject of a number of high resolution absorption and fluorescence studies [1-7]. As a result, considerable information on the active excited and ground state intramolecular mode frequencies for chlorophyll a, (Chl a), Chl b, bacteriochlorophylls, as well as other pigments is available. Raman studies of the ground state modes are more extensive and have been the subject of recent reviews [8,9]. Despite the number of optical studies, however, the Franck-Condon factors associated with the $Q_y \leftarrow S_0$ transition have not been determined even for "isolated" Chl monomers imbedded in host matrices. Nevertheless, it is apparent from the published fluorescence line narrowed (FLN) spectra for the isolated monomers that the linear electron-vibration coupling associated with the Q_y state is weak for all modes [1,2].

The question of whether this is also the case and the determination of the Franck-Condon factors for protein-bound Chl species are important for a number of reasons. Included are the determination of the role of the intramolecular vibrations as acceptor modes for excitation transport from the antenna to the reaction center (RC) complex [10,11] and charge-separation within the RC [12-16]. Another pertains to the theoretical modeling of the absorption profile of the lowest Q_y transition of the special pair in the RC of photosynthetic bacteria [12,17,18].

The above determination for Chl a and b in a light harvesting complex of Photosystem I (PSI-200) is the focus of this paper. Earlier nonphotochemical hole burning (NPHB) [19] studies of a core antenna complex of Photosystem I (devoid of

the Chl a/b polypeptide, enrichment Chl a:P700 ~35:1) demonstrated that rich vibronic hole structure [20,21] can be observed for a protein-bound pigment. Because of our concern that the extensive extraction procedure used to obtain the 35:1 particles may produce a significant amount of inactive (in excitation transfer [19,22]) Chl a, it was decided that further NPHB studies should focus on the more natural PSI-200 particles whose Chl:P700 ratio is ~ 200:1, see following section. It is shown here that exceptionally high quality NPHB vibronic hole spectra are obtainable for PSI-200. As a result, the excited state frequency and Franck-Condon factors for 41 fundamental vibrations have been determined for Chl a (15 for Chl b). All Franck-Condon factors are ≤ 0.04 . These results are discussed in comparison to the available data for Chl a and b monomers in glassy matrices.

Also important for the understanding of transport phenomena in the photosynthetic unit is the determination of the linear electron-phonon (protein) coupling strength. This coupling is a measure of the protein reorganization energy associated with excitation of the Q_y state. NPHB data which speak to the magnitude of this coupling are also presented and discussed. Finally, NPHB data that relate to the time scale of the initial phase of excitation transport within the antenna at 1.6 K are presented and theoretically discussed in terms of the available room temperature time domain data.

EXPERIMENTAL

PSI-200 particles (Chl:P700 ratio 200:1) were isolated from the chloroplast of spinach [23]. This "native" PSI particle contains the full complement of polypeptide subunits that act as light harvesting antenna and the P700 reaction center with its associated electron acceptors [24,25]. The antenna polypeptides are organized into the light harvesting chlorophyll complex (LHCI) containing 100 Chls with a Chl a:Chl b ratio of ~ 3.5 [24,26,27] and the Chl a polypeptides associated with the PSI reaction center core antenna complex C670 [24,26]. Overall, the Chl a:Chl b ratio is ~ 6 [24,28]. The PSI-200 particle retains the structural and functional properties of PSI in thylakoids [24]. The particles were stored at 77 K in a buffered (pH 8.3) glycerol:H₂O mixture containing 0.1% triton X-100 and used as needed.

Optical densities of samples were adjusted to ≤ 0.8 (at the 670.0 nm Chl a absorption maximum) by dilution in a buffered glycerol:H₂O glass forming solvent (pH 8.3) to which 1 mM ascorbic acid has been added. The samples were quickly cooled (<10 minutes) in the dark to 4.2 K in a Janis model 8-DT Super Vari-Temp liquid helium cryostat. All experiments were performed with the sample immersed in superfluid He at 1.6 K.

The burn laser utilized was a Coherent 699-21 ring dye laser. For the vibronic hole experiments, this laser was used broad band (linewidth 0.07 cm^{-1}) with burn intensities of $\sim 1 \text{ W/cm}^2$, DCM laser dye. Moderate resolution ($\sim 0.2 \text{ cm}^{-1}$) of vibronic hole spectra was performed in the transmission mode with a computer controlled double beam spectrometer (1.5 m Jobin-Yvon Model HR 1500) [20]. Output of a 500 W xenon lamp (Canrad Hanovia 960C1980) was dispersed by the spectrometer prior to incidence on the sample. For the high resolution studies of the

zero-phonon holes coincident with λ_B (burn wavelength), burning and reading were performed with the dye laser operating in the single frequency mode (linewidth 0.002 cm^{-1}). Burn intensities were $<1 \text{ } \mu\text{W}/\text{cm}^2$ and for the read scans (30 GHz), performed in transmission, the probe intensity was set 3 orders of magnitude lower than the burn intensity.

RESULTS

Vibronic Hole Structure

Figure 1 shows a pre-burn and hole burned spectrum for PSI-200. The latter was obtained with $\lambda_B = 670.0$ nm located at the center of the origin band for Chl a and a burn intensity (I_B) of 4 W/cm^2 and burn time (τ_B) of 20 min. At this fluence the ZPH (zero-phonon hole) is saturated [29,30]. The difference spectrum, shown as the inset in Fig. 1, reveals more clearly the broad hole (FWHM $\sim 66 \text{ cm}^{-1}$) displaced to lower energy of λ_B by 22 cm^{-1} . It will be argued later that this hole is a pseudo-phonon side band hole (pseudo-PSBH). The combined intensity of the ZPH and pseudo-PSBH can be seen to be compensated by the intensity of the anti-hole to the left of the ZPH, inset spectrum of Fig. 1. Thus, the mechanism for hole production is nonphotochemical [31-34] and must be associated with protein-pigment configurational tunneling induced by excitation [19,32-34]. To our knowledge, the spectra of Fig. 1 provide the best available example in any system for the conservation of absorption intensity associated with NPHB. This conservation is also illustrated in Fig. 2 for NPHB of the origin band of Chl b. Data, presented later, lead to a determination of the Huang-Rhys factor (S) for Chl of ~ 0.8 . Since the intensity of an r -phonon process is governed by the Poisson distribution $\exp(-S)S^r/r!$ [12 and ref. therein], it is readily calculated that $\sim 80\%$ of the Chl a sites whose zero-phonon transition is coincident with λ_B (Fig. 1) are burned. The failure to observe 100% hole burning may be due to spontaneous hole filling [34,35] and/or Chl a in protein configurations not amenable to NPHB. In any event, our concern that in earlier studies on the core antenna complex of PSI the NPHB was due to inactive or unnatural Chl a resulting from the isolation procedure appears to be removed. The

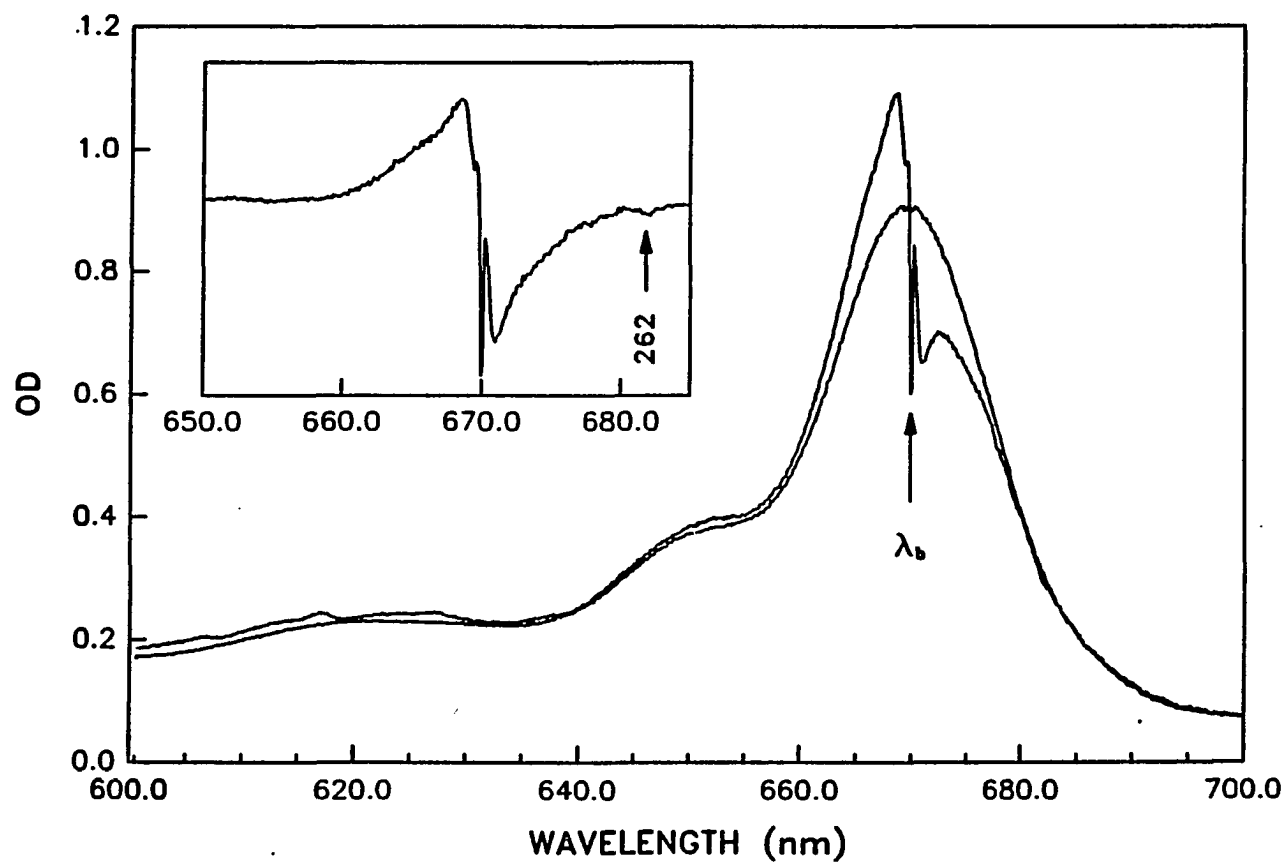


Figure 1. Hole burned spectrum of PSI-200. The burn wavelength $\lambda_B = 670.0$ nm. The broad phonon sideband hole is displaced to the right of λ_B by ~ 25 cm^{-1} . The anti-hole is evident to the left of λ_B . The difference absorption spectrum is shown in the insert. The arrow marks the 262 cm^{-1} Chl a vibration (see text).

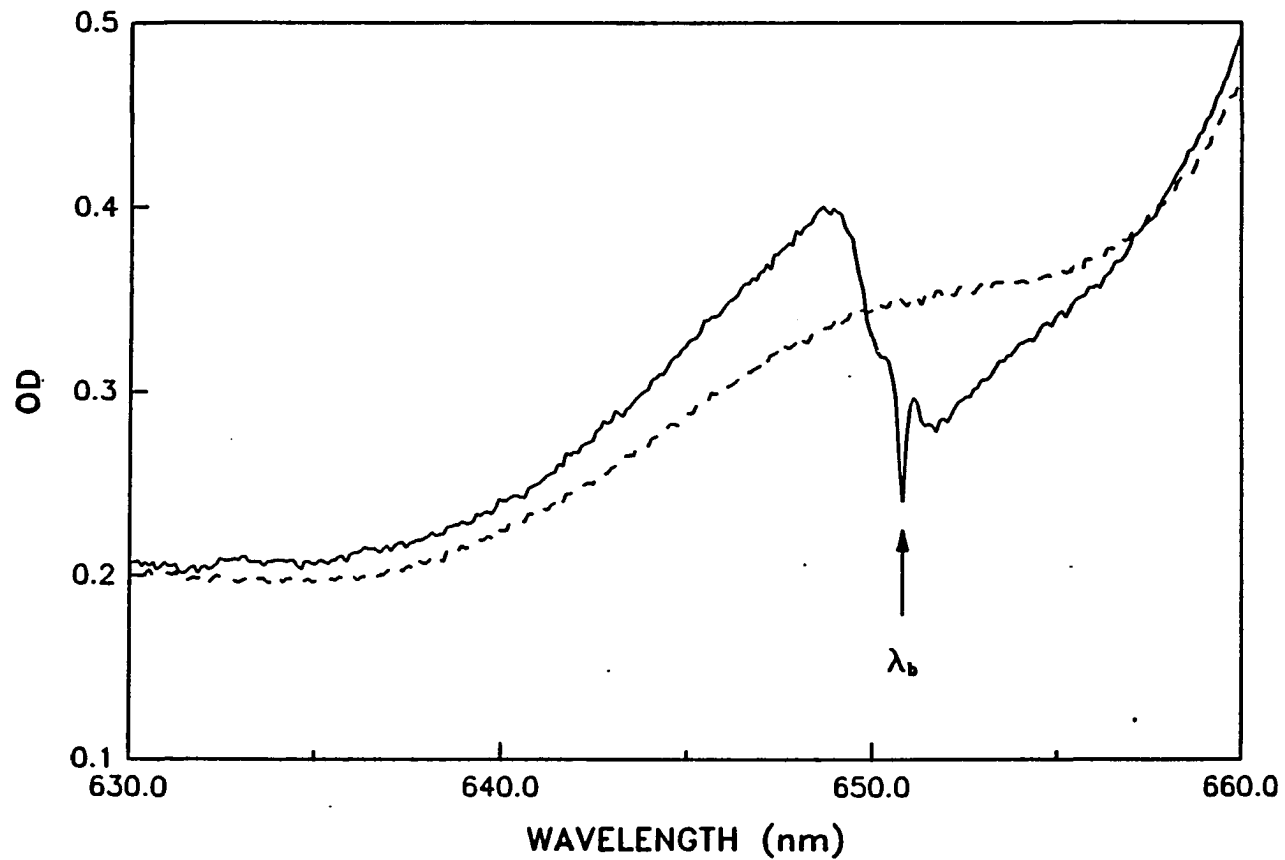


Figure 2. Hole burned spectrum of the origin region of Chl b in PSI-200. The broad phonon sideband is displaced $\sim 22 \text{ cm}^{-1}$. The anti-hole is evident to the left of λ_B . The broken line is the pre-burn absorption.

FWHM of the saturated ZPH measured at a read resolution of 0.2 cm^{-1} is 0.9 cm^{-1} . The FWHM of the ZPH obtained in the short burn time limit (O.D. change $<10\%$) with a read resolution of 0.002 cm^{-1} is 0.025 cm^{-1} (profile not shown). It is well known and understood [35-39] that ZPH widths undergo significant broadening when the short burn time limit is not satisfied. The ZPH width of 0.025 cm^{-1} compares well with those obtained earlier for the core antenna complex (C670) in the short burn time limit [19].

In the pre-burn spectrum of Fig. 1, weak vibronic structure to higher energy of the origin bands of Chl a and b can be discerned. Earlier NPHB studies have demonstrated that, with excitation into congested vibronic absorption regions, vibronic satellite hole structure can be burned into the origin bands [19-21]. The displacements of the satellite holes from this yield the excited state frequencies of the Franck-Condon active modes. This is illustrated in Fig. 3 for $\lambda_B = 650.1 \text{ nm}$ excitation which results in the appearance of extensive vibronic hole structure in the origin band of Chl a. The associated difference spectrum is shown in Fig. 4, where several of the prominent holes are labeled by their excited state vibrational frequency (in cm^{-1}). By tuning λ_B , it is possible to map out the frequencies for all active modes. Difference spectra for $\lambda_B = 635.0$ and 616.1 nm are shown in Figs. 5 and 6, respectively, which show activity for Chl b in addition to Chl a. The excited state fundamental vibrational frequencies for Chl a and b are tabulated in Tables I and II. Also included are the measured Franck-Condon factors. With reference to Table I, these factors were obtained as follows: the spectrum shown in Fig. 1 was used to determine the hole (ZPH + pseudo-PSBH) intensity ratio of the 262 cm^{-1} mode to the origin band whose ZPH is coincident with λ_B . This ratio was then scaled by the ratio of the optical densities of the pre-burn spectrum at ω_B and

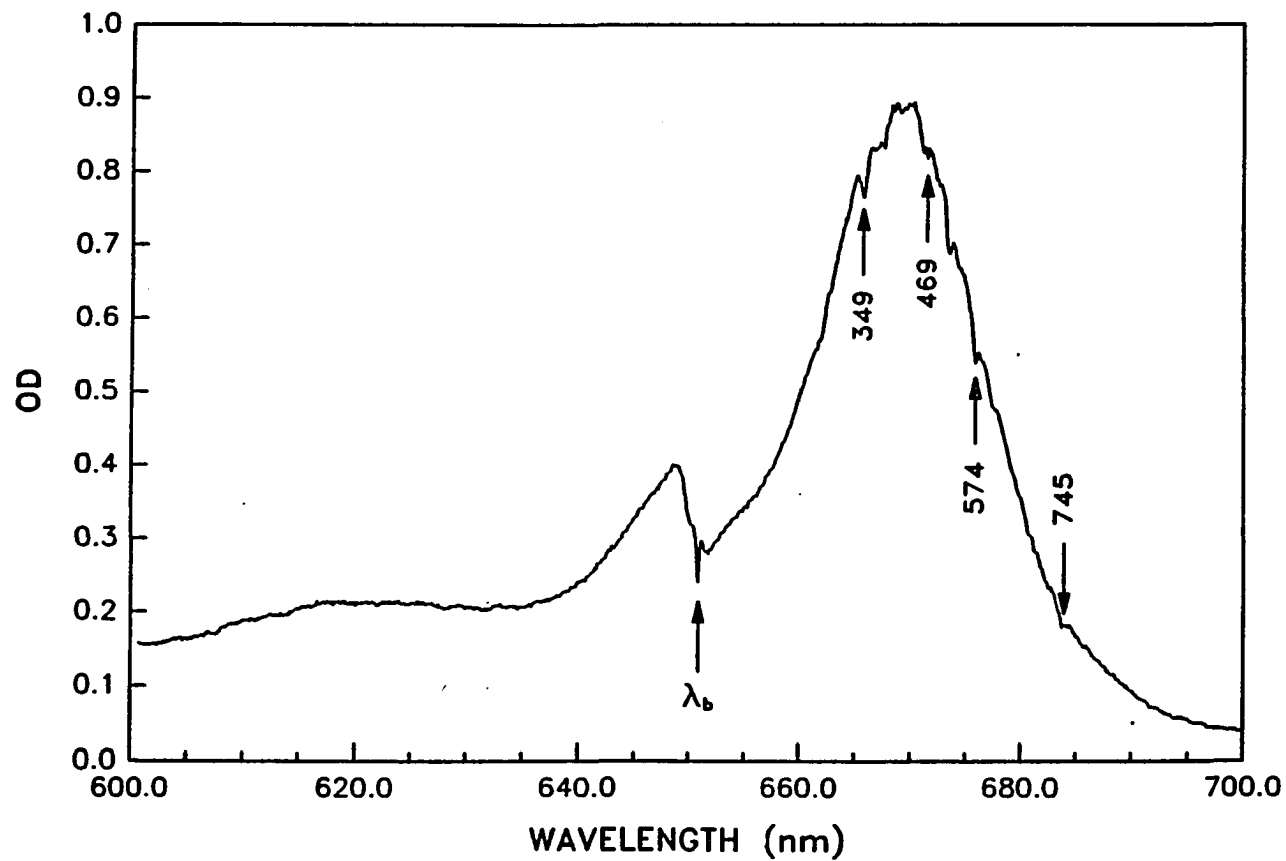


Figure 3. The hole burned spectrum of PSI-200 at 1.6 K for burn $\lambda_B = 650.1$ nm. Satellite holes are labeled with excited state vibrational frequencies (cm^{-1}).

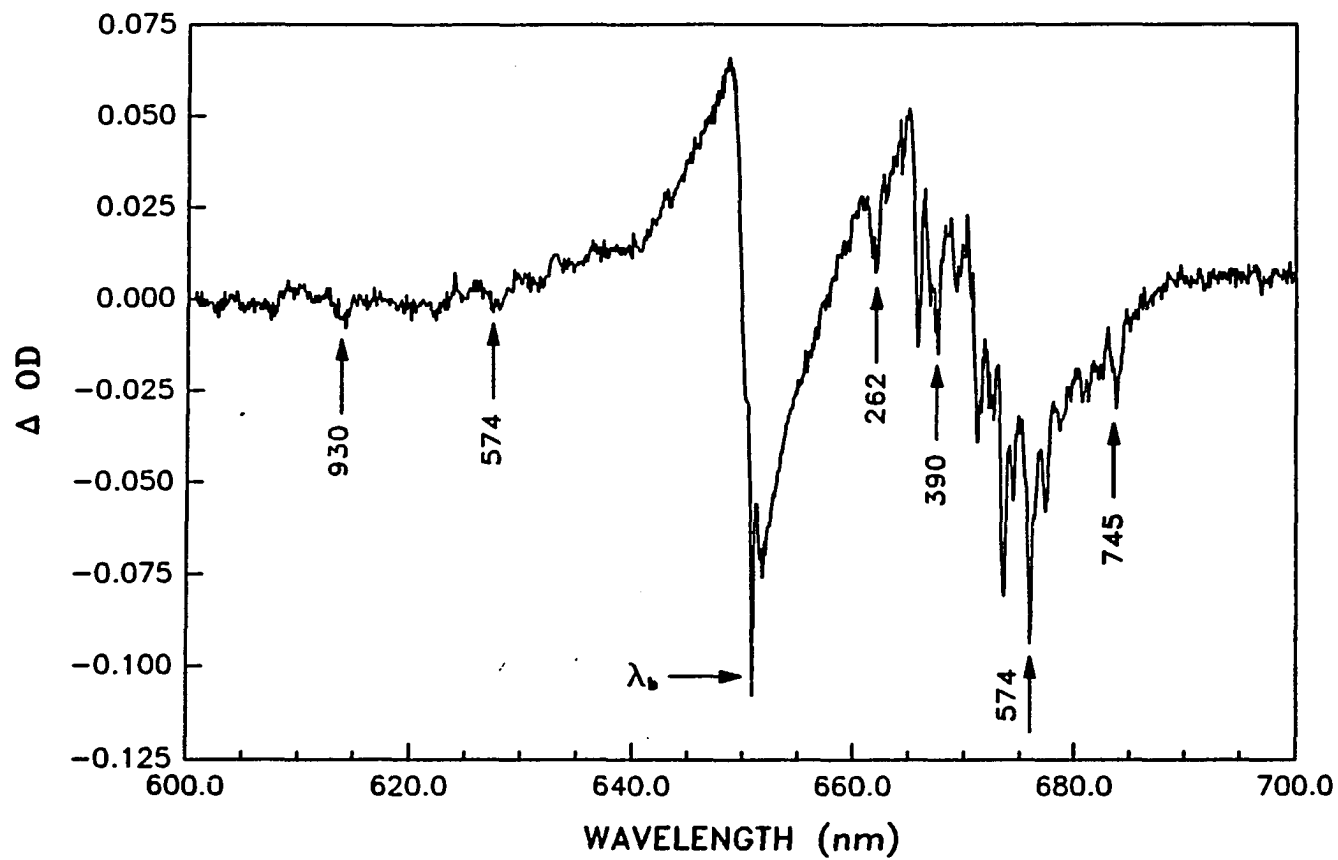


Figure 4. The difference hole burned spectrum of PSI-200 at 1.6 K for burn $\lambda_B = 650.1$ nm. Satellite holes are labeled with excited state vibrational frequencies (cm^{-1}).

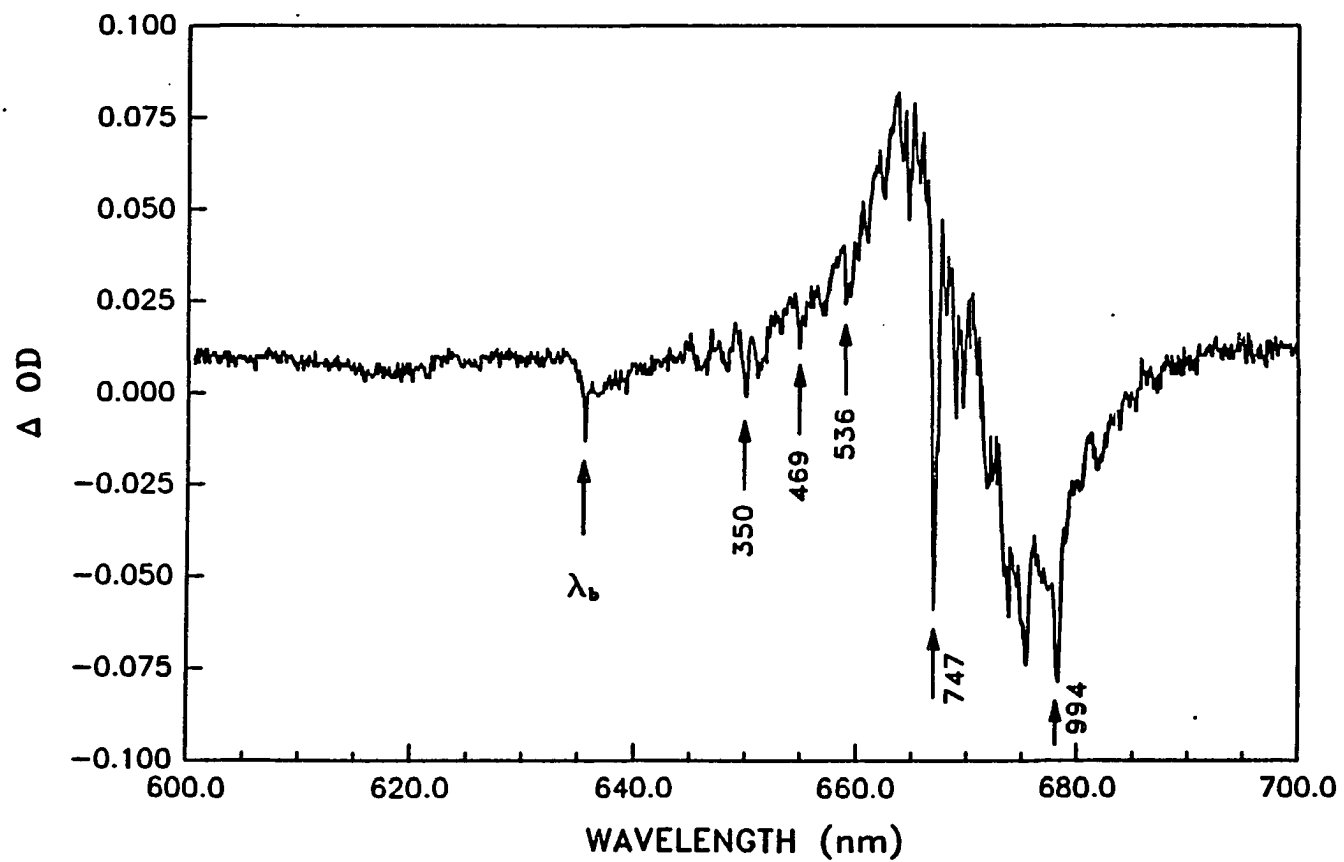


Figure 5. The difference hole burned spectrum of PSI-200 at 1.6 K for burn $\lambda_B = 635.0$ nm. Satellite holes are labeled with excited state vibrational frequencies (cm^{-1}).

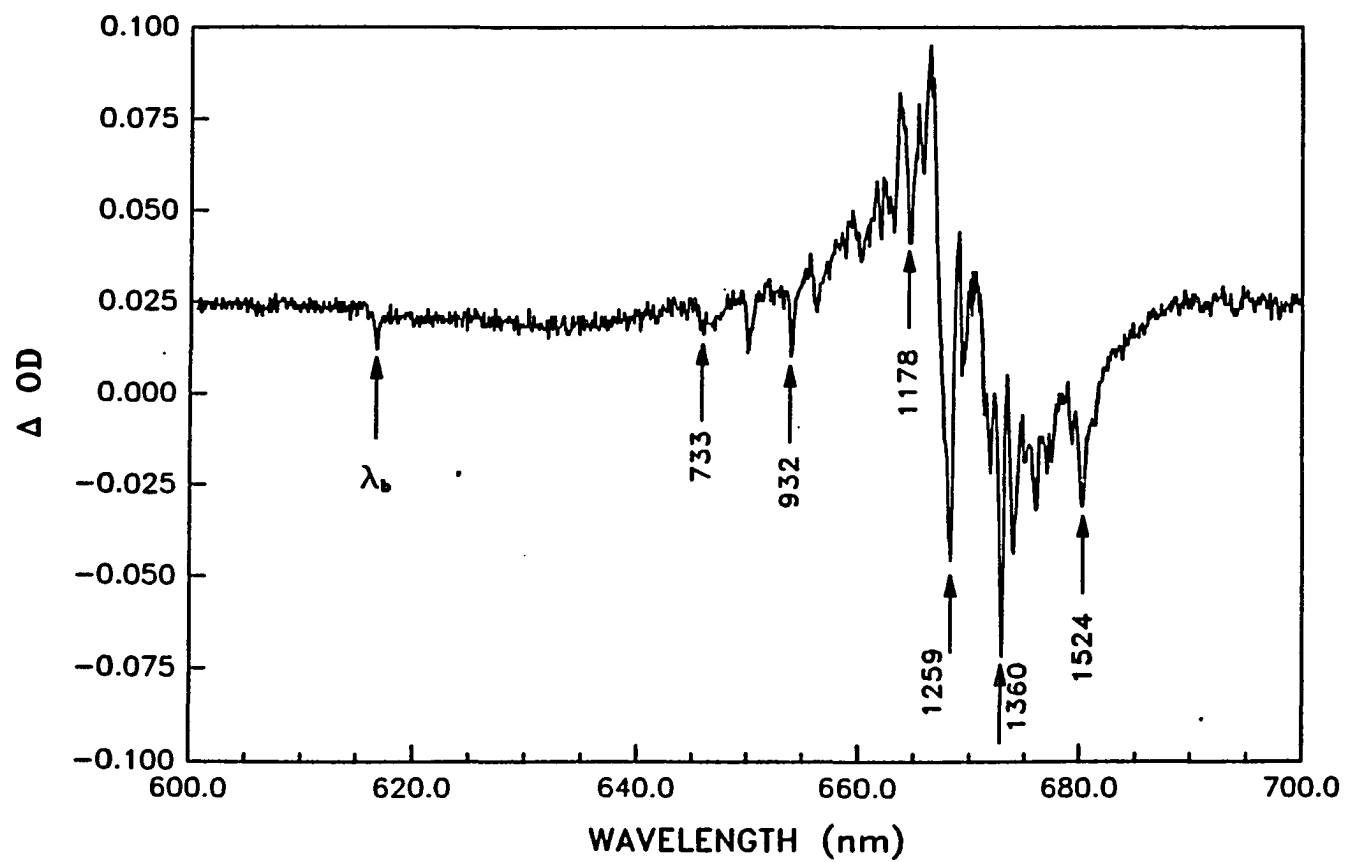


Figure 6. The difference hole burned spectrum of PSI-200 at 1.6 K for burn $\lambda_B = 616.1$ nm. Satellite holes are labeled with excited state vibrational frequencies (cm^{-1}).

Table I. PSI-200 S_1 vibrational frequencies (cm^{-1}) and Franck-Condon factors for Chla obtained by nonphotochemical hole burning at 1.6 K

S_1 Vibrational Frequencies ^b	Franck-Condon Factors ^b	Fluorescence (relative intensity) ^a	
		S_1	S_0
262	0.012	263 (3)	260
283	0.004		
390	0.015	390 (2)	390
425	0.007		
469	0.019	465 (2)	470
501	0.007		
521	0.017	515 (1)	520
541	0.009		
574	0.025	570 (2)	570
588	0.005	583 (1)	
607	0.012	600 (1)	
638	0.009	635 (1)	
692	0.015	688 (1)	
714	0.010		
746	0.044	748 (3)	745
771	0.007	765 (1)	
791	0.014	785 (1)	
805	0.012		
819	0.005		
855	0.009		
864	0.007		
874	0.007	880 (1)	
896	0.013	890 (1)	
932	0.025	925 (1)	915
994	0.028		
1009	0.005	1005 (1)	
1075	0.012	1075 (2)	
1114	0.009	1110 (2)	

^aFrom ref. 2.

^bThis work.

Table I. (continued)

S_1 Vibrational Frequencies ^b	Franck-Condon Factors ^b	Fluorescence (relative intensity) ^a	
		S_1	S_0
1178	0.018	1168 (2)	1185
1203	0.012	1195 (1)	
1259	0.041	1250 (5)	
1285	0.011	1275 (1)	
1340	0.011	1345 (3)	1385
1364	0.032	1372 (2)	
1390	0.018	1395 (1)	
1411	0.005	1415 (1)	1430
1433	0.009		
1455	0.006		
1465	0.006		
1504	0.010	1510 (3)	1525
1524	0.032	1530 (2)	1545

ω_B-262 . Since the resulting ratio is $\ll 1$ it is, to a very good approximation, equal to the Franck-Condon factor given as 0.012 in Table I. Because the mode frequency changes between the S_0 and S_1 states are small (see last column of Table I), the Franck-Condon factor is just the Huang-Rhys factor S_{262} . The remaining Franck-Condon factor (S values) in Table I were obtained from S_{262} by utilizing the measured ZPH intensity of each vibronic hole relative to that of 262 with due account being given to optical density differences in the pre-burn spectrum, *vide supra*. The spectra in Figs. 4-6 yielded the data given in Table I.

Avarmaa and Rebane [1,2] have previously determined the excited state mode frequencies and relative intensities for Chl a (mono-ligated) in a diethyl ether glass from vibronically excited fluorescence line narrowed spectra. Their data are given in the third column of Table I. More recently, the same technique has been used for PSI-200 [40]. There is generally good agreement between these PSI-200 and the Chl a/diethyl ether data. Comparison of the data in the third column of Table I with those of the first and second columns is revealing. The protein-Chl a interactions are apparently sufficiently weak to produce only slight frequency changes. Furthermore, there are similarities between the relative vibronic intensities of Chl a in PSI-200 and Chl a/diethyl ether. Because of the high degree of vibrational congestion in the S_1 state of Chl a, the degree of dependence of these intensities on the host medium apparent in Table I could be due to excited state mode mixing (Duschinsky effect) [41] modulated by the medium [42].

No activity by Chl a modes with a frequency less than 262 cm^{-1} was observed in the hole burned spectra of PSI-200 or in ref. (19). Thus, it appears that the 140 cm^{-1} mode observed for Chl a in n-octane by Plantenkamp and co-workers [7] is

peculiar to the n-octane host. The Franck-Condon factor for a 140 cm^{-1} mode of Chl a in PSI-200 would have to be $\leq 4 \times 10^{-4}$ in order to escape detection by NPHB.

The procedure described above for Chl a was used to obtain the Franck-Condon factors for Chl b in LHCI, Table II. Significantly less vibrational information for Chl b is provided by NPHB because the Chl b/Chl a content ratio in PSI-200 is $\sim 1/6$ and the Chl b origin band lies on the high energy tail of the Chl a origin, Fig. 1. As is the case for Chl a, the agreement between the excited state mode frequencies of Chl b in LHCI and as a mono-ligated monomer in the diethyl ether glass is good. There also appears to be some dependence of the relative vibronic intensities on the host medium, Table II.

An important conclusion that can be drawn from the data in Tables I and II is that the linear electron-intramolecular vibration coupling for both Chl a and b in PSI-200 is very weak with the maximum Huang-Rhys factor S measured being ~ 0.04 . The linear electron-phonon coupling is considerably stronger than that for any of the intramolecular vibrations as will now be discussed.

Phonon Sideband Hole Structure

In the presence of linear electron-phonon coupling, a phonon sideband hole (PSBH) is predicted on both the high and low energy side of the ZPH coincident with λ_B [12 and refs. therein]. The former has been referred to as the real PSBH [36,37] since it builds on the ZPH, i.e., the intensity of the PSBH relative to that of the ZPH is governed by S , the Huang-Rhys factor. In contrast, the low energy PSBH is referred to as the pseudo-PSBH [36,43] since it is the result of the burning of sites (whose zero-phonon frequencies lie lower than ω_B) which absorb ω_B via their phonon sideband. Short burn time limit model calculations of the ZPH and

Table II. PSI-200 S_1 vibrational frequencies (cm^{-1}) and Franck-Condon factors for Chlb obtained by nonphotochemical hole burning at 1.6 K

S_1 Vibrational Frequencies ^b	Franck-Condon Factors ^b	Fluorescence (relative intensity) ^a S_1
255	0.010	255 (1)
315	0.009	310 (2)
350	0.021	345 (3)
374	0.012	375 (2)
563	0.015	560 (1)
681	0.009	680 (1)
733	0.005	732 (2)
752 (shoulder)		750 (2)
757	0.006	
833	0.005	832 (2)
840	0.005	
983	0.010	980 (2)
1045	0.007	1040 (1)
1090	0.006	1087 (4)
1143	0.010	1140 (5)

^aFrom ref. 2.

^bThis work.

PSBHs have recently been presented for S -values ranging from 1 to 8 [12]. It is only in the short burn time limit that the intensities of the ZPH and pseudo-PSBH can be used to determine S . In the long burn time limit (e.g. ZPH saturated), the pseudo-PSBH intensity relative to that of the ZPH can be significantly greater than that expected on the basis of the S -value and the aforementioned Poisson distribution. This is the situation for Fig. 1 where it is apparent that if the pseudo-PSBH hole intensity were used to determine S , a value much greater than unity would be obtained. It is also apparent that, with NPHB, the appearance of the anti-hole to higher energy of the ZPH prevents a determination of the real PSBH.

Figure 7 shows the dependence of the ZPH and pseudo-PSBH on burn time (τ_B) for $I_B = 10 \text{ mW/cm}^2$ and $\lambda_B = 669.5 \text{ nm}$. The dominance of the one-phonon hole at $\omega_B - 22 \text{ cm}^{-1}$ indicates that $S \lesssim 1$. In the short burn time limit the ZPH:(ZPH + one-phonon pseudo-PSBH) intensity ratio is given by $(1+S)^{-1}$. The calculated values of S for $\tau_B = 1, 5, 10$ and 20 min are 0.8, 1.0, 1.1 and 1.2, respectively. Thus, a reasonable estimate of S is 0.8. An earlier study of the core antenna complex of PSI had yielded $S \lesssim 0.9$ for Chl a [19]. As a check on the value of 0.8 for S , the one-phonon hole profile for $\tau_B = 1 \text{ min}$ in Fig. 7 was analytically fit and subtracted from the pseudo-PSBH profile for $\tau_B = 20 \text{ min}$ after scaling to match the peak pseudo-PSBH intensity at $\omega_B - 22 \text{ cm}^{-1}$. The resulting spectrum exhibited a 2-phonon hole at $\omega_B - 2 \times 22 \text{ cm}^{-1}$ whose integrated intensity is ~ 0.23 that of the one-phonon + two phonon hole profile. The corresponding theoretical ratio is $2^{-1}S/(1+2^{-1}S)$ which, when set to 0.23, yields $S=0.6$. This is in reasonable agreement with 0.8 considering the interference from the anti-hole.

Extensive studies of the dependence of S and ω_m (mean phonon frequency) on λ_B for both Chl a and Chl b have not yet been performed. Preliminary studies

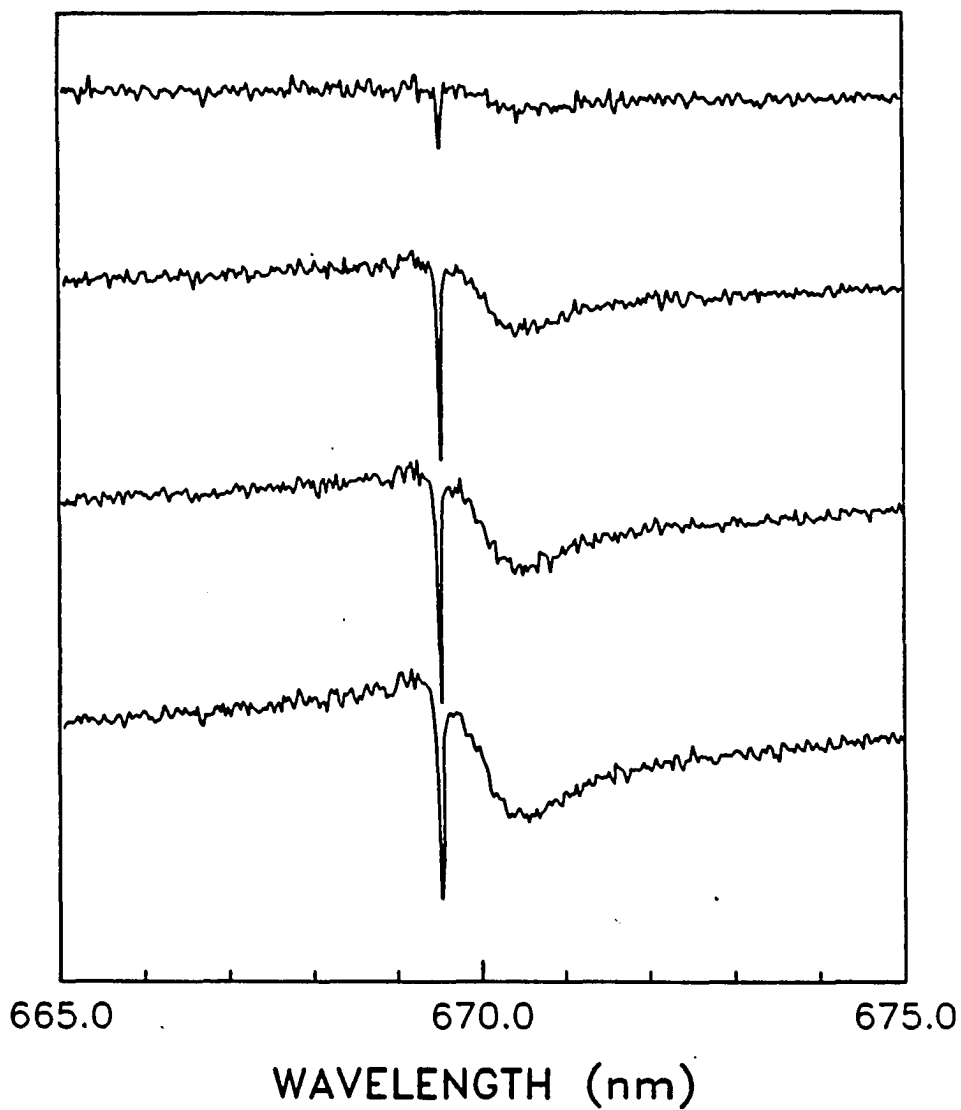


Figure 7. Time dependent zero-phonon and pseudo-phonon development for PSI-200. The burn wavelength is 669.5 nm. Burn times (from top to bottom) are 1, 5, 10, 20 min. Burn intensity was 10 mW/cm^2 . The OD scale is equivalent for all spectra. The tailing feature to the left of λ_{P} is the anti-hole.

with $\lambda_{\text{B}} = 677.2$ and 650.2 nm (Chl b excitation) indicate that the coupling strength does not vary significantly between these two wavelengths. Thus, it appears likely that the linear electron-phonon coupling will be weak ($S \sim 0.8$) for all Chl monomers which contribute significantly to the $S_1(Q_y) \leftarrow S_0$ absorption system. However, this coupling is significantly stronger than that associated with the intramolecular modes for which $S \lesssim 0.04$, *vide supra*.

DISCUSSION

The present work on PSI-200 and earlier studies on the core antenna complex of PSI [19] have shown that the Huang-Rhys factor S for antenna Chl a is ~ 0.8 . In this section the role of phonons as mediators for excitation transport within the core antenna complex will be focused on. The details of this mediation will depend on whether the phonons observed in this work are delocalized protein modes or resonant (pseudo-localized) phonons with a large amplitude of vibration centered on the excited pigment. For example, the familiar Dexter-Förster energy transfer theory [44,45], with its donor-acceptor spectral overlap criterion, is based on the precept of localized vibrations. The underlying theory for excitation transport involving delocalized phonons is fundamentally different [46]. Also important is the question of the accuracy with which regular antenna pigment array models can describe excitation transport. Organization of the antenna into subunits, containing several strongly interacting Chl molecules, would necessitate the incorporation of delocalized exciton structure for the subunits into the model. For the case of the green bacterium *Prosthecochloris aestuarii*, whose antenna structure has been determined [47,48], the basic structural unit is a trimer of subunits. Within a subunit nearest neighbor center to center distances between 11 and 14 Å exist. For such short distances, excitonic structure within the subunit should be very important [49,50]. Recent picosecond pump-probe depolarization studies have yielded data consistent with energy transfer occurring between exciton states of different subunits of *P. aestuarii* [51]. It has also recently been suggested, on the basis of pump-probe [52] and picosecond fluorescence decay [53] data, that excitonic

structure may also be important for the understanding of energy transfer in the core antenna complex of PSI.

In our earlier NPHB studies of the core antenna complex of PSI [19], it was pointed out that an understanding of the relationship between the dynamical information provided by time domain and hole burning techniques depends on an understanding of the factors discussed above. For a zero-phonon hole which is homogeneously broadened by the initial step of excitation transport (viewed as a T_1 process), the time (τ_i) associated with this step is given by $(\pi c \Gamma_h)^{-1}$, where Γ_h is the FWHM of the ZPH, in cm^{-1} [54]. For C670 of the core antenna complex and $\lambda_B = 660.2, 670.3$ and 678.1 nm, zero-phonon holewidths of $0.047, 0.036$ and 0.031 cm^{-1} were reported for $T = 1.6$ K [19]. Our studies on PSI-200 ($I_B < 1 \mu\text{W}/\text{cm}^2$) have yielded Chl a holewidths of 0.025 and 0.028 cm^{-1} at $\lambda_B = 670.2$ and 678.3 nm (hole profiles not shown), respectively. Further studies are required to determine whether there are significant differences in holewidths for C670 and Chl a of PSI-200. A holewidth of 0.05 cm^{-1} was obtained for Chl b of LHCI in PSI-200 at $\lambda_B = 650.3$ nm, 1.6 K (hole profile not shown). The important point for the ensuing discussion is that the holewidths yield τ_i values in the range of 200-400 psec [19]. For the calculations described later, for the core antenna complex, a value of $\tau_i = 300$ psec is used.

Picosecond fluorescence decay measurements on PSI core antenna complexes of varying P700 enrichment by Owens and co-workers [22,53] have yielded data, which when analyzed in terms of the Pearlstein model [55] for excitation transport in a regular array of Chl a, lead to a value of ~ 0.2 psec for the average nearest neighbor single site transfer (SST) time at 283 K. This time should be compared with $\tau_i \sim 300$ psec at 1.6 K. If the SST time was 0.2 psec at 1.6 K, the ZPH width

would be $\sim 50 \text{ cm}^{-1}$. Thus, within the framework of the regular array model, one is faced with the problem of understanding why the SST time increases by more than 3 orders of magnitude as the temperature is reduced from 283 to 1.6 K. Such an understanding is impossible unless, perhaps, diagonal energy disorder for Chl a is built into the regular array model. Although it is clear that the C670 absorption profile is contributed to by at least three different Chl a components [3,53,56], our NPHB data establish that each component suffers from significant inhomogeneous line broadening. Thus, excitation transport cannot be understood without consideration of diagonal energy disorder. In the presence of such disorder and vanishing linear electron-phonon coupling, excitation transport would cease in the low temperature limit.

Temperature Dependence of Excitation Transport in the Core Antenna Complex

To our knowledge, electronic excitation transport theories have not been applied to any antenna complex for which the linear electron-phonon coupling strength has been determined. We proceed to do so now utilizing our data presented earlier as well as the results from time domain experiments on the core antenna complex of PSI [22,52,53]. The objective is to determine the extent to which simple regular and subunit-structured antenna models can account for the T-dependence of the initial step of excitation transport. By simple we mean, in part, that in the former model only nearest neighbor (monomer) hops are considered while in the latter model only a single nearest neighbor subunit hop is considered. Overall transport to the RC following excitation of an antenna donor state could involve multiple hops. Intramolecular Chl a modes are not taken into account in the calculations of this sub-section since no mode with an appreciable Franck-Condon

factor exists which has a frequency $< 262 \text{ cm}^{-1}$, Table I. A donor to acceptor energy gap larger than 262 cm^{-1} that plays a significant role in excitation transport within the core antenna seems unlikely.

Quantum mechanical theories for EET from a donor (D) to acceptor (A) molecule processes have been developed for the cases where the phonons are localized [10,11,45] and delocalized [13,14,46]. The case of delocalized phonons would be applicable when the phonon displacement amplitudes involve molecules whose collective spatial extent exceeds the distance between D and A. For our purposes we need only consider the low and high T limits of the theories. For delocalized phonons [13,14]:

$$\tau_{DA}^{-1} = A \exp(-\tilde{S}) \tilde{S}^P / P! \quad , \text{ low T } (\hbar\omega_m \gg kT) \quad (1)$$

and

$$\tau_{DA}^{-1} = A \left(\frac{\hbar\omega_m}{4\pi\tilde{S}kT} \right)^{1/2} \exp(-\tilde{\epsilon}/kT), \text{ high T}, \quad (2)$$

where

$$A = \frac{2\pi}{\hbar^2 \omega_m} V^2 \quad (3)$$

and

$$\epsilon = (\Delta E + S\hbar\omega_m)^2 / 4S\hbar\omega_m \quad (4)$$

In (1) and (2), τ_{DA}^{-1} is the rate constant for downward transfer from the excited state $|D^*A\rangle$ to $|DA^*\rangle$, i.e., the pure electronic energy gap $\Delta E = E(DA^*) - E(D^*A) < 0$.

Furthermore, p is an integer closest in value to $|\Delta E|/\hbar\omega_m$, where ω_m is the mean phonon frequency. In Eqn. 3, V is the pure electronic matrix element that involves coupling of $|D^*A\rangle$ and $|DA^*\rangle$ through the intermolecular potential energy. The Huang-Rhys factor, S , is embellished with a "twiddle" to underscore the fact that $S\hbar\omega_m$ is the protein-pigment reorganization energy associated with the electronic excitation transfer from D to A . Thus, it is not equal or simply related to the value of $S \sim 0.8$ discussed earlier. The S of 0.8 is associated with the reorganization energy associated with the transition of a monomer Chl a from its ground to excited (Q_y) state. Our preliminary studies indicate (vide supra) that S is quite insensitive to λ_B within the Chl a absorption band of PSI-200. Thus S must be significantly smaller than 0.8, which is physically reasonable since the transport involves electronic excitation transfer in a medium that provides delocalized phonons for mediation. For the model calculations presented below, $S = 0.1, 0.2$ and 0.5 are utilized.

For the case of localized phonons the low and high T limiting expressions for τ_{DA}^{-1} are [13]:

$$\tau_{DA}^{-1} = A \exp(-2S) \sum_{r=0}^{\infty} \left(\frac{S^r}{r!} \right) \left(\frac{S^{r-p}}{(p-r)!} \right), \text{ low } T \quad (5)$$

and

$$\tau_{DA}^{-1} = A \left(\frac{\hbar\omega_m}{8\pi S k T} \right)^{1/2} \exp(-\varepsilon/kT), \text{ high } T, \quad (6)$$

where A is given by Eqn. 3 and

$$\varepsilon = (\Delta E + 2S\hbar\omega_m)^2 / 8S\hbar\omega_m \quad (7)$$

The physical meaning of S is as just defined above. From Eqn. (5) it is particularly apparent that the localized phonons created by downward EET can reside either entirely on D or A or be shared between the two. This is, of course, consistent with the D-A spectral overlap criterion of Dexter-Förster theory and the fact that the reorganization energy for EET is $2Sh\omega_m$, i.e., the reorganization energy for $D^* \rightarrow D$ and $A \rightarrow A^*$ is, in each case, $Sh\omega_m$.

Table III gives the results of calculations, performed with Eqns. 1 and 2, appropriate for the regular monomer array model and delocalized phonons. They are given for a high T value of $\tau_{DA} = 1.0$ psec. As discussed earlier, Owens et al. [22,53] determined a value for the average single site transfer time equal to 0.2 psec at room T. However, for the square or cubic lattice models they employ, τ_{DA} would be 4-6 times this value based on nearest neighbor considerations. This is the reason why we consider the value of $\tau_{DA} = 1.0$ psec (high T). The low temperature value which corresponds to 1.0 psec is 750 psec. The latter value is 300 psec multiplied by the factor 2.5 (rather than 5) since at 1.6 K only downward excitation transfer is possible. For the regular array we assume that diagonal energy disorder places one-half of the nearest neighbors to higher energy of the donor. A single value for ΔE is employed in the theory. Other parameter values utilized are $\omega_m = 20 \text{ cm}^{-1}$ (observed) and $S = 0.1, 0.2$ and 0.5 . The values of $|\Delta E|/hc$ listed are those which provide agreement with the experimentally determined $\tau_{DA}(\text{high T})/\tau_{DA}(\text{low T})$ ratio. Also given are the corresponding values of V and the nearest neighbor (D-A) center to center distance R . This distance was calculated using the result from Pearlstein and Hemenger [50] that $|V| \sim 250 \text{ cm}^{-1}$ for $R = 12.6 \text{ \AA}$ and the fact that $|V| \propto R^{-3}$. From Table III it would appear that the V and R values calculated with $\tau_{DA} = 1$ psec (high T) for delocalized phonons are physically

Table III. Regular monomer array model. τ_{DA} (low temperature) = 750 psec, τ_{DA} (high temperature) = 1 psec. Calculations performed with Eqns. 1 and 2 for delocalized phonons; Eqs. 3 and 4 for localized phonons. F_l and F_h are τ_{DA}^{-1}/A (see Eqns. 1, 2, 3) for low and high temperature, respectively

	$ \Delta E /hc$	$F_l \times 10^5 / F_h \times 10^2$		$V(\text{cm}^{-1})/R(\text{\AA})$	
<u>Delocalized Phonons</u>					
0.1	71	2.0	1.6	32	25
0.2	82	4.0	3.1	23	28
0.5	109	5.3	3.8	21	29
<u>Localized Phonons</u>					
0.8	180	3.8	3.0	24	28

reasonable for a regular array model since $R \sim 26 \text{ \AA}$ and $V \sim 27 \text{ cm}^{-1}$. We believe that S values of 0.1-0.2 are more consistent with our λ_B -dependent NPHB data than an S as large as 0.5.

Table III also gives the results of calculations performed with Eqns. 5 and 6 for the regular array model and localized phonons. Values of S and ω_m equal to 0.8 and $\omega_m = 20 \text{ cm}^{-1}$ were used. For $\tau_{DA} = 1 \text{ psec}$ (room T), $V = 24 \text{ cm}^{-1}$ and $R = 28 \text{ \AA}$ are calculated from the fit to the T-dependence of τ_{DA} . These values, like the corresponding ones in Table III for delocalized phonons, appear to be physically reasonable. However, for localized phonons $|\Delta E| \sim 180 \text{ cm}^{-1}$ while for delocalized phonons $|\Delta E| \sim 80 \text{ cm}^{-1}$. The former value seems rather large for a regular array with diagonal energy disorder, since the inhomogeneous linewidths for Chl a is $\sim 300 \text{ cm}^{-1}$ [57]. Thus, for the regular array it appears that delocalized phonons ($\omega_m \sim 20 \text{ cm}^{-1}$) could mediate excitation transport in a manner consistent with the T-dependent data.

Very recently, Causgrove and coworkers [52] have performed picosecond pump-probe depolarization studies on C670 of PSI particles at room T. The data indicate that excitation transport within the core antenna complex should be modeled in terms of hops between subunits (clusters) containing several Chl a. Although a precise determination of the nearest neighbor subunit hopping time from the data must await a structure determination, the model calculations of ref. (52) indicate that a value of $\tau_{DA} \sim 10 \text{ psec}$ is a reasonable estimate for the calculations which follow. Now D and A are viewed as donor and acceptor subunits. Results analogous to those of Table III are presented in Table IV for $\tau_{DA} = 10 \text{ psec}$ (high T) and $= 300 \text{ psec}$ (low T). Interestingly, Table IV shows that there is little to

Table IV. Subunit model. τ_{DA} (low temperature) = 300 psec, τ_{DA} (high temperature) = 10 psec. F_l and F_h are τ_{DA}^{-1}/A (see Eqns. 1, 2, 3) for low and high temperature, respectively

S	$ \Delta E /hc$	$F_l \times 10^3 / F_h \times 10^2$		$V(\text{cm}^{-1})/R(\text{\AA})$	
<u>Delocalized Phonons</u>					
0.1	42	3.3	10.6	4.0	50
0.2	52	3.4	9.8	4.2	49
0.5	76	2.4	7.3	4.8	47
<u>Localized Phonons</u>					
0.8	140	1.1	4.5	6.1	43

distinguish between the cases of localized and delocalized phonons. We note at the outset that the approach described earlier for the determination of R is highly questionable for the subunit-model. Indeed, even if a structure confirming and elucidating subunits were available, the question of the choice for R would remain (e.g. edge to edge vs. center to center). Another problem stems from the fact that one could reasonably expect subunit excitonic structure to be important. As a result, the excitonic levels of a subunit involved in transport could have transition dipole strengths which differ significantly from those of a monomer. An increased transition dipole would decrease the R -values given in Table IV. In *P. aestuarii* [47,48], the nearest neighbor subunit-subunit center to center distance is $\sim 34 \text{ \AA}$ while the edge to edge distance is $\sim 24 \text{ \AA}$. Recent electron microscopy data on LHC-II (light harvesting complex) associated with PSII [58] indicate that the nearest subunit-subunit center to center distance could be larger than 34 \AA . With these data and the reservations expressed above (on the calculation of R) in mind we cannot argue that the subunit-model is incompatible with the T -dependent data.

To summarize, the observed T -dependence for the initial step of excitation transport can be accounted for, using existing multi-phonon excitation transport theories, equally well by the simple regular array or subunit-structure models.

However, the regular array model does not appear to be tenable since the integrated intensity of the Chl a fluorescence of PSI-200 is only weakly dependent on temperature between ~ 4 and 300 K [40]. The data of ref. (40) show that the fluorescence intensity of Chl a increases by only $\sim 60\%$ as the temperature is decreased to 4 K . The weak dependence on temperature has also been recently observed by Wachtveitl et al. [59]. As already noted, Owens et al. [22,53] have given a reasonable interpretation for their fluorescence decay data for the core

antenna complex in terms of the regular array model. The fluorescence lifetime associated with the Chl a which are active (effective) in excitation transport to the RC is linearly proportional to the effective antenna size (no. active Chl a/RC) [22]. The active Chl a constitute ~ 90% of the Chl a of the core antenna complex [22]. The data analysis of Owens et al. [22,53] indicates that at 283 K the trapping of the antenna excitation is close to being diffusion controlled (motion limited). At this temperature the rate constant for trapping of the antenna excitation by the RC, k_{tr} , is the inverse of the measured fluorescence decay time [53]. For an illustrative calculation we consider $\tau_{fl} \sim 40$ psec for an effective antenna size of ~ 60 [22]. Thus at 1.6 K, $k_{tr} = (40 \text{ psec})^{-1}(0.2/300) = 1.7 \times 10^7$, corresponding to a trapping time of ~ 60 nsec. The SST times at room T and 1.6 K are 0.2 and 300 psec, respectively. The natural and observed lifetimes of Chl a monomer are 15 and 5 nsec [60]. Owens et al. [22,53] have determined that the remaining 10% of the antenna Chl a (vide supra) have a lifetime corresponding to the monomer and point out that the static fluorescence would be dominated at room T by these inactive monomers. With the above lifetimes of 15 and 5 nsec and a trapping time of 60 nsec, it is apparent that the static fluorescence intensity should increase dramatically (~ x10) as the temperature is reduced from room T to 1.6 K. The fact that it doesn't (vide supra) indicates that at 1.6 K the static fluorescence is still dominated by the ~ 10% inactive Chl a, i.e., excitation transport by and trapping of the ~ 90% Chl a (active at room T) by the RC is still effective at helium temperatures. This is inconsistent with the prediction of the regular array model for a SST time of 300 psec at 1.6 K. For PSI-200, the static fluorescence data also show that the Chl b fluorescence is very weak [61] relative to that from Chl a between ~ 4 and 300 K [40]. Thus, the trapping of Chl b excitation is also still efficient at low T.

Whether or not the subunit structure model can account for the weak T-dependence of the antenna Chl a static fluorescence and the dynamical data cannot be satisfactorily explored at this time since a structure for the antenna is not available. Nevertheless, we can calculate a minimum fluorescence quantum yield for the active Chl a at 1.6 K by assuming that 300 psec (from hole burning) represents an "effective" core antenna trapping time. This time and the natural and radiative monomer lifetimes of 15 and 5 nsec yield a quantum yield of 0.02. The quantum yield of the 10% inactive Chl a is ~ 0.3 [60]. These quantum yields and the composition percentages predict a minimum percentage increase in the static fluorescence intensity of $\sim 60\%$ as the temperature is decreased from room T to 1.6 K. This prediction is in agreement with the data of ref. [40]. However, it is apparent that if 300 psec were to be viewed as a nearest neighbor subunit-subunit exciton transfer time and if several transfers of this type occurred prior to trapping at the RC, the predicted increase could be considerably greater than 60%.

With regard to the subunit structure model it is germane to note that recent exciton-exciton annihilation studies on antenna mutants of Rb. sphaeroides have shown that the fundamental energy transfer rate constant decreases by a factor of 12 as the temperature decreases from 300 K to 4 K [62]. This ratio is not so different from the one obtained from Table V (subunit model calcs.) where $\tau_{DA} \sim 10$ psec (high T) and $\tau_{DA} = 300$ psec (low T).

Absence of Satellite Hole Structure Due to Excitation Transfer

The broad satellite hole located at $\sim -22 \text{ cm}^{-1}$ relative to the ZPH has been viewed as a pseudo-PSBH, Figs. 1, 2, 7. Another interpretation is that it is a manifestation of hole burning of sites populated by downward excitation transfer

from the excited isochromat at λ_B . However, such an interpretation is very unlikely to be correct since the results of Fig. 7 prove that, at short burn times, the growth rate of the satellite hole is slower than that of the ZPH. This follows, in part, from the fact that for the most efficient NPHB system known, oxazine 720 in a glycerol glass, the rate constant for hole formation is $2 \times 10^7 \text{ s}^{-1}$ for the initial few percent of the burn [34]. For most systems $k_{\text{NPHB}} \lesssim 10^4 - 10^5 \text{ s}^{-1}$ [63]. Since the absorption cross-sections for oxazine 720 and Chl a are comparable, the lower burn powers used for oxazine 720 in ref. (34) compared to this work indicate that $k_{\text{NPHB}}(\text{Chl a}) \lesssim 10^7 \text{ s}^{-1}$ [34]. Therefore, one deduces that $\tau_{\text{DA}}^{-1} = (300 \text{ psec})^{-1} \gg k_{\text{NPHB}}$ for Chl a. Consequently the -22 cm^{-1} satellite hole, if due to excitation transfer, would burn faster than the ZPH, contrary to observation. Thus, it is concluded that the satellite hole is a pseudo-PSBH. Additional support for this assignment comes from the observation that the satellite hole is also observed for Chl b, Fig. 2, since efficient trapping of the Chl b excitation in LHCI by the Chl a of LHCI or the core occurs at 1.6 K, vide supra.

Nevertheless, the absence of any apparent satellite hole structure due to downward excitation transfer might appear to be at odds with the inequality $\tau_{\text{DA}}^{-1} \gg k_{\text{NPHB}}$. However, it would not be provided that downward excitation transfer from ω_B (burn frequency) results (via a hierarchy of events) in a more or less equal probability for excitation of Chl a molecules whose zero-phonon excitation frequency lies lower than ω_B or if direct excitation transfer from the core antenna Chl a (whose zero-phonon transitions are in resonance with ω_B) occurs to the RC at 1.6 K. The latter possibility was mentioned earlier and will be explored further in the following sub-section. The implications of the former for the absorption profile are essentially the same as those from "uniform" white light

irradiation of the absorption profile. The absorption spectrum is invariant to such irradiation since, at any frequency in the absorption profile, there is a dynamic equilibrium between burning and filling.

Finally, we make a few remarks on the implications of subunit excitonic structure on holewidths. If we admit that such structure contributes to the Chl a C670 absorption profile, it follows, given the existence of inhomogeneous broadening, that a burn at λ_B would likely probe different exciton levels belonging to different subunits. Nevertheless, a holewidth corresponding to 300 psec could also serve as a lower limit for decay from upper to lower exciton levels of a given subunit. Such decay would not occur by the mechanisms discussed earlier, but by one that depends on the modulation of the electronic energy transfer integral by phonon displacements [64,65]. For the case of the lowest triplet exciton band of anthracene, it has been established that decay of the upper exciton level to the lowest (23 cm^{-1} lower in energy than the upper) occurs by this mechanism in 5 psec at helium temperatures [66]. The longer time scale for this process in the core antenna complex might be understood if the energy spacing between adjacent exciton levels is significantly larger than the frequency of the phonon(s) responsible for the aforementioned modulation. For anthracene, the relaxation occurs by one-phonon emission. Two- and higher-phonon emission processes are significantly less probable. Another possible explanation for a long 300 psec exciton decay is that the structural arrangement of pigments in the subunits is such as to provide oscillator strength only to the lowest energy exciton level.

**Possible Role of Intramolecular Modes in large Energy Gap Excitation
Transfer**

The discussion thus far has centered on the possible roles of low frequency phonons as acceptor modes for downward excitation transfer within the core antenna. Although the hole burning determination of ~ 300 psec for τ_{DA} represents, in a strict sense, a lower limit, it is difficult to understand how τ_{DA} could be much longer given the weak dependence of the static Chl a fluorescence on temperature. However, the interpretation of $\tau_{DA} \sim 300$ psec is problematic. The possibility that it might correspond to an average time for direct antenna subunit to RC transfer was raised. Such a mechanism, even if important at low temperatures, might not be important at room temperature. That is, subunit to subunit excitation transfer could be facile at high temperature but not so at low temperature, leaving direct subunit to RC transfer as the residual operative mechanism at 1.6 K.

To explore this possibility we have performed calculations on the low temperature rate for direct transfer from C670 to P700 (primary electron donor state) utilizing the intramolecular Franck-Condon factors in Table I for an energy gap $\Delta E/hc \sim -640 \text{ cm}^{-1}$. For such a large gap, the phonons cannot mediate efficient direct transfer by themselves. Participation of intramolecular modes must, therefore, be considered. Equations 1 and 5 are readily modified to take this into account by inclusion of the one-quantum Franck-Condon factor for the intramolecular mode. We define p as the integer closest in value to $(-\Delta E/hc + \omega_{\text{intr}})/\omega_m$, where ω_{intr} is the intramolecular mode frequency and ω_m is the mean phonon frequency equal to 20 cm^{-1} . It is required that p not be negative. With this in mind we can single out from Table I the 521, 584 and 607 cm^{-1} modes since their Franck-Condon factors are relatively large and because they lead to relatively small values of p , the number

of phonons required for energy conservation. In the absence of experimental data, it is assumed that the Franck-Condon factors for the intramolecular modes of P700 are the same as for antenna Chl a. Only the results of the calculations performed with Eqn. 1 (suitably modified) will be given here. Modification of this equation involves its multiplication by twice [10,13] the Franck-Condon factor for the intramolecular mode. S for the problem at hand is taken as the difference between its value for the antenna complex ($S \sim 1$) [19, this work] and P700 ($S \sim 5.5$) [12]. The rate constant for transport from the antenna to P700 is the sum of the rate constants calculated for each intramolecular mode considered. The value of $\tau_{DA} = 300$ psec and experimental Franck-Condon factors yield a value of 2 cm^{-1} for V . Interesting, however, is the result that the $\tau_{DA}(\text{high temperature})/\tau_{DA}(\text{low temperature})$ ratio is ~ 0.3 . That is, the rate of excitation transport is slower at high temperature than low temperature contrary to the experimental data. Thus although direct large gap transport from the antenna to P700 may be viable at low T , such transport would appear not to be important at high T .

CONCLUSION

This work establishes that spectral hole burning is a powerful high resolution spectroscopic technique for the determination of both the frequencies and Franck-Condon factors of intramolecular and phonon modes associated with the excited electronic states of pigment-protein complexes. The level of detail provided for the antenna of PSI-200 is unprecedented but there is every reason to suggest that nonphotochemical hole burning can provide comparable data for other light harvesting complexes. Data of the above types of essential input for theoretical studies which seek to distinguish between different mechanisms for excitation transport. We have attempted to illustrate this by performing calculations, for simple structural models of the core antenna complex, which explore the temperature dependence of excitation transport within the core antenna and from the antenna to the RC of PSI. It is gratifying that the existing multi-phonon excitation transport theories with the above data can account for the marked slow down of excitation transport as the temperature is reduced. Nevertheless, it is clear that the utility of the data presented here cannot be fully realized until the antenna structure is determined and correlated with more detailed spectroscopic data on the underlying structure of the Q_y absorption profile. Ultra-fast measurements of the temperature dependence of excitation transport within the core antenna complex of PSI are also required. Finally, the data and calculations for PSI indicate that it is the low frequency protein phonons, and not the intramolecular modes, that mediate excitation transport within the antenna and from the antenna to the RC.

REFERENCES

1. Avarmaa, R. A.; Rebane, K. K. *Chemical Physics* 1982, 68, 191.
2. Avarmaa, R. A.; Rebane, K. K. *Spectrochimica Acta* 1985, 41A, 1365.
3. Renge, I.; Muring, K.; Sarv, P.; Avarmaa, R. *J. Phys. Chem.* 1986, 90, 6611.
4. Renge, I.; Muring, K.; Avarmaa, R. *J. Lumin.* 1987, 37, 207.
5. Fünfshilling, J.; Williams, D. F. *Photochem. and Photobiol.* 1977, 26, 109.
6. Bykovskaya, L. A.; Litvin, F. F.; Personov, R. I.; Romanovskii, Yu. V. *Biophysics* 1980, 25, 8.
7. Platenkamp, R. J.; Den Blanken, H. J., Hoff, A. J. *Chem. Phys. Lett.* 1980, 76, 35.
8. Lutz, M. *Adv. Infrared and Raman Spectroscopy*, 1984, 11, 211.
9. Tasumi, M.; Fujiwara, M. In Spectroscopy of Inorganic-based Materials Clark, R. J. H., Hester, R. E., Eds.; Wiley: New York, 1987, p 407.
10. Yomosa, S. *J. Phys. Soc. of Japan* 1978, 45, 967.
11. Sarai, A.; Yomosa, S. *Photochem. Photobiol.* 1980, 31, 589.
12. Hayes, J. M.; Gillie, J. K.; Tang, D.; Small, G. J. *Biochim. Biophys. Acta* 1988, 932, 287.
13. Jortner, J. *J. Chem. Phys.* 1976, 64, 4860.
14. Jortner, J. *Biochim. Biophys. Acta* 1980, 604, 193.
15. Bixon, J.; Jortner, J. *J. Phys. Chem.* 1986, 90, 3760.
16. Friesner, R.; Wertheimer, R. *Proc. Natl. Acad. Sci. USA* 1982, 79, 2138.

17. Won, Y.; Friesner, R. *Proc. Natl. Acad. Sci. USA* 1987, 84, 5511.
18. Won, Y., Friesner, R. *J. Phys. Chem.* 1988, 92, 2208.
19. Gillie, J. K.; Hayes, J. M.; Small, G. J.; Golbeck, J. H. *J. Phys. Chem.* 1987, 91, 5524.
20. Fearey, B. L.; Carter, T. P.; Small, G. J. *J. Phys. Chem.* 1983, 87, 3600.
21. Hayes, J. M.; Fearey, B. L.; Carter, T. P.; Small, G. J. *Int. Rev. Phys. Chem.* 1986, 5, 175.
22. Owens, T. G.; Webb, S. P.; Mets, L.; Alberte, R. S.; Fleming, G. R. *Proc. Natl. Acad. Sci. USA* 1987, 84, 1532.
23. Mullet, J. E.; Burke, J. J.; Arntzen, C. J. *Plant Physiol.* 1980, 65, 814.
24. Malkin, R.; Ortiz, W.; Lam, E.; Bonnerjea, J. *Physiol. Vég.* 1985, 23, 619.
25. Golbeck, J. H. *J. Membrane Sci.* 1987, 33, 151.
26. Lam, E.; Ortiz, W.; Mayfield, S.; Malkin, R. *Plant Physiol.* 1984, 74, 650.
27. Haworth, P.; Watson, J. L.; Arntzen, C. J. *Biochim. Biophys. Acta* 1983, 724, 151.
28. Ortiz, W.; Lam, E.; Ghirardi, M.; Malkin, R. *Biochim. Biophys. Acta* 1984, 766, 505.
29. Burned to maximum hole depth.
30. Moerner, W. E.; Lenth, W.; Bjorklund, G. C. In Persistent Spectral Hole-Burning: Science and Application, Moerner, W. E., Ed.; Springer-Verlag: West Berlin, 1988, p 251.
31. Hayes, J. H.; Small, G. J. *Chem. Phys.* 1978, 27, 151.

32. Small, G. J. In Spectroscopy and Excitation Dynamics of Condensed Molecular Systems, Agranovich, V. M., Hochstrasser, R. M., Eds.; North Holland:Amsterdam, 1983,p 515.
33. Hayes, J. M.; Jankowiak, R.; Small, G. J. In Persistent Spectral Hole-Burning: Science and Applications, Moerner, W. E., Ed.; Springer-Verlag:West Berlin, 1988, p 153.
34. Jankowiak, R.; Small, G. J. Science 1987, 237, 618.
35. Jankowiak, R.; Shu, L.; Kenney, M. J.; Small, G. J. J. Lumin. 1987, 36, 293.
36. Friedrich, J.; Swalen, J. D.; Haarer, D. J. Chem. Phys. 1980, 73, 705.
37. Friedrich, J.; Haarer, D. Angew. Chem. Int. Eds. Engl. 1984, 23, 113.
38. van den Berg, R.; Völker, S. Chem. Phys. Lett. 1986, 127, 525.
39. Völker, S. J. Lumin. 1987, 36, 251.
40. Johnson, S. G.; Small, G. J. Chem. Phys. Lett., 1989, 155, 371.
41. Duschinsky, F. Acta Physicochim. 1937, 7, 551.
42. Small, G. J. J. Chem. Phys. 1971, 54, 3300.
43. Hayes, J. H.; Small, G. J. Chem. Phys. 1978, 27, 151.
44. Förster, T. Naturwiss. 1946, 33, 166; Ann. Physik 1948, 2, 55; Z. Naturforsch. 1949, 417, 321.
45. Dexter, D. L. J. Chem. Phys. 1953, 21, 836.
46. Soules, T. F.; Duke, C. B. Phys. Rev. B 1971, 3, 262.
47. Fenna, R. E.; Ten Eyck, L. F.; Matthews, B. W. Biochem. Biophys. Res. Commun. 1977, 75, 751.

48. Tronrud, D. E.; Schmid, M. F.; Matthews, B. W. *J. Mol. Biol.* 1986, 188, 443.
49. Philipson, K. D.; Sauer, K. *Biochemistry* 1972, 11, 1880.
50. Pearlstein, R. M.; Hemenger, R. P. *Proc. Natl. Acad. Sci. USA* 1978, 75, 4920.
51. Causgrove, T. P.; Yang, S.; Struve, W. S. *J. Phys. Chem.* 1988, 92, 6790.
52. Causgrove, T. P.; Yang, S.; Struve, W. S. *J. Phys. Chem.* 1988, 92, 6121.
53. Owens, T. G.; Webb, S. P.; Alberte, R. S.; Mets, L.; Fleming, G. R. *Biophysical Journal* 1988, 53, 733.
54. Berg, M.; Walsh, C. A.; Narasimhan, L. R.; L. Hau, K. A.; Fayer, M. D. *Chem. Phys. Lett.* 1987, 139, 66.
55. Pearlstein, R. M. *Photochem. Photobiol.* 1982, 35, 835.
56. Shiozawa, J. A.; Alberte, R. S.; Thornber, J. P. *Arch. Biochem. Biophys.* 1974, 165, 388.
57. Gillie, J. K.; Fearey, B. L.; Hayes, J. M.; Small, G. J.; Golbeck, J. H. *Chem. Phys. Lett.* 1987, 134, 316.
58. Li, J. *Proc. Natl. Acad. Sci. USA* 1985, 82, 386.
59. Wachtveitl, J.; Krause, H. In Progress in Photosynthesis Research, Biggins, J., Ed.; Martinus Nijhoff Publishers: Dordrecht, 1987, p 87.
60. Brody, S. S.; Rabinowitch, E. *Science* 1958, 125, 555.
61. Chl *b* fluorescence is <3% of the resonant Chl *a* fluorescence, see ref. 40.
62. Vos, M.; van Dorssen, R. J.; Amesz, J.; van Grondelle, R.; Hunter, C. N. *Biochim. Biophys. Acta* 1988, 933, 132.

63. Carter, T. P.; Fearey, B. L.; Hayes, J. M., Small, G. J. *Chem. Phys. Lett.* 1983, 102, 272.
64. Davydov, A. S. Theory of Molecular Excitons; Plenum:New York, 1971.
65. Johnson, C. K.; Small, G. J. In Excited States, Lim, E. C., Ed.; Academic Press:New York, 1982; vol. 6, p 97.
66. Port, H.; Mistelberger, K.; Rund, D. *Mol. Cryst. Liq. Cryst.* 1979, 50, 11.

ADDITIONAL RESULTS

It is interesting to consider how dispersion in phonon frequencies can alter the values of $\Delta E/hc$, V , and R obtained in Paper II. Table I and II present results for regular monomer array and subunit model, respectively, with delocalized phonons of frequencies $\hbar\omega_m = 10 \text{ cm}^{-1}$ and 30 cm^{-1} . Comparing Table I and II with Tables III and IV of Paper II reveals that a phonon frequency of $\hbar\omega_m = 10 \text{ cm}^{-1}$ gives results similar to that for $\hbar\omega_m \sim 20 \text{ cm}^{-1}$. In the regular array model $\Delta E/hc$ values for $\hbar\omega_m = 10 \text{ cm}^{-1}$ are less than the corresponding values with $\hbar\omega_m \sim 20 \text{ cm}^{-1}$. Lower frequency phonons could serve to enhance EET in a regular monomer array model. Determination of the structure of the antenna protein would aid interpretation. The values of $\Delta E/hc$ for $\hbar\omega_m = 30 \text{ cm}^{-1}$ appear not to be physically reasonable since the inhomogeneous line width for Chl a is 300 cm^{-1} (see Paper II) [110].

Noticeably absent from Table II are the values for $S=0.1$ for subunit model with $\hbar\omega_m = 30 \text{ cm}^{-1}$. It was not possible to account for the temperature dependence of EET using a value of $S=0.1$ (the best calculated value is $\tau_{DA}=37 \text{ psec}$). This behavior is hinted at for $S=0.1$ in Table I for $\hbar\omega_m = 30 \text{ cm}^{-1}$ and is common to all the calculations if S is made small enough. Remember that the corrected energy term is given by

$$\epsilon = (\Delta E + S\hbar\omega_m)^2 / 4S\hbar\omega_m$$

with $S\hbar\omega_m$ being the reorganization strength. For the calculations presented here, if $\epsilon \gtrsim 1000 \text{ cm}^{-1}$ then, it is not possible to account for the temperature dependence of

Table I. Regular monomer array model and delocalized phonons^a

S	$ \Delta E /hc$	$F_l \times 10^5 / F_h \times 10^2$		$V(\text{cm}^{-1})/R(\text{\AA})$	
$\hbar\omega_m = 10 \text{ cm}^{-1}$					
0.1	32	8.8	6.4	11	35
0.2	39	8.7	6.2	12	35
0.5	54	6.8	5.0	13	34
$\hbar\omega_m = 30 \text{ cm}^{-1}$					
0.1	148	0.009	0.007	584	10
0.2	135	1.1	0.85	54	21
0.5	171	2.8	0.022	34.3	25

^a τ_{DA} (low temperature) = 750 psec, τ_{DA} (high temperature) = 1 psec. F_l and F_h are τ_{DA}^{-1}/A (see Eqns. 1, 2, 3 of Paper II) for low and high temperature, respectively.

Table II. Subunit model and delocalized phonons^a

S	$ \Delta E /hc$	$F_l \times 10^5 / F_h \times 10^2$		$V(\text{cm}^{-1})/R(\text{\AA})$	
$\hbar\omega_m = 10 \text{ cm}^{-1}$					
0.1	40	0.38	3.1	5.2	46
0.2	47	0.59	4.1	4.5	48
0.5	64	0.47	3.8	4.7	47
$\hbar\omega_m = 30 \text{ cm}^{-1}$					
0.2	180	0.007	0.06	67	20
0.5	210	0.094	0.71	18.8	30

^a τ_{DA} (low temperature) = 300 psec, τ_{DA} (high temperature) = 10 psec. F_l and F_h are τ_{DA}^{-1}/A (see Eqns. 1, 2, 3 of Paper II) for low and high temperature, respectively.

the EET using $S=0.1$. Physically, this suggests that at some point the energy separation between chromophores (ΔE) overwhelms the ability of the phonons to mediate EET. This is similar to the problem of direct large energy transport between C670 and P700 discussed in Paper II. No Franck-Condon active excited state vibrational modes have been observed in the $\Delta E/hc$ range presented in Tables I and II. Phonons must therefore mediate EET with $\hbar\omega_m \sim 30 \text{ cm}^{-1}$ being an upper energy limit.

Spectral diffusion and dephasing processes in glasses manifest themselves in spectral hole burning by broadening the hole profile [111-113]. The excitation depopulation lifetime T_1 is calculated by

$$T_1 = \frac{1}{\pi\Delta\nu_{\text{hole}}}$$

if spectral diffusion and dephasing processes (T_2^* processes) are ignored. In this case, excitation depopulation lifetimes calculated from $\Delta\nu_{\text{hole}}$ are shorter than the actual value. For this reason we report a lower limit of $\tau_{\text{DA}} = 300 \text{ psec}$.

The maximum rate for EET can be calculated by setting $-\Delta E = S\hbar\omega_m$ [89]. The rate constant at low temperature is readily calculated from

$$\tau_{\text{DA}}^{-1}(\text{low } T) = \tau_{\text{DA}}^{-1}(\text{high } T) \times \frac{e^{-S} S^p / p!}{(\hbar\omega_m / 4\pi S k T)^{1/2}}$$

with $p = \Delta E / \hbar\omega_m = S$. Table III gives $\tau_{\text{DA}}(\text{low } T)$ and $\Delta\nu_{\text{hole}}$ for delocalized phonons within the regular monomer array and subunit model for the antenna. $\tau_{\text{DA}}(\text{low } T)$ is much shorter than observed experimentally. The hole profiles are not

Table III. Optimum Low Temperature Transfer Time

S	τ_{DA} (psec)	Δv_{hole} (cm^{-1})
<u>Regular Array</u> ^a		
0.1	0.38	28
0.2	0.32	24
<u>Subunit Model</u> ^b		
0.1	3.8	1.4
0.2	3.2	1.7

^a τ_{DA} (high T) = 1 psec.

^b τ_{AD} (high T) = 10 psec.

dominated by the broadening which would have been suspected if the calculated τ_{DA} was greater than 300 psec. For example, if the maximum rate for EET was ~ 600 psec ($\Delta\nu_{\text{hole}} = 0.02 \text{ cm}^{-1}$), then since the experimental holewidths are $\sim 0.03 \text{ cm}^{-1}$ ($\tau_{DA} = 300$ psec) other processes such as spectral diffusion and dephasing that broaden the holes could be dominating the relaxation process being measured.

Further experiments are needed, however, to define the influence of spectral diffusion and dephasing in the antenna complex. It is not necessarily to be expected that the rate of EET is at its maximum because this could lead to a inefficient bottleneck of the excitation waiting to be photoconverted at the RC.

The Stark effect is a general term used to label the influence of electric fields on atomic or molecular spectroscopy. A molecule placed in an electric field $m = v + \alpha F$, undergoes a change in potential energy caused by work done on the dipole. The potential change, V , is [114]

$$V = -\int_0^F m \, dF = -\mu \cdot F - \frac{1}{2} F \cdot \alpha \cdot F$$

where μ is the permanent dipole moment and α is the polarizability tensor. If θ is the angle between the dipole and electric field, then

$$V(F) = -\Delta\mu F \cos\theta - 1/2 \Delta\alpha F^2$$

with $\Delta\mu = \mu_e - \mu_g$ is the difference of the electric dipole moment of the excited (e) and ground (g) state and $\Delta\alpha$ the polarizability difference. $F = fE$ with E being the externally applied field and $f = (\epsilon_0 + 2)/3$, the Lorentz local-field correction for a dielectric constant ϵ_0 . The field induced changes allows one to probe the molecular

dipole and polarizability and intermolecular interactions. For example, Stark effect can be used to split the n-fold orientation degeneracy of impurities doped into molecular crystals by altering the field along a particular molecular axis. The observed effect is a splitting of the electronic transition (splitting of the spectral line) with an energy difference

$$\Delta E = 2F\Delta\mu \cos\theta.$$

For excitonic states, Stark effect can alter the resonance between states. For a review of Stark effect on molecular crystals see ref. 114.

The Stark effect is easily studied in molecular crystals since the linewidths at low T are narrow. It is more difficult in amorphous materials since the linewidth is large (several hundred cm^{-1}), however, site selective spectroscopies, in particular spectral hole burning, produce narrow features which allows us to investigate Stark effect in these systems. The Stark effect on spectral holes is not as straight forward as for crystals. The hole shape calculation must account for the shifting of molecular electronic transitions in and out of resonance with the burn frequency. The calculations must also include an integration over all dipole orientation angles since the dipoles are not aligned as in a molecular crystal [115,116].

The Stark effect results in a shift in the transition frequency which is displayed in spectral hole burning by a broadening [$E_{\text{laser}} \perp E_{\text{field}}$] or splitting [$E_{\text{laser}} \parallel E_{\text{field}}$] of the hole profile for a parallel dipole moment and transition moment [115,116]. The frequency shift is given by

$$h\Delta\nu = -f\Delta\mu \cdot F - \frac{1}{2} f^2 F \cdot \Delta\alpha \cdot F$$

where E is the external field given in V/d , f is the Lorentz field factor, $\Delta\mu$ is the change in dipole moment and $\Delta\alpha$ is the polarizability of the molecule. Second order effects have never been observed so the frequency shift simplifies to

$$h\Delta\nu = -f \Delta\mu \cdot F.$$

The slope of the plot of holewidth (broadening) or hole splitting versus the electric field is used to calculate $\Delta\mu$ in the ground to excited state electronic transition.

The Stark effect absorption spectra for the RC of *Rps. viridis* demonstrates a large change in the dipole moment between the ground and excited state (~ 9 D) indicating substantial charge transfer character for the primary electron donor [117]. This is consistent with the hole burned spectra for the RCs of PSU which shows a strong electron-phonon coupling [118,119]. Such charge transfer characteristic would have important consequence in discussing EET in antenna systems. Although no spectral evidence for charge transfer in the antenna exist, Stark effect spectroscopy provides a simple check.

Stark effect is not observed for the Chl in the core antenna complex of PSI. The uncertainty in the holewidths is $\sim 0.002 \text{ cm}^{-1}$ and the maximum applied E field was $\sim 750 \text{ V/cm}$. A value for the dielectric constant for the protein complex is not available and will be taken as that for polymers, $\epsilon_0=3.0$ [117]. The calculation gives $\Delta\mu < 0.1$ D for the core antenna Chl. The change in the dipole is small consistent with weak linear electron-phonon coupling and electron-vibrational coupling. This implies that the excited state potential surface is not greatly perturbed from the

ground state. The measured $\Delta\mu$ for Zn-tetrobzoporphin in poly(vinyl butyral) is $\sim 0.2D$ and for isobacteriochlorin in n-octane $\Delta\mu \sim 1.6D$ [118,119].

No evidence for spontaneous hole refilling (SPHF) or laser induced hole refilling (LIHF) has been observed. This observation also removes global spectral diffusion and anti-hole reversion through external two level systems, processes speculated to be active in ionic dyes doped into polymers [111,113], as active processes in the antenna. More data such as hole growth and hole refilling studies are needed before a complete picture can be forwarded.

This work demonstrates that spectral hole burning is an important new tool for studying dynamical processes in protein bound complexes. A number of interesting new results have been presented to answer important questions, but, a number of new questions have also arisen. A more complete understanding of EET in the antenna system of PSI awaits more thorough investigation of protein effects on hole burning and structure determination.

REFERENCES

1. Lotshaw, W. T.; Alberte, R. S.; Fleming, G. R. *Biochim. Biophys. Acta* 1982, 682, 75.
2. Gulotty, R. J.; Fleming, G. R.; Alberte, R. S. *Biochim. Biophys. Acta* 1982, 682, 322.
3. Gulotty, R. J.; Mets, L.; Alberte, R. S.; Fleming, G. R. *Photochem. Photobiol.* 1985, 41, 487.
4. Owens, T. G.; Webb, S. P.; Mets, L.; Alberte, R. S.; Fleming, G. R. *Proc. Natl. Acad. Sci. U.S.A.* 1987, 84, 1532.
5. Owens, T. G.; Webb, S. P.; Mets, L.; Fleming, G. R. *Biophys. J.* 1988, 53, 733.
6. Fetisova, Z. G.; Freiberg, A. M.; Timpmann, K. E. *Nature* 1988, 334, 633.
7. Searle, G. F. W.; Tamkivi, R.; van Hoek, A.; Schaafsma, T. J. *J. Chem. Soc., Faraday Trans. 2* 1988, 84, 315.
8. Mimuro, M.; Tamai, N.; Yamazaki, I. *FEBS Lett.* 1987, 213, 119.
9. Gillbro, T.; Sundström, V.; Sandström, A.; Spangfort, M.; Andersson, B. *FEBS Lett.* 1985, 193, 267.
10. Avarmaa, R. A.; Kochubey, S. M.; Tamkivi, R. P. *FEBS Lett.* 1979, 102, 139.
11. Avarmaa, R.; Renge, I.; Muring, K. *FEBS Lett.* 1984, 167, 186.
12. Sundström, V.; van Grondelle, R.; Bergström, H.; Akesson, E.; Gillbro, T. *Biochim. Biophys. Acta* 1986, 851, 531.
13. Bergström, H.; Sundström, V.; van Grondelle, R.; Akesson, E.; Gillbro, T. *Biochim. Biophys. Acta* 1980, 852, 279.
14. Causgrove, T.; Yang, S.; Struve, W.S. *J. Phys. Chem.* 1988, 92, 6121.

15. Causgrove, T.; Yang, S.; Struve, W.S. *J. Phys. Chem.* 1988, 92, 6790.
16. Den Hollander, W. T. F.; Bakker, J. G. C.; van Grondelle, R. *Biochim. Biophys. Acta* 1983, 725, 492.
17. Bakker, J. G. C.; van Grondelle, R.; Den Hollander, W. T. F. *Biochim. Biophys. Acta* 1983, 725, 508.
18. Dobek, A.; Deprez, J.; Geacintov, N. E.; Paillotin, G.; Breton, J. *Biochim. Biophys. Acta* 1985, 806, 81.
19. Vos, M.; van Grondelle, R.; van der Kooij, F. W.; van de Poll, D.; Amesz, J.; Duysens, L. N. M. *Biochim. Biophys. Acta* 1986, 850, 501.
20. Vos, M.; van Dorssen, R. J.; Amesz, J.; van Grondelle, R.; Hunter, C. N. *Biochim. Biophys. Acta* 1988, 933, 132.
21. Renge, I.; Muring, K.; Avarmaa, R. *Biochim. Biophys. Acta* 1984, 766, 501.
22. Renge, I.; Muring, K.; Vladkova, R. *Biochim. Biophys. Acta* 1988, 935, 333.
23. Muring, K.; Renge, I.; Avarmaa, R. *FEBS Lett.* 1987, 223, 165.
24. Gillie, J. K.; Hayes, J. M.; Small, G. J.; Golbeck, J. H. *J. Phys. Chem.* 1987, 91, 5524.
25. Gillie, J. K.; Small, G. J.; Golbeck, J. H. *J. Phys. Chem.* 1989, 93, 1620.
26. Knox, R. S. In Primary Processes of Photosynthesis; Barber, J., Ed.; Elsevier: Amsterdam, 1977, p 56.
27. Knox, R. S. In Photosynthetic Membranes and Light Harvesting Systems; Staehelin, L.; Arntzen, C., Eds.; Springer-Verlag: Berlin, 1986, p 286.
28. Geacintov, N. E.; Breton, J. *CRC Crit. Rev. Plant. Sci.* 1987, 5, 1.

29. van Grondelle, R. *Biochim. Biophys. Acta* 1985, 811, 147.
30. Holzwarth, A. R. In The Light Reactions; Barber, J., Ed.; Elsevier: Amsterdam, 1987, p 95.
31. Pearlstein, R. M. In Photosynthesis; Ames, J. Ed.; Elsevier: Amsterdam, 1987, p 299.
32. Franck, J.; Teller, E. *J. Chem. Phys.* 1938, 6, 861.
33. Frenkel, J. *Phys. Rev.* 1931, 37, 17; *Phys. Rev.* 1931, 37, 1276.
34. Peierls, R. *Ann. d. Physik* 1932, 13, 905.
35. Emerson, R.; Arnold, W. A. *J. Gen. Physiol.* 1932, 15, 391.
36. Emerson, R.; Arnold, W. A. *J. Gen. Physiol.* 1932, 15, 191.
37. Gaffron, H.; Wohl, K. *Naturwissenschaften* 1936, 24, 81; *Naturwissenschaften* 1936, 24, 103.
38. Govindjee; Govindjee, R. In Bioenergetics of Photosynthesis; Govindjee, Ed.; Academic; New York, 1975, p 2.
39. Robinson, G. W. *Brookhaven Symposia in Biology* 1967, 19, 16.
40. Bay, Z.; Pearlstein, R. M. *Proc. Natl. Acad. Sci. U.S.A.* 1963, 50, 1071.
41. Pearlstein, R. M. *Photochem. Photobiol.* 1982, 35, 835.
42. Harris, C. B.; Zwemer, D. A. *Ann. Rev. Phys. Chem.* 1978, 29, 473.
43. Munn, R. W.; Silbey, R. *Mol. Cryst. Liq. Cryst.* 1980, 57, 131.
44. Fayer, M. D.; Harris, C. B. *Phys. Rev. B* 1974, 9, 748; *Phys. Rev. B* 1974, 10, 1784.
45. Stevenson, S. H.; Connolly, M. A.; Small, G. J. *Chem. Phys.* 1988, 128, 157.

46. Fayer, M. D.; Harris, C. B. *Chem. Phys. Lett.* 1974, 25, 149.
47. Johnson, S. G.; Small G. J. *Chem. Phys. Lett.* 1989, 155, 371.
48. Johnson, C. K.; Small, G. J. In Excited States; Lim, E. C., Ed.; Academic: New York, 1982; Vol. 6, p 97.
49. Kenkre, V. M.; Knox, R. S. *Phys. Rev. B* 1974, 9, 5279.
50. Kenkre, V. M.; Knox, R. S. *Phys. Rev. Lett.* 1974, 33, 803.58.
51. Kenkre, V. M.; Knox, R. S. *J. Lumin.* 1976, 12, 187.
52. Paillotin, G. *J. Theor. Biol.* 1972, 36, 223.
53. Paillotin, G. *J. Theor. Biol.* 1976, 58, 219.
54. Paillotin, G.; Swenberg, C. E.; Breton, J.; Geacintov, N. E. *Biophys. J.* 1979, 25, 513.
55. Paillotin, G. In Advances in Photosynthesis Research; Sybesma, C., Ed.; Martinus Nijhoff/Dr. W. Junk: The Netherlands, 1984, Vol. 1, p 5.
56. Pearlstein, R. M. In Advances in Photosynthesis Research; Sybesma, C., Ed.; Martinus Nijhoff/Dr. W. Junk: The Netherlands, 1984, Vol. 1, p 13.
57. Förster, T. *Discuss. Faraday Soc.* 1959, 27, 7.
58. Borisov, A. Y. In The Photosynthetic Bacteria; Clayton, R. K., Sistrom, W. R., Ed.; Plenum; New York, 1978, p 323.
59. Montroll, E. W. *J. Math. Phys.* 1969, 10, 753.
60. Seely, G. R. *J. Theor. Biol.* 1973, 40, 173; *J. Theor. Biol.* 1973, 40, 189.
61. Shipmann, L. L. *Photochem. Photobiol.* 1980, 31, 157.

62. Knox, R. S. *J. Theor. Biol.* 1968, 21, 244.
63. Kudzmaukas, S.; Valkunas, L.; Borisov, A. Y. *J. Theor. Biol.* 1983, 105, 13.
64. Borisov, A. Y. *Biofizika* 1967, 12, 630.
65. Borisov, A. Y.; Fetisova, Z. G. *Molekulyarnaya Biologia* 1971, 5, 509.
66. Altmann, J. A.; Beddard, G. S.; Porter, G. *Chem. Phys. Lett.* 1978, 58, 54.
67. Scherz, A.; Parson, W. *Photosynthesis Research* 1986, 9, 21.
68. Rafferty, C. N.; Bolt, J.; Sauer, K.; Clayton, R. K. *Proc. Natl. Acad. Sci. U.S.A.* 1979, 76, 4429.
69. Monger, T. G.; Parson, W. W. *Biochim. Biophys. Acta* 1977, 460, 393.
70. Cogdell, R. J.; Thornber, J. P. *FEBS Lett.* 1980, 122, 1.
71. Loach, P. A.; Parkes, P. S.; Miller, J. F.; Hinchigeri, S.; Callahan, P. M. In Molecular Biology of the Photosynthetic Apparatus; Steinbeck, K. E., Ed.; Cold Spring Harbor Laboratory: New York, 1985, p 197.
72. Zuber, H.; Sidler, W.; Füglistaller, P.; Brunisholz, R.; Theiler, R. In Molecular Biology of the Photosynthetic Apparatus; Steinbeck, K. E., Ed.; Cold Spring Harbor Laboratory: New York, 1985, p 183.
73. Kramer, H. J. M.; Grondelle, R.; Hunter, C. N.; Westerhuis, W. H. J.; Amesz, J. *Biochim. Biophys. Acta* 1984, 765, 156.
74. Matthews, B. W.; Fenna, R. E. *Acc. Chem. Res.* 1980, 13, 309.
75. Tronrud, R. E.; Schmid, M. E.; Matthews, B. W. *J. Mol. Biol.* 1986, 188, 443.
76. Pearlstein, R. M.; Hemenger, R. P. *Proc. Natl. Acad. Sci. U.S.A.* 1978, 75, 4920.
77. Li, J. *Proc. Natl. Acad. Sci. U.S.A.* 1985, 82, 386.

78. Kuhlbrandt, W. *Nature* 1984, 307, 478.
79. Joliot, A.; Joliot, P. *C. R. Acad. Sci.* 1964, 258, 4622.
80. Butler, W. L. *Ann. Rev. Plant Physiol.* 1978, 29, 345.
81. Englman, R. *Non-Radiative Decay of Ions and Molecules in Solids*; North Holland: Amsterdam, 1979.
82. Dexter, D. L. *J. Chem. Phys.* 1953, 21, 836.
83. Kubo, R. *Phys. Rev.* 1952, 86, 929.
84. Kubo, R.; Toyozawa, Y. *Progress of Theor. Phys.* 1955, 13, 160.
85. Soules, T. F.; Duke, C. B. *Phys. Rev B* 1971, 3, 262.
86. Duke, C. B. *Mol. Cryst. Liq. Cryst.* 1979, 50, 63.
87. Marcus, R. A. *J. Chem. Phys.* 1956, 24, 966.
88. Marcus, R. A. *Annu. Rev. Phys. Chem.* 1964, 15, 155.
89. Marcus, R. A. *Faraday Discuss. Chem. Soc.* 1982, 74, 7.
90. Hopfield J. J. *Proc. Natl. Acad. Sci. U.S.A.* 1974, 71, 3640.
91. Jortner, J. *J. Chem. Phys.* 1976, 64, 4860.
92. Sarai, A. *Chem. Phys. Lett.* 1979, 63, 360.
93. *Tunneling in Biological Systems*; Chance, B.; DeVault, D. C.; Frauenfelder, H.; Marcus, R. A.; Schieffer, J. R.; Sutin, N., Eds.: Academic: New York, 1979.
94. DeVault, D.; Chance, B. *Biophys. J.* 1966, 6, 825.

95. Devault, D. *Quar. Rev. Biophysics* 1980, 13, 387.
96. Yomosa, S. *J. Phys. Soc. Japan* 1978, 45, 967.
97. Jortner, J. *Biochim. Biophys. Acta* 1980, 594, 193.
98. Jortner, J. *J. Phys. Chem.* 1986, 90, 3795.
99. Marcus, R. A.; Sutin, N. *Biochim. Biophys. Acta* 1985, 811, 265.
100. Marcus, R. A. In Supramolecular Photochemistry; Balzani, V. Ed.; D. Reidel: New York, 1987, p 45.
101. Levich, V. G. In Physical Chemistry: An Advanced Treatise; Eyring, H.; Henderson, D.; Jost, W., Eds.; Academic: New York, Vol. 9B, 1970.
102. Jortner, J. *J. Am. Chem. Soc.* 1980, 102, 6676.
103. Laubereau, A.; Von Der Linde, D.; Kaiser, W. *Phys. Rev. Lett.* 1971, 27, 802.
104. Laubereau, A.; Wochner, G.; Kaiser, W. *Opt. Commun.* 1975, 14, 175.
105. Holstein, T.; Lyo, S. K.; Orbach, T. *Comments Solid State Phys.* 1978, 8, 119.
106. Holstein, T.; Lyo, S. K.; Orbach, R. *J. Lumin.* 1979, 18/19, 634.
107. Huang, K.; Rhys, A. *Proc. R. Soc. Lond. A* 1950, 204, 406.
108. Dogonadze, R. R.; Kuznetsov, A. M.; Vorotyntsev, M. A. *Phys. Stat. Sol. B* 1972, 54, 125.
109. Watson, G. N. A Treatise on the Theory of Bessel Functions; University Press: New York, 1945.
110. Gillie, J. K.; Fearey, B. L.; Hayes, J. M.; Small, G. J.; Golbeck, J. H. *Chem. Phys. Lett.* 1987, 134, 316.

111. Jankowiak, R.; Small, G. J. *Science* 1987, 237, 618.
112. Friedrich, J.; Haarer, D. In Optical Spectroscopy of Glasses; Zschokke, I., Ed.; Reidel: Dordrecht, Netherlands, 1986, 149.
113. Hayes, J. M.; Jankowiak, R.; Small, G. J. In Persistent Spectral Hole-Burning: Science and Application; Moener, W. E., Ed.; Springer-Verlag: West Berlin, 1988, 153.
114. Hochstrasser, R. M. *Acc. Chem. Res.* 1973, 6, 263.126.
115. Meixner, A. J.; Renn, A.; Bucher, S.E.; Wild, U. P. *J. Phys. Chem.* 1986, 90, 6777.
116. Maier, M. *Appl. Phys. B* 1986, 41, 73.
117. Lockhart, D. J.; Boxer, S. G. *Biochemistry* 1987, 26, 664.125.
118. Hayes, J. M.; Small, G. J. *J. Phys. Chem.* 1986, 90, 4928.
119. Hayes, J. M.; Gillie, J. K.; Tang, D.; Small, G. J. *Biochim. Biophys. Acta* 1988, 932, 287.
118. Kador, L.; Haarer, D.; Personov, R. *J. Chem. Phys.* 1987, 86, 10.
119. Kador, L.; Personov, R.; Richter, W.; Sesselmann, Th.; Haarer, D. *Polymer J.* 1987, 19, 61.

ACKNOWLEDGMENTS

This dissertation is dedicated to the loving memory of my brother Alan Stephen Gillie, May 4, 1963 - December 20, 1985. Few events in one's life can be so painful yet so influencing. We will never have the chance now to collaborate in a scientific endeavor as we once dreamed. I miss his companionship, his jokes and animated gestures, but mostly I miss his love. This dissertation is also dedicated to the memory of my grandmother Ethel Gillie whom I wish could share my joy of graduating.

I wish to thank my parents for their encouragement through the years, their love and support, and most of all the patience to answer all the questions three curious boys can ask. I also wish to thank my older brother Michael for all the fun and friendship that only an older brother can provide.

I also express thanks to everyone who has played an important part in my scientific development. I am most grateful to Dr. Gerald J. Small who provided needed guidance while allowing me the freedom to pursue the aspects of this project I found most interesting. His patience and thoughtful discussions were very important. I also thank Dr. John Hayes and Dr. Ryszard Jankowiak for their many discussions through the years. I cannot imagine two better coworkers. To my friends in Dr. Small's group, thanks for all the help and good times. The practical jokes have always been enjoyable.

Finally, I thank my other friends who made my stay at ISU enjoyable. I especially thank my girlfriend, Patrice Christensen, for the good times, companionship and love of the last two years.

This work was performed at Ames Laboratory under contract No. W-7405-eng-82 with the U. S. Department of Energy. The United States government has assigned the DOE Report number IS-T 1403 to this thesis.